# Modelling Composite Fire Behaviour Using Apparent Thermal Diffusivity

V. Urso Miano

Thesis submitted in
Accordance with requirements
of Newcastle University
for the Degree
of Doctor of Philosophy

Supervisors: A.G. Gibson, A.M. Robinson

September 2011

# Abstract

In this study, a new model has been developed for the prediction of thermal profiles for fibre reinforced plastic composites exposed to high heat flux. The model involves expressing the thermal diffusivity of the composite as a function of temperature. Apparent thermal diffusivity (ATD) can take into account the decomposition of the resin, which is endothermic, as well as the consequent changes in specific heat capacity and thermal conductivity of the composite. This offers the possibility of significantly simplifying computational procedures needed for modelling thermal behaviour with decomposition. The possibility of extending thermal analyses to two and three dimensional cases was explored.

Techniques for the direct measurement of the apparent thermal diffusivity are presented for different composite systems over a wide range of temperatures: from ambient to $\sim$ 600 ℃. Two different techniques were needed for different ranges of temperatures: from ambient to 80 ℃ and from 80-100 ℃ to 600 ℃.

To measure the ATD in the low range, a step temperature change was applied to the surface of a slab-shaped piece of material. Theta, the difference between the middle plane temperature and the outer surface temperature was recorded. The value of the thermal diffusivity at each temperature was calculated from the values of theta. The high range measurement involved the application of a linear temperature rise to the surfaces of a slab of material. The ATD was calculated by means of the Laplace heat transfer equation.

The thermal diffusivity function obtained through these measurements was used to model the fire behaviour of these materials under different heat transfer conditions.

Quasi isotropic glass/polyester slab shaped composite specimens were tested under one dimensional heat transfer conditions. A one-sided heat flux was applied to the samples and the remaining surfaces were isolated to obtain repeatable boundary conditions. The temperatures were recorded at different depths within the samples during the exposure. The ATD of this material was measured through the techniques mentioned above and implemented in a one-dimensional heat transfer FORTRAN model.

I-beam shaped pultruded sections were subjected to two-dimensional heat transfer conditions. The temperatures were recorded at different locations on the cold side. Thermal properties were determined by means of the apparent thermal diffusivity of the material and implemented in a two-dimensional FE thermal model.

Carbon fibres reinforced wing box materials were used to perform three dimensional fire tests.

To describe analytically the tests, the ATD was measured along the three principal directions by means of the techniques mentioned before. These data were implemented into finite element models. The suitability of the ATD to model complex cases was verified.

The failure of polyester and phenolic pultrusions under tensile and compressive load and a one-sided heat flux of 50 $kW/m^2$ was studied. A thermal/mechanical model, based on the Henderson equation and laminate theory, was used to model their behaviour. In tension, significant load-bearing capacity was retained over a period of 800 seconds, due to the residual strength of the glass fibres. However, pultruded composites are susceptible to compressive failure in fire, due to the loss of properties when the resin Tg is reached.

The fire reaction properties reported here showed the phenolic pultrusions to perform better than polyesters in all fire reaction properties (time-to-ignition, heat release, smoke and toxic product generation). The measurements under load in fire showed that the phenolic system decayed at a slower rate than the polyester, due mainly to the very shallow glass transition of the phenolic, but also the char-forming characteristic of the phenolic. The behaviour described here for phenolic pultrusions is superior to that reported for some phenolic laminates, the main reason probably being their lower water content.

In all cases the experimental data and the predicted temperatures were compared. The ATD modelling proved capable of capturing the main features of the temperature curves that relate with the effects of fire exposure of composites. This study allowed to determine the characteristics of the ATD curve at different temperatures and relate it to the phenomena occurring to composites exposed to fire.

# Acknowledgements

The project presented here is the product of years of study, experimentation, mistakes and lessons learned. During this time I have been exchanging ideas and thoughts with a great number of people. I have been asked questions and difficult questions. I have been listened to. I have been explained things. Most of the time these interactions that sparkled useful ideas in a confused mind, either consciously or not. Therefore I feel impossible to identify all the contributors to this work. Nevertheless I tried to identify the main and more important ones.

Firstly I would like to thank professor Geoff Gibson for his support, trust, good ideas, good discussions, availability to listen and accept challenges. For being my *vate* in the academic world. And finally I am grateful for the very good time we had around Europe. I owe my gratitude to Roberto Palacin which managed to help me in numerous ways and ease the difficulties of a journey uncertain and impervious such as a PhD research. Thank you to professor Mark Robinson for his support. I am grateful to Dr Magnus Svanberg for helping me on the FE modelling of degrading materials.

I am indebted to my many of my colleagues to support me in many ways. Among them I would like to mention Dr. Cristian Ulianov for his friendship and indefatigable help; Dr Mariano Otheguy for the Spanish lessons, and his endless enthusiasm ; Conor O'Neill for his advice, help, friendship, and cakes; Dr. Craig Hudson for the help with this awkward language called English; Dr Dewan Islam for his lessons; Dr Gaetano La Delfa professional collaboration. It's been a pleasure to solve the world's problems with the *T10 posse*. Thanks to Constandinos Konstantis for his friendship and help.

Thanks to Dr Pierfrancesco Celada and Andrea De Mauro these years have been merrier. I would like to thank Tien Lam 'Andy' Lau for friendship and support with the final draft of this work.

A great thank you goes to my family. Without their help, support and love this thesis would not have been possible. And *dulcis in fundo*, I am grateful to my future wife, Elena Acampora, especially for her support and encouragement to terminate this work during this last difficult year.

This study was funded by *MOMENTUM*, a Marie Curie Research training network.

# Contents

# Chapter 1

# Introduction

Composite materials, and specifically fibre reinforced polymers, offer great advantages compared to traditional structural materials such as metals. Apart from their high specific stiffness and strength, very good corrosion resistance, good acoustic damping properties and the possibility of varying their ply stacking sequence allows to optimize the material to better suit each single application. The existence of different manufacturing processes makes composites applicable to different industry sectors: pultruded composites are largely applied in civil structures such as bridges; prepreg composites offer high fibre volume fractions and high performance for aerospace applications; sandwich composites are widely used in boat building. Different material can be usd in a composite system. Carbon fibres constitute high performance fibres and are used in aerospace applications, together with high performance epoxy resins. Glass fibres and a poly/vinyl ester matrix constitute a cheaper solution, mainly used in boat building. Different materials can be used in a composite system.

One of the main disadvantages of composites in structural applications is their fire behaviour. Once the matrix temperature reaches the glass transition temperature, the compressive strength, being a matrix dominated property, decreases significantly. The tensile strength behaves somewhat better as it depends mainly on the fibres. In addition mechanical properties of fibre reinforcements degenerate at higher tempera-

tures [1]. When heated up to high temperatures (300℃-400℃), the matrix develops heat, smoke, fumes and soot. Smoke suffocation makes the application of composites in transportation hazardous in enclosed spaces. Nevertheless composites are thermally insulating, have slow burn-through properties and their fire behaviour can be modified with the use of additives [1].

Characterizing and modelling the behaviour of composites at high temperatures is important to understand and design safe composite structures with fire hazards. Composites undergo thermal, chemical and physical transformation when exposed to high temperatures. From a thermal perspective the surface exposed to fire will be subjected to radiation, the bulk will conduct heat and there might be parts of the structure that exchange heat by convection with air, water or any other fluid. Chemical reactions will be activated during decomposition changing the transport properties of the materials. Hence different aspects of the fire behaviour of composite materials can be modelled.

## 1.1 Fire reaction and fire resistance

Properties of composites in fire can be divided in *fire reaction* and *fire resistance*. *Fire reaction* properties characterize the early stages of fire, from start of fire exposure to flash over. They include: flammability, oxygen index, smoke toxicity, heat release rate, time to ignition, combustion properties and flame spread rate. The *heat release rate* is an index of the amount and rate of energy released by the material when oxidized, it gives an indication of the contribution of a certain material to a fire. Hence it is the most important fire reaction property of the material [2].

*Fire resistance* properties characterize the fire behaviour of the material from the occurrence of the flash over. Fire resistance is mainly expressed as the ability of the material to withstand a fire, retaining mechanical stiffness and strength necessary to avoid the structure to collapse. Another important fire resistance property is the

capability to impede the fire to spread within the structure, along with burn through resistance and heat insulation.

For a complete description of the fire reaction properties of polymer composites see Mouritz, Gibson [1].

## 1.2 Composites in fire

Polymer composites, when exposed to fire, degrade at around 300℃-400℃. A large variety of volatiles is yielded during degradation, many of which ignite contributing to the spread and growth of the fire. The composition of the product gases is dependent on the polymer constituting the matrix and the nature of the fibres. Organic fibres tend to supply a considerably higher amount of combustible volatiles than non-organic ones. Depending on the nature of the materials constituting the composite some char may be produced once decomposition is completed. Common vinyl ester and polyester resins produce small amounts of char, about 5% of the original resin content. Phenolic and aerospace epoxies produce larger amounts of char, about 50% of the original resin content [3]. The latter effect enables their composites to retain mechanical properties after the complete decomposition of the matrix, in fact the remaining char is capable to hold the fibres together, Easby et al [3].

## 1.3 Decomposition reactions

The effects of fire to composites involve polymer matrix decomposition and, in case, organic fibres decomposition.

Polymer matrices show different reaction mechanisms. Some of them tend to reduce the molecular weight of the polymer: random chain scission, chain-end scission and chain stripping. Cross linking and condensation tend to increase the molecular weight, instead. Random chain scissions break down the long polymer chain into a large number of smaller molecules and they are more likely to occur . Chain-

end scission is a process that involves the release of the links at the ends of the chains. Chain stripping consists of the separation of entire chains from the bulk of the material. Cross linking occurs when further links are established between polymeric chains at relatively low temperatures, 100℃-200℃, and it produces an opposite effect to chain scission. Cross linking is mainly due to post-curing.

Fibres can be organic and non-organic. Among the non-organic fibres we can find the most commonly used glass and carbon ones. Aramid fibres are widely used among the organic ones. Glass fibres start softening at 800℃; their strength starts decreasing at lower temperatures and no chemical reaction occur in fire. Carbon fibres experience oxidation in fire. Gibson [4] experienced reductions of diameter and length in carbon fibres exposed to fire.

Aramid fibres show a main decomposition process at 400℃-500℃.

## 1.4 Characterization of decomposition

The decomposition dynamics of a composite can be characterized through the use of different methods. The most common are: *thermogravimetric analysis (TGA), differential scanning calorimetry (DSC), dynamic mechanical analysis (DMA), dynamic mechanical thermal analysis (DMTA), gas chromatography (GS) and mass spectrometry (MS).* Each single technique gives an understanding of different aspects of the decomposition.

### 1.4.1 Thermogravimetric analysis

The *thermogravimetric analysis*, TGA, consists of the measurement of the weight of a sample while its temperature is risen at a constant rate. The test can be executed in air or using an inert environment. An inert atmosphere makes possible the study of the decomposition without the occurrence of the oxidation of the sample. The oxidation introduces uncertainties in the determination of the testing temperature

being it an exothermic process and TGA data obtained using an inert environment give a more accurate description of the decomposition. The samples are usually very small, their weight is around $50 - 100mg$, in order to assure that the temperature is uniformly distributed in every point of the sample. The samples can be tested in bulk or ground in order to assure better heat exchange conditions between the sample and the surrounding environment. The decomposition of polymers is a rate dependent process, the temperature at which the process occurs depends on the temperature rate applied. Hence for an understanding of the phenomenon it is useful the execution of three TGA tests at three different heating rates. Materials may decompose in one or more stages and thermogravimetric analysis is a way of determining the nature of the decomposition.

### 1.4.2 Differential scanning calorimetry

The technique consists of comparing the quantity of heat required to heat up a sample to the one needed to heat up a reference material at the same rate. The heating rates imposed are usually linear and the specific heat of the reference material needs to be known over the full range of testing temperatures. The technique allows to measure the specific heat capacity, the melting point, the glass transition and the percentage of crystallinity of a polymer.

### 1.4.3 Dynamic thermo-mechanical analysis

The technique consists of performing three point bending tests or torsional tests at different temperatures. It gives the opportunity of locating the occurrence of the glass transition and measuring the evolution of different mechanical properties as function of temperature.

## 1.5 Fire testing of composites

Fire tests of composites aim to determine the fire behaviour properties described above. Fire reaction property tests are characterized by the possibility of using small scale specimens; many fire resistance properties need to be testes at full scale instead, being difficult to predict the behaviour of an entire structure from a simple coupon sample.

### 1.5.1 Cone calorimeter

The cone calorimeter is the most common instrument to measure fire reaction properties through the use of a standardized testing procedure [5]. The apparatus is capable to measure all the fire reaction properties from a small coupon sample, $100mm \times 100mm$, except for the flame spread rate. The heat release of the material is determined indirectly measuring the consumption of oxygen. It uses a truncated cone shaped radiant heater which assures an uniform incident heat flux on the exposed surface of the sample, figure 1.1. Heat fluxes range from 0 to $100kW/m^2$ and the sample can be tested either in a vertical or horizontal position to better reproduce the real condition of use of the tested material.

### 1.5.2 Other fire reaction tests

The ignition and flammability of materials can be measured by the *Limiting oxygen index (Loi)* test. The test allows to measure the minimum amount of oxygen needed to ignite the material and sustain the oxidation process. The specimen is placed in a glass chimney and ignited at the upper end, figure 1.2. A mixture of oxygen and nitrogen flows from the bottom end of the chimney around the specimen. Several tests need to be conducted at different oxygen concentration to determine the lowest one to assure ignition and sustained burning.

In the *radiant panel flame spread* test a sample inclined toward the heater element

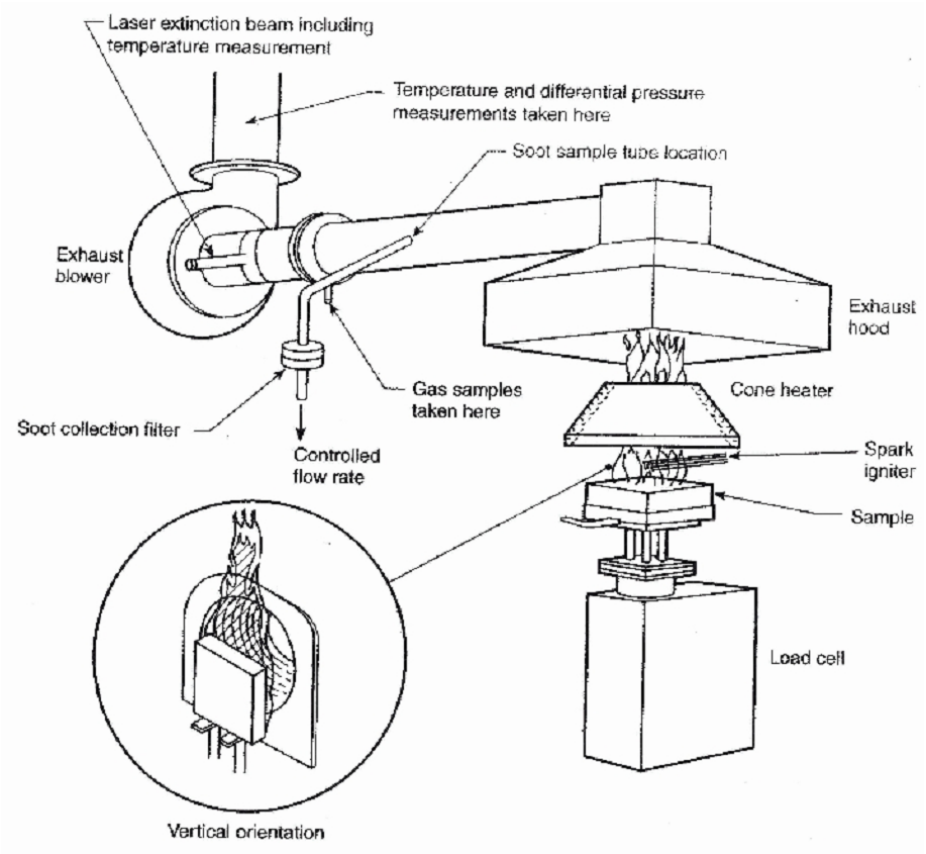


Figure 1.1: Schematic of the cone calorimeter.

Figure 1.2: Limiting oxygen index apparatus.

catches fire at the top end and the downward flame spread rate is measured. The downward spread rate of a flame on a material is not directly related to the upward flame spread and the validity of the test is arguable. Many variants of this test have been developed in order to cover the possible practical situations, upward ,lateral and horizontal flame spread tests.

*Smoke density* tests provide the specific optical density of the smoke yielded when the sample is burning. The production of smoke and its density depend on the conditions of characterizing the fire, such as heat flux, geometries. The relevance of the various versions of these tests is questionable because they fail to reproduce realistic fire conditions.

Figure 1.3: Furnace for large samples tests.

### 1.5.3 Fire resistance tests

*Furnace tests* tend to reproduce real fire condition on real scale composite panels, figure 1.3. The setup consists of an open side furnace to which a composite panel gets attached. The specimens can be loaded to test their structural integrity during fires and they are instrumented with any sort of sensors needed.

# Chapter 2

# Literature review

The implications of the application of composites where there is a hazard of fire or presence of high temperature, were,for the first time, presented comprehensively by Mounitz and Gibson [1]. The study covers all the main aspects of the fire behaviour of composites ranging from the dynamics of decomposition, structural properties in fire, modelling and testing of thermal response and structural integrity, fire safety regulations to health hazards involved in the use of composites in fire. Nevertheless previous to that, several studies were conducted on all different aspects of the topic.

The study presented here focused on the modelling of a wide range of composite systems in fire. Fire modelling has an important role in the design process of composite structures. Reliable models give the opportunity of reducing the number of tests, performing optimization studies, saving time and cost of numerous and expensive tests.

The variety of mechanisms involved in a composite fire leads to a multitude of modelling approaches. Thermal modelling is certainty the most straightforward aspect to be considered. The evolution of the temperature profiles of a composite structure exposed to fire is predicted by this kind of models.

Thermo-mechanical models study the mechanical response of a composite structure to fire. The mechanical properties of a composite, such as its stiffness and

strength, change dramatically in the event of fire. The main causes of those effects are: the softening of the resin at the glass transition temperature, ∼100℃; the thermal decomposition of the resin at higher temperatures, as described in 1.3, it changes the ratio between the matrix and the fibres; the introduction of a further component to the composite system by means of the formation of char. The most common thermo-mechanical models involve a first independent thermal analysis and a following mechanical one, strongly influenced by the previous one. Temperature dependent $A(T), B(T), D(T)$ matrices, from *The Classical Laminate Theory*, are used to predict the mechanical behaviour of the composite in fire [7]. The prediction of the time to failures of composites can be achieved performing residual strength analyses as in [3, 8, 9, 10].

Fire reaction properties such as heat release rate, ignition and flame spread are key properties to model the behaviour of materials in the early stages of fires, the evolution of fires into enclosures and interiors. The heat release rate is influenced by the nature of the material, the portion of its surface involved in the fire and the surrounding boundary conditions. For those reasons enclosure fires reach far higher temperatures than fires in open spaces. Modelling the heat release rate involves the evaluation of the mass loss rate and the heat of decomposition. These properties can be measured with the Cone Calorimeter or predicted using thermal degradation models. Ignition models are usually calibrated using experimental results and state critical conditions at which the ignition occurs. They can be based on a critical temperature, a critical incident heat flux, a critical mass loss rate.

## 2.1 Modelling the fire response of composite materials

The origins of modern pyrolysis models for polymers and composite materials lie on earlier studies in wood fire behaviour, [14, 15]. Burning wood is treated as a two-layered material: the charred material and the unpyrolysed layer. The two layers

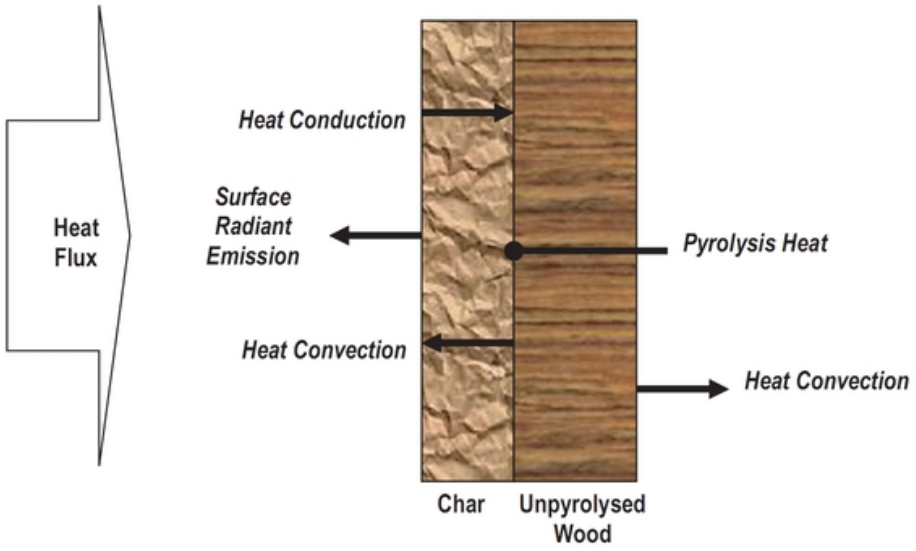


Figure 2.1: Tho-layer schematic for wood pyrolysis.

are separated by the pyrolysis front which moves toward the virgin material. The decomposing material at the pyrolysis front produces flammable volatiles that move through the charred material to the fire, figure 2.1.

Henderson *et al.* [6] formulated a one-dimensional model for the thermal response of phenol-formaldehyde/carbon composites to fire. In this model, the usual energy balance equation used for one-dimension thermal conduction,

$$\rho C_p \frac{\partial T}{\partial t} = \frac{\partial}{\partial x}(k\frac{\partial t}{\partial x}) \tag{2.1}$$

was equipped with two extra terms to take into account the effects of a temperature rise on a composite material. The Henderson equation is formulated as follows:

$$\rho C_p \frac{\partial T}{\partial t} = \frac{\partial}{\partial x}(k\frac{\partial t}{\partial x}) - \dot{m}_g C_{pg}\frac{\partial T}{\partial t} - \frac{\partial \rho}{\partial t}(Q_i + h - h_g) \tag{2.2}$$

where $\rho$ is the density; $C_p$ is the soecific heat; $T$ is the temperature; $t$ is time; $x$ is the through thickness coordinate; $k$ is the thermal conductivity; $\dot{m}_g$ is the volatiles flow rate; $C_{pg}$ is the specific heat of the volatiles; $Q_i$ is the heat of decomposition; $h$ and $hg$ are respectively the enthalpy of the composite and the volatiles.

The middle term on the right hand side describes the effects of resin decomposition, which is a significantly endothermic process and the far right term describes the convective cooling that occurs as a result of the passage of decomposition products through the laminate towards the hot face. It should be noted that the thermal properties in Equation 2.2 are not treated as single point values -they evolve, both with changing temperature and with decomposition of the resin phase. Physical and transport properties of the material were determined experimentally over a wide range of temperatures.

The mass loss was measured through TGA tests. It is a function of temperature and temperature rate and it is modelled using an activation model formulated by Arrhenius [6]. The Arrhenius equation was written in terms of density as follows:

$$\frac{\partial \rho}{\partial t} = -A\rho_0 \left[\frac{\rho - \rho_f}{\rho_0}\right]^n e^{\frac{E}{RT}} \tag{2.3}$$

where $\rho$ the current value of the density $[kg/m^3]$, $\rho_0$ is the initial value of the density, $\rho_f$ is the final value of the density, is $A$ is the pre-exponential factor $[s^-1]$, $E$ is the activation energy $[J/gmol]$, $R$ is the gas constant [8.314 $j/gmolK$], $T$ is the temperature $[K]$, $n$ is the order of reaction [-]. $A$,$E$ and $n$ are the *kinetic parameters* of the decomposition process.

The phenolic resin system showed a two-stage decomposition process, figure 2.2, that Henderson fitted using one set of kinetic parameters for each decomposition stage.

Implementation of the Henderson equation can be achieved using either a finite difference methodology as in Dodds et al. [16] or the finite element method [17]. To date, modelling work has concentrated on one-dimensional (1-D) formulations of the model, which work well for the case of simply shaped flat laminates.

Gibson *et al.* [18] observed interesting properties of glass/polyester composites in fire such as the "slow burn-through effect". It is stated that a $10mm$ thick composite is able to withstand an hydrocarbon fire curve for $20min$ due to its low thermal

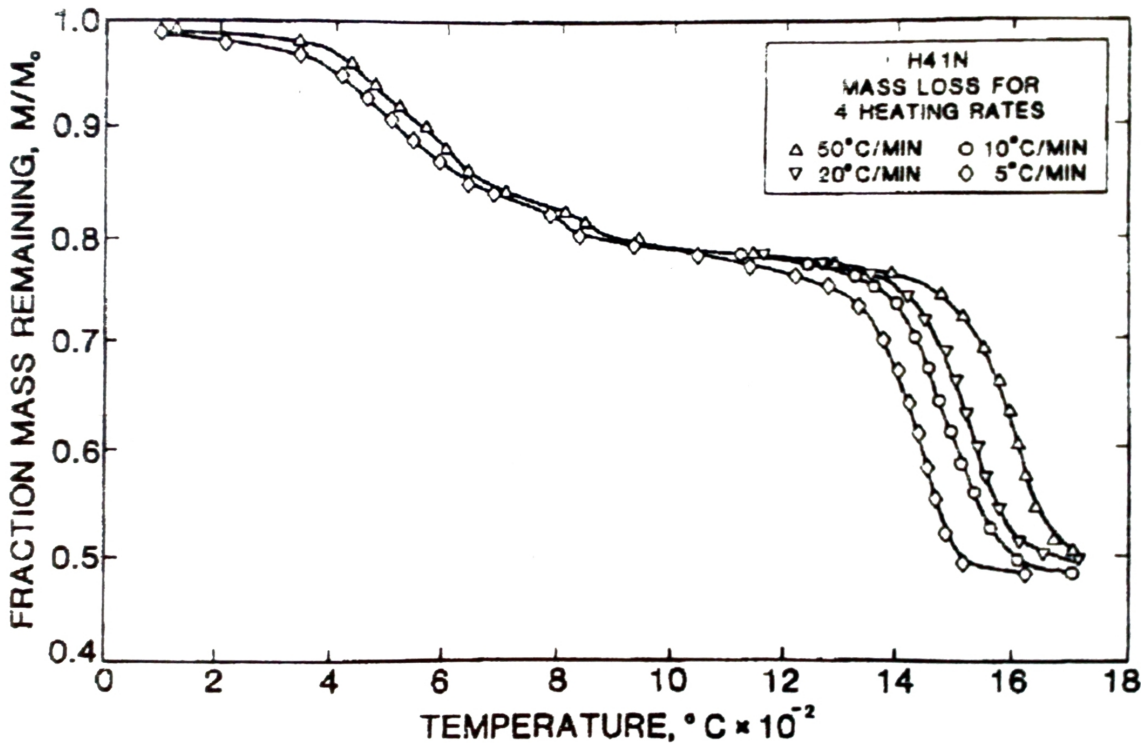


Figure 2.2: TGA data for phenolic/carbon composites from Henderson et al. [6].

conductivity. This enhances the possibility of the development of composite fire protection systems. This effect can be further improved using sandwich with a fire resistant core taking their burn-through resistance to hydrocarbon fires up to about two hours.

The temperature profiles show a plateau in the range of temperature that involve decomposition. This effect was attributed to the decomposition and mass flux of volatiles. The temperature were predicted with the use of explicit one-dimensional finite difference based calculation program based on the Henderson equation, 2.2. The program was used to analyse the effects of the terms mentioned above showing that the mass flux term has a small influence on the phenomenon. This led to the conclusion that the plateau was mainly due to the presence of the matrix decomposition.

A thorough study of the thermal properties of E-glass woven roving fibre mats is presented by Lattimer and Ouellette [19]. The behaviour of the fibres in fire can be coupled with the thermal properties of the resin to model the overall fire response of a

laminate. The study provides emissivity, specific heat and thermal conductivity over a wide range of temperatures. The thermal conductivity increased with temperature and it could be fitted with good approximation with a straight line. The specific heat capacity increases up to 300℃ and then remains constant.

Dodds *et al.* [16] studied the fire behaviour of different composite systems: polyester, epoxy and phenolic glass reinforced laminates. In this work a finite difference one-dimensional computer model was developed to predict the temperature profiles of flat samples exposed to a one-sided hydrocarbon fire curve. It is pointed out that despite the presence of a combustible matrix, thick polymer composites show a good fire resistance due to the low thermal conductivity of the material.

Looyeh *et al.* [17] for the first time developed a one-dimensional finite element model for offshore composites. The model was based on the Henderson equation, 2.2, and it was used to model glass/polyester composites exposed to a hydrocarbon fire. The study is still limited to one-dimensional analyses and to the use of a non commercial code.

There is a great interest, however, in extending the applicability of the model to the 2- and even 3-D cases, to enable complex features such as corners, reinforcing ribs and composite-to-metal interfaces [20] to be accurately modelled.

There are a number of computational difficulties to be overcome in implementing the Henderson model. There can, for instance, be problems of numerical stability due to the nature of the Arrhenius model and the speed at which the decomposition reaction can take place. Such problems can introduce a degree of trial and error into the computation, and the need to shorten the time increment used in finite difference calculations. This can considerably increase both the calculation time and the cumulative error in the calculation. Therefore, avoiding the Arrhenius model and expressing the degree of decomposition of the resin as a simple function of temperature constitutes a significant benefit. This should not lead to undue errors as long as the effective heating rates in the fire do not differ too greatly from those employed in the

thermo-gravimetric measurements used to characterise the resin decomposition.

In extending the treatment to cover the 2-D or 3-D cases two further problems arise:

- the gas convection term in Equation (1), because the direction of the gas flow within the laminate, is not easy to determine for these cases;
- specifying a 2-D or 3-D complex geometry in a finite difference model becomes very demanding task.

The first problem could be overcome by modelling the permeability of the laminate with decomposing resin [22], which would add greatly to the computational burden. Nevertheless it was shown [18] that the effect of the volatile convection term on the overall thermal field is small enough to be neglected in most cases. The second issue can be solved using a commercial finite element package which is much more versatile than in house code, either F.E. or F.D. based, to model complex geometries.

In summary, therefore, the present work involves the development of a model incorporating the following approximations, compared to the Henderson model:

- the Arrhenius temperature dependence of the resin decomposition was ignored, and replaced by a simply temperature-dependent decomposition model;
- the heat transferred by volatile convection within the laminate was ignored.

These simplifications significantly improve the utility of the model in finite difference implementations and in commercial FEA heat transfer packages, especially when extending from 1-D to 2-D and 3-D versions.

Furthermore, this approach was implemented in the commercial finite element package *ANSYS* and validated against experimental results.

### 2.1.1 Thermal properties of composites at high temperature

The main thermal properties used in modelling are *thermal conductivity*, *specific heat capacity* and *density*. These properties can be determined at room temperature

using the rule of mixtures. In the most general case the thermal conductivity is a tensor assuming different values in the 0° direction, the 90° and the through thickness direction. For the through thickness direction, at ambient temperature, the thermal conductivity can be calculated as follows:

$$\frac{1}{k_{com}} = \frac{V_f}{k_f} + \frac{V_m}{k_m} \tag{2.4}$$

The specific heat capacity and the density are scalar properties, only one value is needed to define the property at each point of the material. Hence the specific heat and the density will be calculated as follows at ambient temperature:

$$(C_p)com = \frac{(C_p \rho V)_f + (C_p \rho V)_m}{\rho_f V_f + \rho_m V_m} \tag{2.5}$$

$$\rho_{comp} = \rho_f V_f + \rho_m V_m \tag{2.6}$$

In equations 2.4, 2.5 and 2.6 the subscript *com* refers to the effective property of the composite; $f$ refers to the fibres; $m$ to the matrix; $V$ is the volume fraction; $k$ is the thermal conductivity; $C_p$ is the specific heat and $\rho$ is the density.

As mentioned in 1.3 composites undergo significant changes during a fire and the same happens to their thermal properties. Hence they need to be determined over the same range of temperatures they experience in a fire.

The density of a composite is related to its mass reduction and it is measured through thermogravimetric analyses executed at different temperature rates as described in 1.2 and shown in figure 2.3. The data can be fitted with the use of one or more Arrhenius equations, depending on the number of stages involved in the process [12].

The thermal conductivity of composites need to be evaluated for three material states: a first set of values needs to be evaluated for the virgin material up a temperature at which it is starting to decompose; a second set for the decomposing material, it is actually difficult to define this state; and a last one for the charred material,

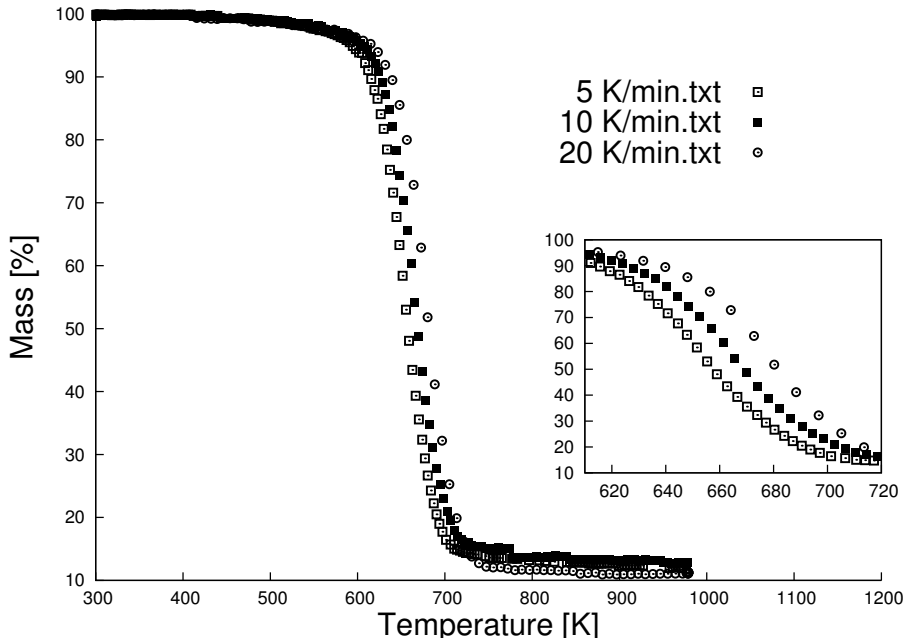


Figure 2.3: TGA data for glass chopped strand mat/polyester composite tested at three different heating rates: $5K/min$, $10K/min$ and $20K/min$. Details of the decomposition region in the frame. Data refer to resin only. Reproduced from Urso Miano and Gibson [11].

which involves just the fibre mat in some cases. The thermal conductivity in all cases, individually, tends to increase with the temperature; generally its values are quite different for the three sets, as shown in figure 2.1.1.

The specific heat , as well as the thermal conductivity, is characterized by three material states: virgin, decomposing and charred material. It is determined using differential scanning calorimetry [13].

There has been the need [22] of simplifying the Henderson approach to provide a model that more closely resembles Laplace's Equation. Therefore, in this work, it is proposed that the resin decomposition can be modelled in a similar manner to a phase change, and the effect incorporated into an effective temperature-dependent specific heat capacity, enabling the resin decomposition endothermic term to be incorporated into the heat conduction term.

Equation 2.2 can be reduced to Laplace's equation with temperature dependent

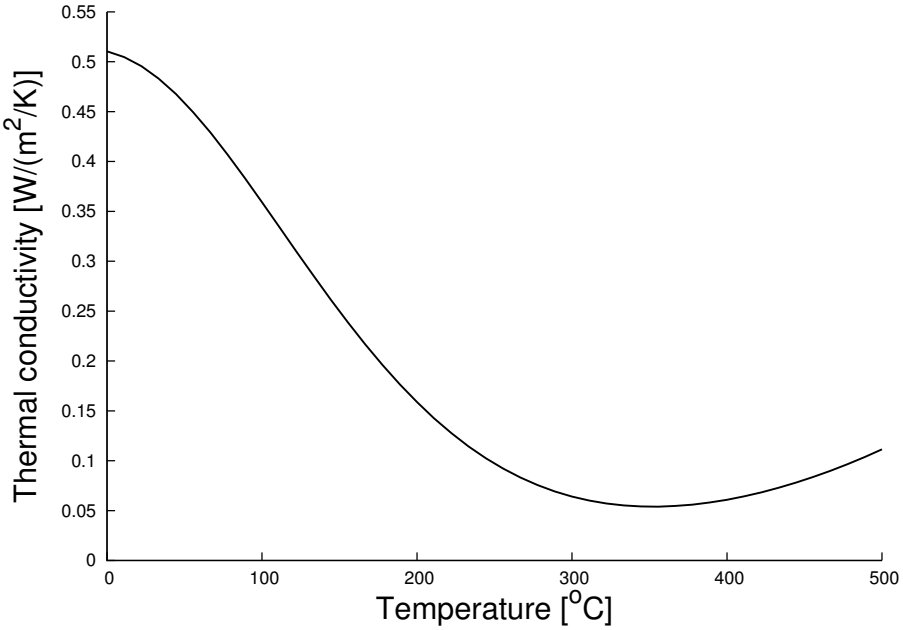


Figure 2.4: Thermal conductivity of glass chopped strand mat/polyester composite.

thermal diffusivity.

$$\frac{\partial T}{\partial t} = \alpha(T)\frac{\partial^2 T}{\partial x^2} \tag{2.7}$$

where $T$ is temperature; $t$ is time; $x$ is the through thickness abscissa; $\alpha$ is the apparent thermal conductivity.

All the thermal parameters of the composite (conductivity, specific heat, density) evolve during fire, as a result of both temperature increase and thermal decomposition [1] and can be lumped together into *apparent* values, leading to an *apparent* thermal diffusivity (ATD) which varies with temperature.

$$\alpha(T) = \frac{k(T)}{\rho(T)C_p(T)} \tag{2.8}$$

where $k$ is the thermal conductivity; $\rho$ is the density; $C_p$ is the specific heat; $T$ is the temperature. However, to obtain the temperature dependence of the ATD several characterization experiments are required for each composite (TGA, density, thermal conductivity etc). A novel direct experimental method for measuring the temperature-dependent ATD, $\alpha(t)$, over the thermal range needed for fire modelling

(∼600℃) is introduced in this work.

Henderson *et al.* [23] suggest a method for the determination of the specific heat and the heat of decomposition of composite materials over a wide range of temperatures, from room temperature up to ∼ 700℃. The technique accounts for the weight loss of the sample due to decomposition using a combination of DSC and TGA data obtained from tests executed at the same heating rate.

## 2.2 Fire behaviour of phenolic pultruded composites

Phenolic resins show superior fire properties compared to common vinyl ester or polyester ones [25, 26]. Mounitz and Mathys [25] study the fire performance of marine phenolic laminates. The materials are subjected to different heat fluxes and different time exposures and then the mechanical properties are evaluated. The study shows that fire affects the mechanical performances of phenolic laminates. No modelling has been carried out in this work.

Mouritz and Gardiner [26] studied the compressive strength of glass/vinyl ester skins with PVC core (referred to as vinyl ester sandwich) and glass/phenolic skins with a phenolic core (referred to as phenolic sandwich) exposed to fire. Ignition time of phenolic sandwiches were roughly ten times bigger than the vinyl ester ones at the same heat flux. The phenolic sandwiches performed somehow better than the vinyl ester ones.

The work offers analytical models for the core shear failure stress due to core shear failure and global buckling as a function of the thicknesses of the damaged region of the sandwich. The thicknesses are measured after each test and no thermal modelling is involved for their evaluation. This approach gives no possibility of predicting the mechanical performance of the material knowing the thermo-mechanical boundary conditions. The mechanical properties are assumed to be negligible for the blackened material and equal to those of the virgin material in the non blackened region. This

two-layer approach ignores the fact that the properties vary gradually from the hot to the cold face. The authors themselves recognize that the uncharred portion reaches temperatures beyond the glass transition point in either cases. Hence in that region some thermal softening and degradation occur anyway, although their extent remains undetermined.

Gibson *et al.* [27] reported some success modelling the resistance of phenolic laminates under load in fire. The thermo-mechanical model approximates the composite exposed to fire to a two-layered structure: one layer with reduced (or zero) mechanical properties, affected by the fire and a second one still undamaged. The stiffness or strength are evaluated linearly combining the ones assigned to the two layers weighting them with their thicknesses as a fraction of the total thickness. This approach ignores the fact that in reality mechanical properties vary gradually with temperature. The compressive strength of the laminates appeared affected more than the tensile one. The reason is that the compressive strength is matrix dominated. Once all the resin is depleted the fibres retain tensile strength at high temperatures but they can not bear any compressive loads.

It should be borne in mind that some phenolic composites, particularly those produced by low temperature curing used by Feih *et al.* [28], can be prone to severe delamination behaviour during fire, due mainly to the pressure generated by the vaporisation of water that can be present in the laminate from the curing operation. It has been shown [28] that it is necessary to remove this water to achieve good fire properties. In the case of pultrusions the elevated temperature cycle involved in cure appears to be very effective in accomplishing this. A secondary factor may be fibre architecture: it may be that the woven fabric reinforcement often employed in cold-cured laminates contains more intrinsic weak points for delamination than the three layer structure of mats and unidirectional composite used in pultrusions.

The investigation suggested here consists of a thorough characterization of the mechanical properties of phenolic and polyester pultrusions. The tensile and com-

pressive strength, the longitudinal and transverse stiffness are measured at different temperatures ranging from ambient temperature to $\sim 300$℃, were they stabilize.

The thermo-mechanical model consists of two parts. The first part is an independent thermal model that predicts the temperature profiles through the thickness of the material using the thermal properties of the material and the specified boundary conditions. The second one is represented by a temperature dependent mechanical model that evaluates the the mechanical properties of the pultruded material as the thermal damage progresses in time.

# Chapter 3

# COM_FIRE

## 3.1 Introduction

*COM_FIRE* is a FORTRAN program , developed at the Centre of Composite Materials Engineering (CCME), School of Mechanical and System Engineering, Newcastle University, for predictions of thermal response of composite laminates in fire.

The program COM_FIRE was initially developed in 1994 for predictions of thermal resistance of thick GFRP laminates when exposed (with one of its two faces) to hydrocarbon fire only, based on the one-dimensional (1D) model [18] using finite difference (FD) numerical analysis approach. The newer current version of the program can be used to predict thermal responses of composite laminates exposed to range of different heating sources. Also, the program can accommodate various types of resin systems and fibre reinforcements.

## 3.2 Governing equations

A 1D FD element cut from the composite laminate under examination with a unit cross-sectional area and a length of $\Delta x$ in the through-thickness direction is shown in figure 3.1:

The rate of change of internal energy inside the 1D FD element can be expressed

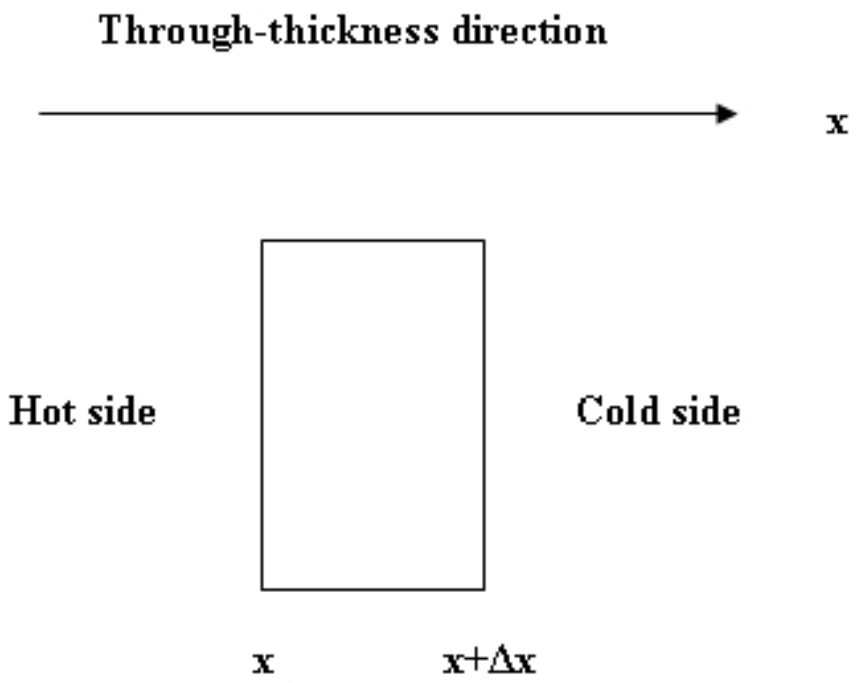


Figure 3.1: Finite difference element and coordinate system.

as follows:

$$\frac{\partial}{\partial t}(\rho_{com} h_{com})(\Delta x) \tag{3.1}$$

where $\rho_{com}$ denotes the density of the composite material and $h_{com}$ represents the enthalpy of the material. Internal energy change of the element due to conventional heat conduction is given by:

$$\frac{\partial}{\partial x}\left(k_{com}\frac{\partial T}{\partial x}\right)(\Delta x) \tag{3.2}$$

where $k_{com}$ is the thermal conductivity of the composite material and $T$ is the temperature of the material element. The internal energy change of the element due to gaseous mass flow (from the cold side to the hot side) is represented by:

$$\frac{\partial}{\partial x}\left(\dot{M}_g h_g\right)(\Delta x) \tag{3.3}$$

where $\dot{M}_g$ denotes gaseous mass flux, or rate of gaseous mass flow, and $h_g$ denotes

enthalpy of the gases generated during decomposition. And finally the internal energy change of the element due to heat generation or absorption is:

$$-Q_p \frac{\partial \rho_{com}}{\partial t}(\Delta x) \tag{3.4}$$

where $Q_p$ denotes heat of decomposition and is negative for endothermic reaction.

Having assumed that there is no accumulation of gases generated in the composite during fire exposure, considering energy conservation of the element under examination leads to the following non-linear partial differential equation:

$$\frac{\partial}{\partial t}(\rho h)_{com}(\Delta x) = \frac{\partial}{\partial x}\left(k_{com}\frac{\partial T}{\partial x}\right)(\Delta x) + \frac{\partial}{\partial x}(\dot{M}h)_g(\Delta x) - Q_p\frac{\partial \rho_{com}}{\partial t}(\Delta x) \tag{3.5}$$

With some simple substitutions equation 3.5 can be rewritten in the form of equation 2.2.

### 3.2.1 Thermal degradation

When the hot surface of a composite sample exposed to a fire reaches a sufficiently high temperature, chemical reactions within the composite body may begin to occur and its resin component degrades to form gaseous products. The nth order Arrhenius formulation, equation 2.3, is adopted in thermal analysis to simulate the decomposition process of the resin system involved.

The four kinetic parameters that appear in equation 2.3, i.e. $E$, $A$, $n$ and $\rho_f$, can be derived from processing thermogravimetric data using either Anderson's single heating rate technique [29], or Friedman's multiple heating rate technique, [30]. In this version, $n = 1$ is assumed.

Although thermogravimetric tests of a resin system may be conducted at different heating rates, resulting in a set of TGA curves, the kinetic parameters of the resin system derived from processing TGA data, in theory, should be independent of heating rate. One may have the kinetic parameters of a resin system required for running this

program by averaging values derived from relevant TGA data with different heating rates [31].

### 3.2.2 Boundary conditions

The heat exchange process or the energy transfer from a heating source to a composite laminate sample during the exposure time period is controlled by thermal interaction between the specified heating source surrounding the front hot face (HF) and the hot face of the sample itself through thermal radiation and natural convection. In fire situations, radiation is always the main mechanism in energy transfer and no forced heat convection is assumed in the analysis.

The total heat flux, $q$, into the front hot face of a composite sample is determined according to the following equation:

$$q = \sigma(\epsilon_s \alpha_m T_s^4 - \epsilon_m T_k^4) + h_{nc}(T_{sc} - T_c) \tag{3.6}$$

where $q$ is the heat flux into the hot face of the sample $[W/m^2]$; $T_{sc}$ is the surrounding temperature of heating source $[K]$; $T_c$ is the temperature of the hot face of the sample $[K]$; $T_s$ is the surrounding temperature of heating source $[K]$; $T_k$ is the temperature on hot face of the sample $[K]$; $h_nc$ is the heat transfer coefficient through natural convection $[W/(m^2C)]$; $\epsilon_s$ is the emissivity of heating source [-]; $\alpha_m$ is the absorptivity of the HF material of the sample [-]; $\epsilon_m$ is the emissivity of the HF material of the sample [-]; $\sigma$ is the Stefan-Boltzmann constant $[56.7 \times 10^{-12} W/(m^2 K^4)]$.

The first term on the right hand side of equation 3.6 represents the energy transfer to the sample from the heating source through thermal radiation, which follows the familiar Stefan-Boltzmann law. The second term represents the part of energy transfer to the sample through natural thermal convection from the heating source.

For a solid material, heat radiation is a matter of surface effects. Under such circumstances, emissivity is just a function of the material itself and the surface finish. For hot gases or flames in combustion process, however, radiation is no longer

a surface effect. Flames in an open space or inside a furnace should be treated as selective emitters. For prediction purposes, evaluation of flame emissivity under specified conditions is necessary since its value is usually a complex function of field temperatures. To measure the surrounding temperature of a heating source in a fire test, $T_s$, thermocouples should be placed in such positions which are close to the front hot face of the sample within the boundary layer thickness of the fluid flow.

It is noted that when conducting a fire test against a composite sample, some localised flash over may occur during the test, which will affect measurements of the surrounding temperature of the heating source considerably. A good practice is to place a number of thermocouples around different positions for the measurement and later to take the averaged data as the input to run this program for predictions.

It is indicated in [32] that in fire situations, most hot surfaces, smoke particles or luminous flames may have an emissivity between 0.7 and 1.0. This was also the finding revealed in [33].

In general, emissivity of the hot face of a FRP composite laminate sample, $\epsilon_m$, can be taken as 0.8, and in most practical cases, absorptivity of the hot face of the sample, $\alpha_m$, can be taken as 1.0. The values of emissivity and absorptivity are based on tests developed at Newcastle University for the development of COM_FIRE [33].

The heat transfer coefficient for natural convection, $h_{nc}$, adopted in this program is calculated using the following approximate equation [31] for a vertical wall surface of not over one metre high above the ground:

$$h_{nc} = 1.31(\theta^{\frac{1}{3}}) \qquad for\ 10^9 < Gr < 10^{12} \tag{3.7}$$

where $\theta$ is the difference between the surrounding temperature of the heating source and the temperature of the front hot face of the sample (in ℃), and $Gr$ denotes the Grashof number. The adoption of equation 3.7 means that the flow boundary layer of circulating air on the vertical surface due to natural convection is turbulent, resulting in large Grashof number.

For lower range of Grashof number, which means that the flow of air due to natural convection will remain laminar on the boundary layer of the sample surface, the following equation may be used for evaluating the heat transfer coefficient [31]:

$$h_{nc} = 1.42 \left(\frac{\theta}{l}\right)^{\frac{1}{4}} \qquad for\ 10^4 < Gr < 10^9 \tag{3.8}$$

where $l$ denotes the characteristic linear dimension in the particular case. For example, $l$ may be taken as the distance between the centre of the exposed hot face and the ground floor during the test.

It should be noted that during a fire situation the effect of natural convection, in the majority of cases, is small compared to the effects due to heat radiation.

There are three options in this program for thermal boundary conditions on cold face of the laminated sample under examination:

- thermally insulated;
- natural convection plus free radiation;
- connected with a steel plate of a given thickness.

Thermal boundary condition on the back face of the steel plate can be either thermally insulated or natural convection combined with free radiation.

## 3.3 Thermal properties at high temperature

It is clear that thermal properties of FRP composites are resin volume fraction-dependent. These properties may vary considerably at high temperatures due to:

- changes in resin volume fraction;
- changes in composition of the materials due to chemical reactions.

In this program, the initial density, thermal conductivity and specific heat of a given virgin composite material are evaluated for a specified fibre volume fraction,

$V_f$, according to equations 2.4, 2.5 and 2.6

Re-evaluation of density of the composite material is repeated at each node and each time step during computation to account for changes caused by resin decomposition. The predicted Remaining Resin Content, in percentage, at a time and for a layer at a given depth in the through-thickness direction of the composite is called RRC in the analysis.

No density change in E-glass fibres is expected for temperatures up to about 1000℃. Carbon fibres and aramid fibres may undergo oxidation or decomposition action at high temperatures, resulting in changes in density of the composite material. But such effects are not included in the analysis for the time being since relevant information or data are not available. Effects of gases or air filled in the voids within the skeleton composite material on density change during fire exposure are also ignored.

Although it has been found unsatisfactory to use the above formulas for estimating thermal conductivity and specific heat of composites at high temperatures, for simplicity, it is assumed in this program that the derived initial values of $k_{com}$ and $C_{p,com}$ are independent of temperature.

The inaccuracy in predictions caused by the above simplicity assumption is to be resolved either by directly inputting measured thermal properties of the composite at high temperatures when running the program, or by adopting a modified Rule of Mixtures in the program for evaluating thermal conductivity and specific heat of composites undergoing decomposition at high temperatures.

It is expected that adopting the initial value of thermal conductivity of virgin composite material at room temperature as those at high temperatures might lead to an over-estimation of the actual thermal conductivity of the porous laminate, resulting in a conservative prediction of thermal responses of the composite material in fires.

It is suggested that at least, the following two factors are to be taken into account in formulating a modified Rule of Mixtures:

- The existence of gases or air in the voids generated during decomposition of the composite material;
- different type of fibre reinforcement in the composite, leading to different ways of contact of one individual fibre with another in the through-thickness direction.

## 3.4 Type of Heating Source

Five different types of heating sources are considered in this program and these include:

- The hydrocarbon (HC) curve, which is automatically defined by the program;
- the SOLAS fire curve, which is automatically defined by the program;
- a constant incident heat flux, which is specified by the value of heat flux and the relevant emissivity of the heating source;
- an experimentally or theoretically defined temperature vs time curve in an input data file describing the thermal environment surrounding the front surface of the composite sample under examination;
- an experimentally or theoretically defined temperature vs time curve in an input data file describing temperatures on the front hot surface of the composite sample.

The final type is associated with no particular heating source. This special type of 'heating source' is designed for predictions to be compared with predictions obtained from running commercial FEA or FDA packages in a conventional thermal analysis, where thermal boundary conditions are usually defined as temperatures on boundary surfaces as a function of time. For thermal analysis in most of commercial packages, effects of decomposition reactions in materials at high temperatures are usually not included.

## 3.5 Fourier Number in Heat Transfer Analysis

The Fourier number is a dimensionless parameter that characterizes heat conduction:

$$F_o = \frac{\alpha t}{b^2} \tag{3.9}$$

where $\alpha$ is the thermal diffusivity; $t$ is the characteristic time; $b$ is the length through which conduction occurs.

The suggested value of the Fourier number in heat transfer analysis when running this program is between 0.02 and 0.05. These values are found to be suitable for most cases where the laminate thickness ranges from a few mm to about $25mm$.

Reducing the value of the Fourier number may lead to an improvement in accuracy in predictions for a given time step. Meanwhile, however, the accumulative error in predictions may be hence largely increased due to increased total number of time steps for a given fire exposure time period. Compromise seems to be the right decision.

## 3.6 Numerical Scheme

*Discretisation of laminates:*

- In the 1D modelling, the laminate is discretised automatically by the program in the through-thickness direction with fifty one nodes, forming uniform 50 one-dimensional FD elements or layers in any cases.

*The numerical scheme adopted:*

- The non-linear partial differential equation 2.2 [18] governing the heat transfer process from a heating source to a composite laminate is numerically solved using a straightforward explicit finite difference method and iteration procedure.
- The iteration procedure is required in dealing with thermal boundary conditions.

# Chapter 4

# Application of COM_FIRE: phenolic and polyester pultrusions

## 4.1 Introduction

This work was undertaken in collaboration with Fiberline Composites and involved polyester and phenolic pultruded sections. Pultruded composites are increasingly employed for structural applications, some of which may be sensitive to fire. For that reason, glass/phenolic pultrusions, which have better fire reaction properties (smoke, heat release, time to ignition, etc.), are sometimes used as an alternative to the more commonly employed glass/polyester. The purpose of this investigation was to develop a methodology for the fire characterisation and modelling of pultruded composites and to compare the structural behaviour of phenolic and polyester pultrusions under load in fire.

Recently, an improved structural approach has been developed for studying the behaviour of composites under load in fire [3, 10, 27, 45, 46, 47]. This involves the application of a constant, one sided heat flux to a small laminate sample under constant tensile or compressive stress. The heat flux can be provided either by a radiant electrical element [10, 45] or a calibrated gas burner [3, 27]. Mechanical

measurements are aided by a thermal model, based on the approach adopted by Henderson [6] for the prediction of the temperature evolution through composite laminates.

## 4.2 Experimental

Pultruded glass/phenolic and glass/polyester sections were supplied by Fiberline Composites. These were in the form of structural box sections in which the laminate was 8 $mm$ thick. Like many types of pultruded section, these products were manufactured with a three layer structure as shown in figure 4.1. In this form of construction, a unidirectional core provides the main strength and stiffness to the section. The core is protected on both sides from mechanical and chemical damage by layer of continuous strand mat (swirl mat), in which the fibre orientation lies randomly in the plane of the laminate. The total thickness of the laminate section in this case was 8 $mm$, the skin thickness being 1.5 $mm$. Flat specimens cut from these sections can therefore be regarded as *subelements* of a typical pultruded composite structure.

The Fiberline products were manufactured using the *die injection* version of the pultrusion process, in which no wet resin is exposed to the working environment. General engineering properties of the sections are given in [48]. The phenolic resin was an acid cured resin and the polyester resin was conventional halogenated polyester of the type widely used in structural applications.

## 4.3 Fire reaction properties

The fire reaction properties of the pultruded laminates were measured using a cone calorimeter [49] and are compared in table 4.1. The results underline the well known differences between phenolic and polyester resin fire reaction properties, namely, extended time to ignition, reduced heat release rate and reduced toxic product evolution in the case of the phenolic. As mentioned above, one aim of this study was to investi-

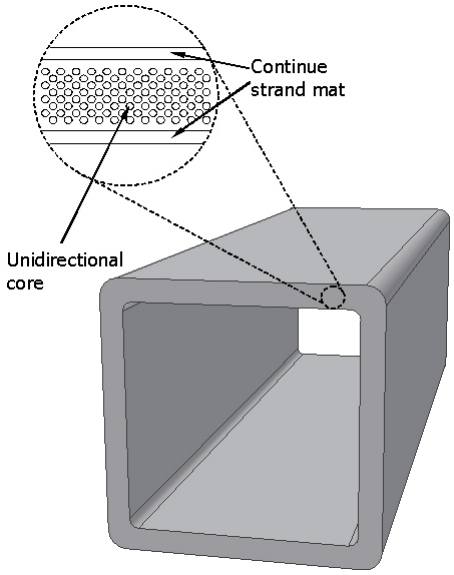


Figure 4.1: Three layer structure commonly employed in pultruded sections: unidirectional core and continuous strand mat (CSM) skins. Testpieces were cut from this section.

| Fire reaction properties | Phenolic | Polyester |
|---|---|---|
| Time to ignition, $[s]$ | 150 | 17 |
| Peak heat release rate, $[kW/m^2]$ | 124 | 309 |
| Average HRR (over 10 min) , $[kW/m^2]$ | 72 | 112 |
| Average smoke production (specific extension area), $[m^2/kg]$ | 197 | 828 |
| Average mass loss rate, $[g/s]$ | 0.044 | 0.066 |
| Average CO yield, $[kg/kg]$ | 0.02 | 0.06 |
| Average $CO_2$ yeld | 1.8 | 1.7 |

Table 4.1: Fire reaction properties (cone calorimeter, 75 $kW/m^2$) for phenolic and for polyester pultrusions.

gate whether the fire reaction benefits of using phenolic resin would also be reflected in better mechanical performances of the phenolic pultrusions, both at high temperature and in fire.

## 4.4 Mechanical properties

To model the structural behaviour of a composite laminate in fire, material constants such as longitudinal and transverse stiffness, tensile and compressive strengths are needed as a function of temperature [3, 7]. Experiments were therefore developed and carried out to measure these properties up to high temperature [3]. The results of these tests needed to be fitted as a function of temperature, so a fitting function

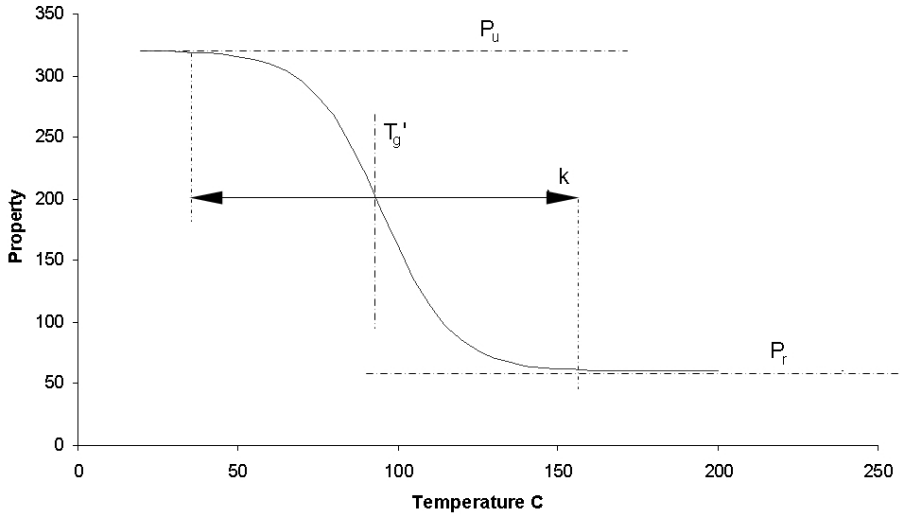


Figure 4.2: Schematic of property variation v. temperature with four parameter relationship of equation 4.1.

was required. Between ambient temperature and the point at which they begin to decompose, many thermosetting resins go through a single large transition, the glass transition. The following empirical fitting function has been proposed [3, 10, 27, 45, 46, 47] based on the shape of the hyperbolic tan function

$$P(T) = P_U - \left(\frac{P_U - P_R}{2}\right) 1 + tanh[k(T - T_g')] \tag{4.1}$$

where $P_U$ and $P_R$ are the unrelaxed and relaxed property values respectively, $k$ is a constant describing the breath of relaxation, $T$ is the absolute temperature and $T_g$ is the absolute temperature of the mechanical glass transition. This relationship is shown schematically in figure 4.2

### 4.4.1 Tensile strength

Dog bone shape samples were used for tensile testing of pultruded material specimens, several tests being carried out over a temperature range from 25 ℃ up to 400 ℃. Instead of performing the tensile measurements in an oven, a small jig was designed (figure 4.3), comprising an aluminium jacket containing a cartridge heater. This was used to maintain a uniform temperature along the gauge length during the test, an

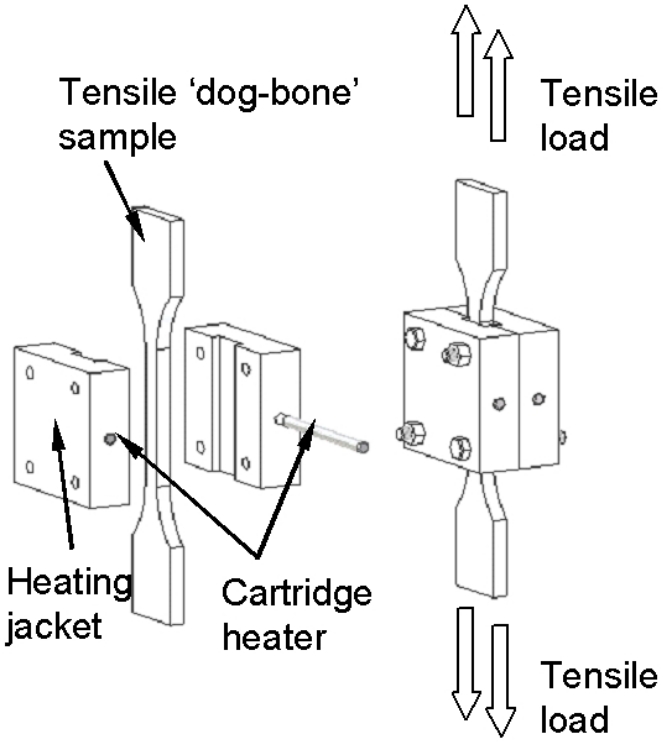


Figure 4.3: Temperature controlled heating jig for measurement of tensile strength at high temperature: only gauge length region of sample is heated, to avoid grip failures.

arrangement that enabled the specimen ends to be kept cold, thus preventing the material from slipping in the grips. Longitudinal tests were carried out on both the full three layer section of the pultrusion and on the unidirectional core material, with the skins removed, the results being shown in figure 4.4. The room temperature tensile strength of unidirectional composites is often modelled using the well known *law of mixtures* relationship

$$\sigma_{UL} = \sigma_{f,UL} V_f + \sigma'_m (1 - V_f) \tag{4.2}$$

where $\sigma_{UL}$ is the failure strength of the composite, $\sigma_{f,UL}$ is the failure strength of the fibres, $\sigma'_m$ is the stress in the matrix at the failure strain of the fibres and $V_f$ is the fibre volume fraction.

It can be seen from figure 4.4 that the fall in the strength of the unidirectional composite due to the resin glass transition is significantly greater than that predicted

by putting $\sigma' = 0$ in equation 4.2. This effect was not found to be due to any spurious experimental effects, such as grip slippage. It therefore required some special consideration. The most probable explanation is the loss of the composite effect.

Below the resin $T_g$, the *uniform strain* assumption applies, so all the reinforcement is subjected to the same strain level, by virtue of being encapsulated in the resin. The result of this will be that most of the fibres will fail at the average failure strain of the fibres. However, nominally unidirectional reinforcement will, in reality, be imperfectly aligned due to variations in the way the fibre tows are packed into the die during manufacture. There may also be path differences between the lengths of fibre incorporated into a particular product sample.

Once the resin modulus has fallen to a low value, their effects will become prominent in increasing the range of composite strains over which the fibres will fail, the overall result being a fall in the failure stress of the composite to a value lower than that of the $\sigma_{UL}V_f$ term in equation 4.2.

This effect, which has not been widely discussed in literature, warrants further investigation and modelling. At high temperature, both the polyester and the phenolic pultrusions maintained a high value of tensile strength [47], although at lower level than that predicted by equation 4.2. This is largely determined by the fibre strength. The strength of the polyester samples was found to fall off more rapidly, and to a lower level than that of the phenolic ones. The transition region for the phenolic appears much broader than that for the polyester.

### 4.4.2 Compressive strength

A compression testing jig was designed to provide both temperature control and buckling suppression. This is shown in figure 4.5. The samples were heated in the jig to the desired temperature, then loaded up to compressive failure. Tests were again performed at temperatures from 20 ℃ up to 400 ℃. The compressive stress-strain curves were all found to follow the familiar saw tooth profile associated with

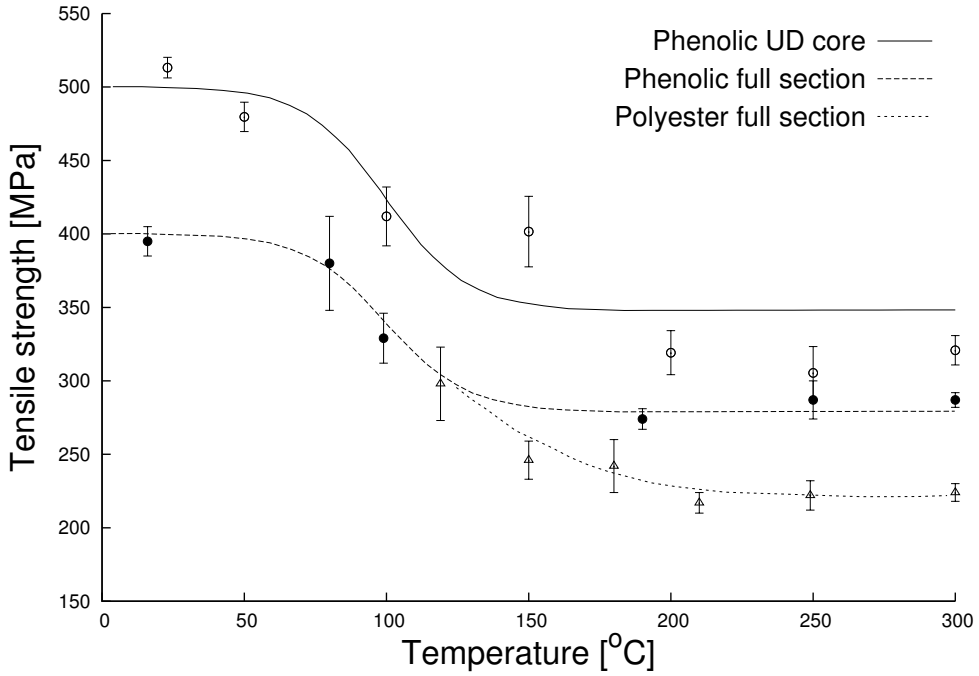


Figure 4.4: Tensile strength of pultruded phenolic and polyester sections as a function of temperature.

compression tests on composites.

The failure mechanism in compression is different from that in tension and involves the formation of a localised band of kinked material [50, 51], probably triggered by the shear deformation of any slightly misaligned material. Figure 4.6 shows the compressive strength of the phenolic and polyester pultrusions against temperature. The curves show a steep drop for temperatures above the transition region, there being little benefit in this case from the high temperature strength of the glass. Once again, the transition region for the phenolic appears to be broader than that for the polyester.

### 4.4.3 Longitudinal and transverse stiffness

Flexural modulus measurements were carried out using three point bend creep tests with rectangular specimens having a length/depth ratio of at least 16. The bending rig was placed inside a temperature controlled oven, as shown in figure 4.7. Once a stable value of the required temperature had been reached, the load was applied

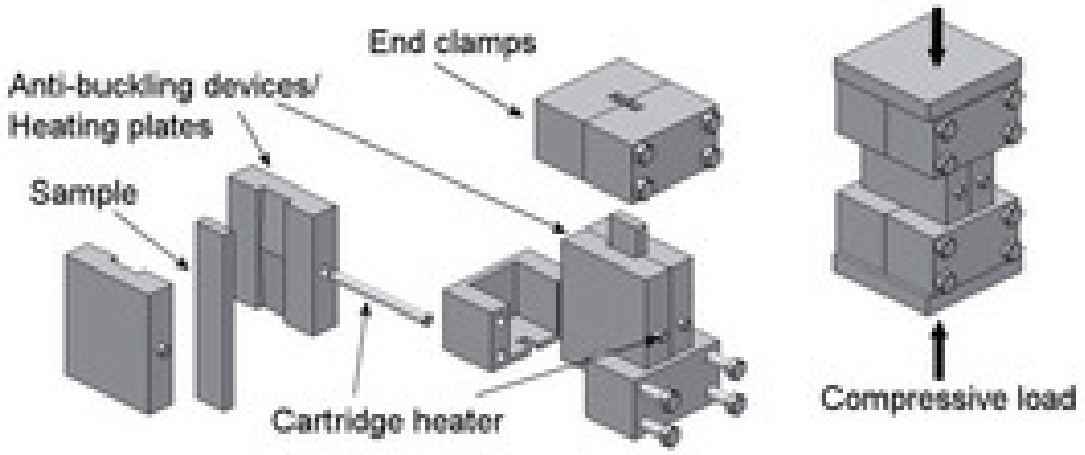


Figure 4.5: Jig for measurement of compressive strength at high temperature, showing combined temperature controlled heating block and antibuckling guide.

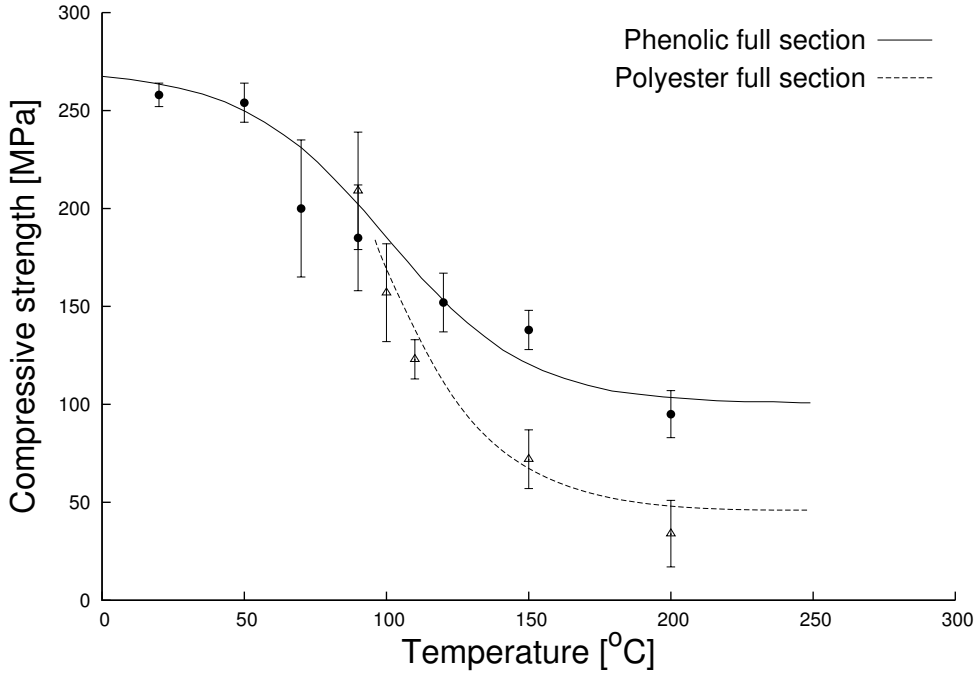


Figure 4.6: Compressive strength of pultruded phenolic and polyester sections as a function of temperature

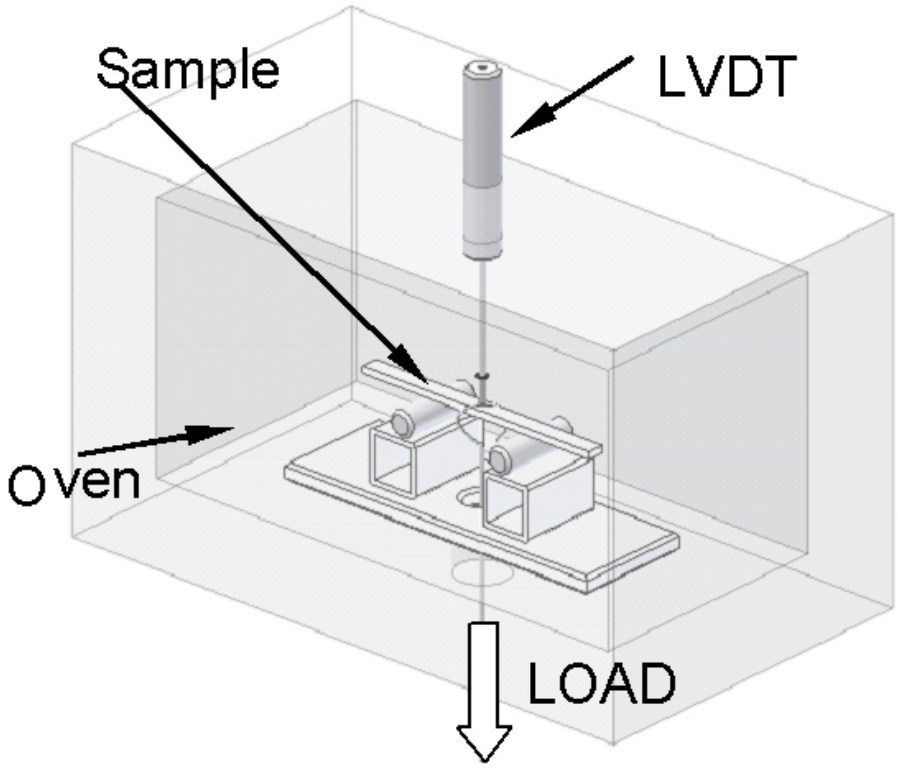


Figure 4.7: Temperature controlled rig for measurement of flexural modulus

in a form of a dead weight. The deflection was measured with an LVDT transducer and recorded after 100 $s$ loading time, enabling the 100 $s$ Young modulus to be determined. Figure 4.8 shows the longitudinal and transverse moduli $E_1$ and $E_2$ respectively as a function of temperature for the polyester and phenolic pultrusions.

Measurements were performed for both the full section material and the core. In the case of the polyester pultrusion, the data show the familiar drop in magnitude as it passes through the transition region. The modulus drop for the polyester, like the fall in tensile strength, is larger than would be predicted by the law of mixtures of moduli, again implying effects due to fibre misalignment. The phenolic material shows a much smaller fall in stiffness, even in the resin sensitive transverse direction and again, the transition region can be seen to be very broad. The parameters used to describe all the composite mechanical properties as a function of temperature, using equation 4.1, are given in table 4.1.

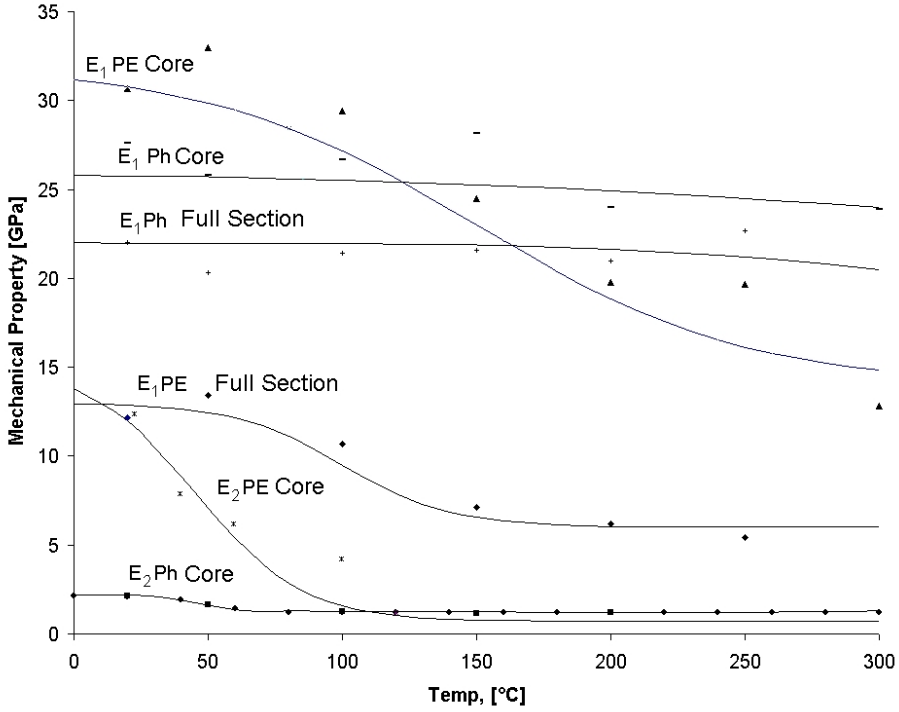


Figure 4.8: Flexural moduli (100 s) of pultruded phenolic and polyester sections as a function of temperature

| Polyester pultrusions | | | | |
|---|---|---|---|---|
| Parameter | PU, $[MPa]$ | PR, $[GPa]$ | Tg, [°C] | k, [-] |
| $\sigma_{T1}$ Core | 354.0 | 242.0 | 150 | 0.03 |
| $\sigma_{T1}$ Full material | 230.0 | 220.0 | 150 | 0.03 |
| $\sigma_{C1}$ Full material | 320.0 | 60.0 | 95 | 0.045 |
| $E_1$ Core | 32.0 | 14.0 | 150 | 0.01 |
| $E_1$ Full material | 13.0 | 6.0 | 100 | 0.025 |
| $E_2$ Core | 15.2 | 0.7 | 45 | 0.025 |

Table 4.2: Parameters used to describe mechanical properties of polyester pultrusions as a function of temperature: PU and PR are expressed in MPa for strengths and GPa for stiffness values.

| Phenolic pultrusions | | | | |
|---|---|---|---|---|
| Parameter | PU, $[MPa]$ | PR, $[GPa]$ | Tg, [°C] | k, [-] |
| $\sigma_{T1}$ Core | 500 | 347 | 100 | 0.035 |
| $\sigma_{T1}$ Full material | 400 | 278 | 100 | 0.035 |
| $\sigma_{C1}$ Full material | 270 | 100 | 100 | 0.02 |
| $E_1$ Core | 26 | 22 | 300 | 0.005 |
| $E_1$ Full material | 22 | 19 | 300 | 0.05 |
| $E_2$ Core | 2.12 | 1.2 | 50 | 0.06 |

Table 4.3: Parameters used to describe mechanical properties of phenolic pultrusions as a function of temperature: PU and PR are expressed in MPa for strengths and GPa for stiffness values.

## 4.5 Fire testing under load

Rectangular tensile specimens for fire testing under load were machined, 500 $mm$ long and 75 $mm$ wide. The test configuration is shown in figure 4.9. The samples were subjected to a constant tensile load and simultaneous constant heat flux from the propane burner, which was calibrated *in situ*, as 50 $kW/m^2$ based on hot face temperature and distance from the front of the burner to the front of the sample. The heat flux was kept constant throughout the test by monitoring a hot face thermocouple. The rear face of the sample was insulated with kaowool to prevent heat loss and to achieve the most reproducible thermal boundary condition. The time taken for the sample to fail, from the moment the burner was turned on, was recorded as time to failure for several loads. Ultimate tensile strength was also determined, and denoted with a failure time of 1 $s$.

The fire testing arrangement under compressive load is shown in figure 4.10. Samples, 120 $mm$ long and 100 $mm$ wide, were cut from the 10 mm thick pultruded laminate and were held in a constrained compression jig, similar in principle, to the Boeing compression after impact test jig [52]. The purpose of this was to suppress global buckling of the samples during testing while at the same time allowing samples with a large surface area to be exposed to heat flux.

Once in place, the samples were loaded with a constant compressive load, exposed to a propane burner flame and calibrated by means of a slug type heat flux meter to produce a heat flux of 50 $kW/m^2$ at the specimen surface. The time to compressive failure of the sample was recorded for several different applied loads.

### 4.5.1 Results and discussion

Time to failure measurements were performed for both phenolic and polyester pultrusions under one sided heat flux. Both tensile and compressive failure events were observed to occur with little warning. The tensile stress rupture curves (figure 4.11),

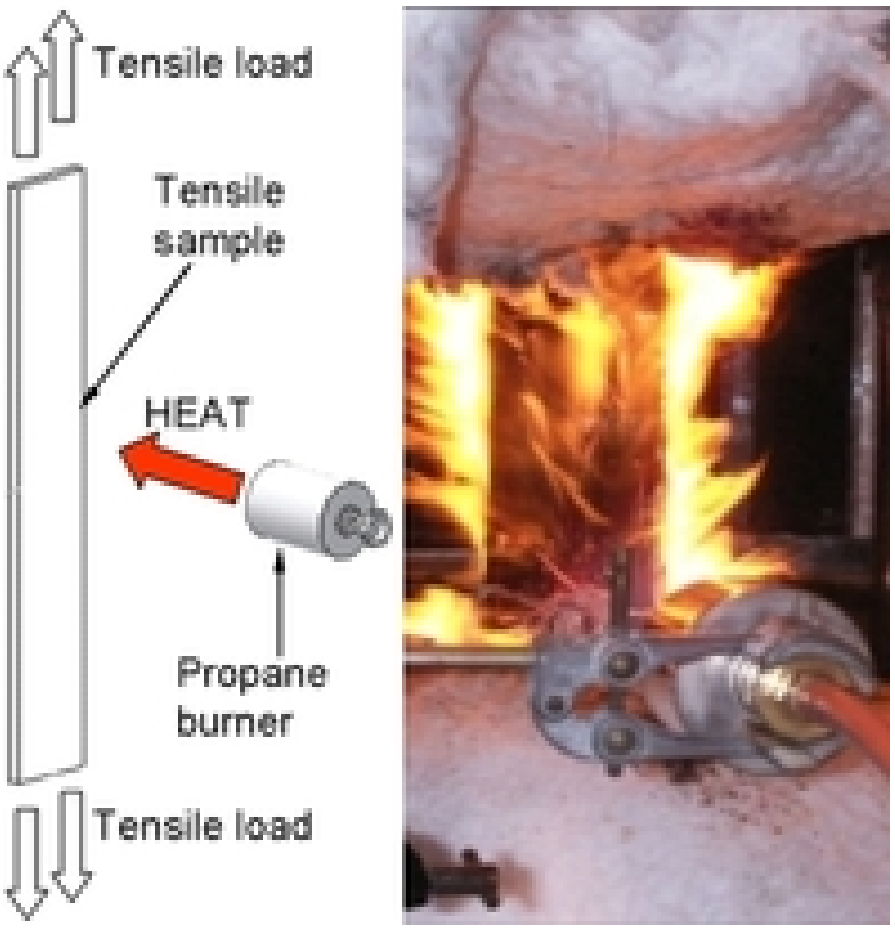


Figure 4.9: Test sample under tensile load subject to one sided heat flux using propane burner: rear face insulation of sample is not shown here

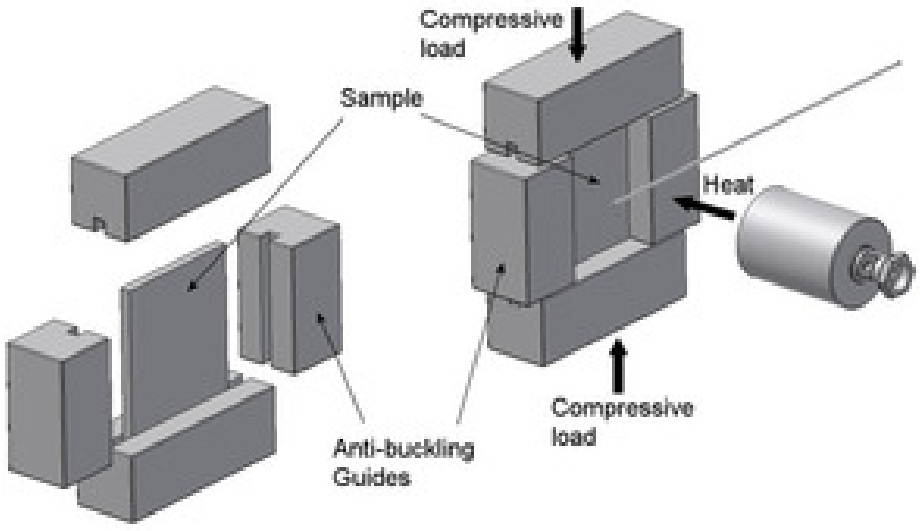


Figure 4.10: Fire test in compression, using propane burner as one sided heating source: note use of antibuckling guides; rear face of sample was thermally insulated

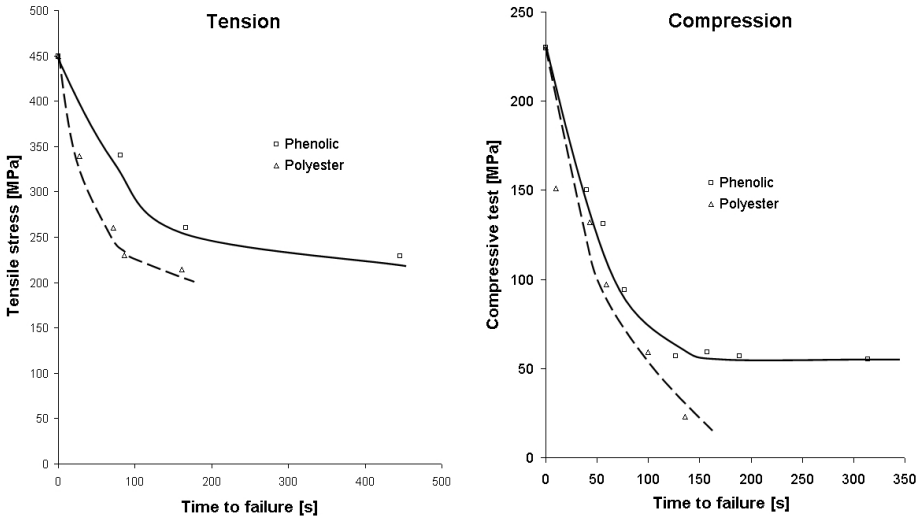


Figure 4.11: Measured and modelled fire test results for phenolic and polyester sections under tensile and compressive load at heat flux of 50 $kW/m^2$

for both types of material, exhibit a fairly high level of residual strength, due to glass retaining a proportion of its strength at high temperatures. By contrast, the compressive stress rupture firecurves show a more rapid decline in strength, to a lower final value. This limited residual strength in compression has been observed with other composites systems in [45, 53, 47] and is mainly attributable to the bulk of the matrix material reaching its glass transition temperature.

## 4.6 Modelling

### 4.6.1 Thermal model

The thermal model COM_FIRE, based on the Henderson equation [6], has been developed to predict the temperature distribution in a composite exposed to heat flux. The version of the model described here is, in essence, a one-dimensional heat transfer relationship, which takes account of conduction, resin pyrolysis and the effect of the decomposition products passing through the laminate. The one-dimensional governing equation was described earlier in section (2.2).

The composite transport properties in equation 2.2 evolve as a function of temper-

| | |
|---|---|
| $A$(polyester), $[s^{-1}]$ | $1.29 \times 10^{13}$ |
| $E$(polyester), $[J/(mol\ K)]$ | $2 \times 10^5$ |

Table 4.4: Kinetic parameters for decomposition of polyester resin.

| | |
|---|---|
| $A$(phase I), $[s^{-1}]$ | 5 |
| $E$(phase I), $[J/(mol\ K)]$ | $27.2 \times 10^3$ |
| $A$(phase II), $[s^{-1}]$ | 68 |
| $E$(phase II), $[J/(mol\ K)]$ | $65.2 \times 10^3$ |
| Mass remaining after phase I, [%] | 87 |

Table 4.5: Kinetic parameters for decomposition of phenolic resin.

ature and resin decomposition. The second term takes account of the cooling effect of decomposition reaction gases diffusing through the laminate thickness.

The heat consumed by the decomposition of the resin is modelled by the third term on the right hand side of equation 2.2. Thermogravimetric analysis (TGA) was used to determine the mass loss rate under controlled heating conditions, and the relevant material parameters may be evaluated using the Arrhenius rate equation, 2.3.

### 4.6.2 TGA analysis

As mentioned above, TGA provides the main input parameters for the thermal model: A, n and E. The analysis also provides a measure of the amount of the char left when the resin is spent. The polyester resin TGA parameters are shown in table 4.4.

The decomposition process of the phenolic resin takes place in two stages. The process can be modelled using two sets of kinetic parameters and two Arrhenius equations. The rate parameters are shown in table 4.5. A carbonaceous residue of $\sim$55% is left when the decomposition is complete. This char formation is a useful attribute of phenolic resin, as it is capable of bearing some load. Also, of course, material remaining as char does not contribute to heat release. By contrast, the polyester resin decomposes in one stage and its residual resin content is $\sim$6%, so any resin is left to carry any load. The TGA curves for the phenolic and polyester resins are compared in figure 4.12.

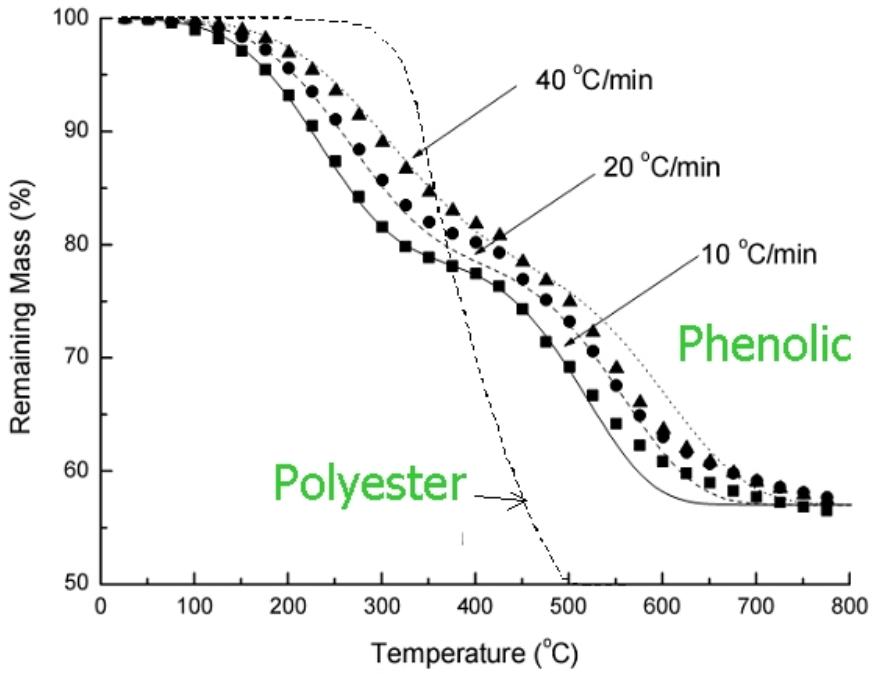


Figure 4.12: Thermogravimetric analysis curves, showing comparison between decomposition of phenolic and polyester resin

## 4.7 Thermal and residual resin profiles

Figures 4.13 and 4.14 show the modelled profiles of temperature and residual resin content through the polyester and phenolic laminates as a function of time. The temperature profiles show an initial plateau, which corresponds to the absorption of heat by the resin decomposition process. In the phenolic case, the residual resin profiles show some evidence initially of the two stage decomposition process. The char formation in the phenolic case ensures that the resin content falls only to ∼55%, whereas in the polyester case, the residual content is almost 0.

## 4.8 Modelling behaviour under load

The laminate analysis failure model requires input from the thermal model described in the previous section, namely, temperature evolution and residual resin content through the thickness of the material. It also requires mechanical properties as a

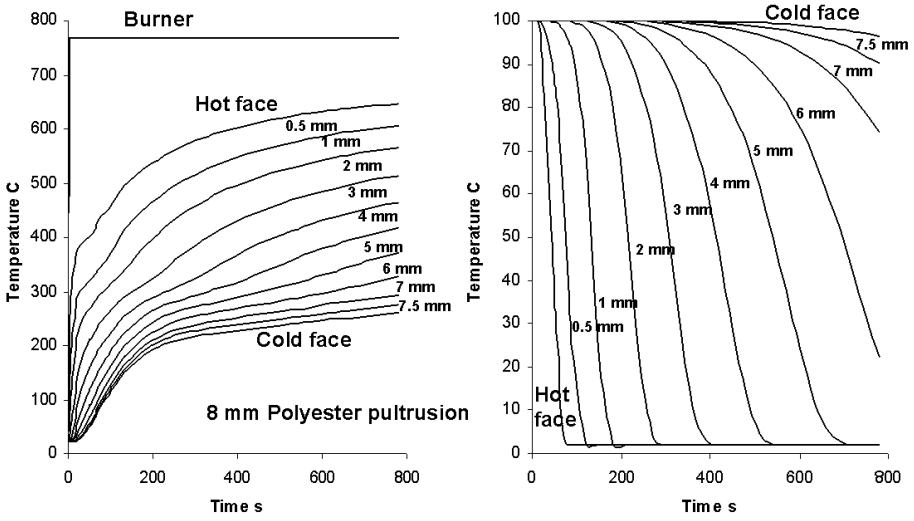


Figure 4.13: Modelled thermal profiles (left) and residual resin profiles (right) at various depths for 8 mm thick three layer pultruded polyester glass laminate, subject to one sided heat flux of 50 $kW/m^2$.

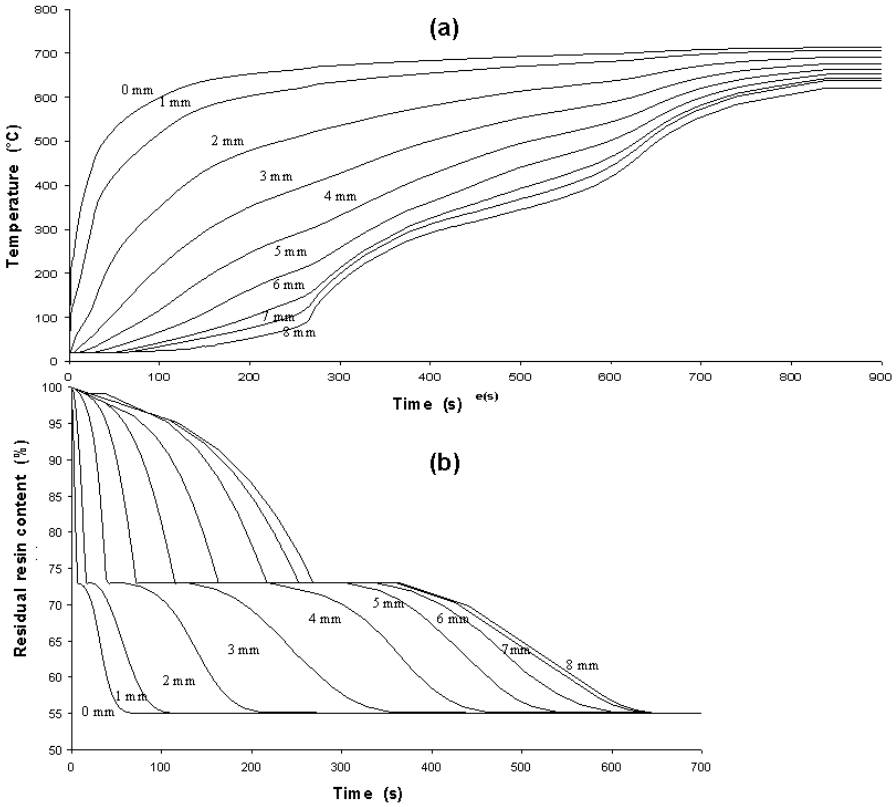


Figure 4.14: a) modelled thermal profiles and b) residual resin profiles at various depths for 8 mm thick three layer pultruded phenolic glass laminate, subject to one sided heat flux of 50 $kW/m^2$.

function of temperature, detailed above. The calculation steps involved in the model are shown in figure 4.15.

The transformed stiffness matrix $\bar{Q}$ of each layer of the composite is calculated as a function of temperature. The $\bar{Q}$ matrix is used to calculate the $A$, $B$ and $D$ matrices as a function of temperature:

$$A = \sum_{k=1}^{n} \int_{h_{k-1}}^{h_k} \bar{Q} dx \; ; \; B = \sum_{k=1}^{n} \int_{h_{k-1}}^{h_k} \bar{Q} x dx \; ; \; D = \sum_{k=1}^{n} \int_{h_{k-1}}^{h_k} \bar{Q} x^2 dx \tag{4.3}$$

In this case, account needs to be taken of the variation of properties through each ply, due to the changes in temperature and residual resin content. This requires a numerical integration in addition to the conventional ply by ply summation. The applied loads (in plane forces and bending moments) are related to the resulting deformations (mid plane strains and curvatures) through the familiar $ABD$ matrix relationship :

$$\begin{bmatrix} N \\ M \end{bmatrix} = \begin{bmatrix} A & B \\ B & D \end{bmatrix} \begin{bmatrix} \epsilon_0 \\ k \end{bmatrix} \tag{4.4}$$

where $N$ and $M$ are the matrices of normal loads and bending moments, and $\epsilon_0$ and $k$ are the mid plane strains and curvatures. When the input parameters are loads, it is often preferable to employ the fully inverted version

$$\begin{bmatrix} \epsilon_0 \\ k \end{bmatrix} = \begin{bmatrix} A' & B' \\ B' & D' \end{bmatrix} \begin{bmatrix} N \\ M \end{bmatrix} \tag{4.5}$$

In order to use laminate theory, the material has been considered to be composed of three layers, with the properties of each layer varying with temperature and resin content. The data for the core were determined experimentally, but it was not possible for the continuous strand mat (CSM) outer layers because they were calculated using a combination of sandwich beam theory and data from literature. The data describing compressive strength as a function of temperature were determined entirely experimentally, as described above. In this case, splitting the material into its three

layers was deemed unnecessary. This was due to the almost negligible effect the CSM needle weave layers would have on the materials compressive strength. The sandwich beam method considers the material as a typical sandwich beam and utilises the expression

$$E_{Full} = E_{UD}\frac{t_1^3}{t_2^3} + E_{CSM}\left(\frac{t_2^3}{t_2^3} - \frac{t_1^3}{t_2^3}\right) \tag{4.6}$$

where $E_{Full}$ is the flexural modulus of the full section of material, $E_{UD}$ is the flexural modulus of the core material and $E_{CSM}$ is the flexural modulus of the skin material. The thickness of the full section is $t_2$ and the thickness of the core material is $t_1$. This calculates the flexural modulus for the CSM skins from the flexural modulus of both the core material $E_{UD}$ and the full section $E_{Full}$ (both obtained experimentally). The resulting flexural modulus $E_{CSM}$ is the same in both perpendicular and longitudinal directions. It was found that all the mechanical properties of the core and skin material could be described with equation 4.1. As mentioned above, the fitting parameters are shown in table 4.2 and 4.3.

## 4.9 *ABD* matrix evolution

Figure 4.16 shows the evolution of the $ABD$ matrix components for an 8 $mm$ polyester pultrusion using the laminate failure model and the corresponding predictions for the 8 $mm$ phenolic pultrusion.

The $A$ matrix components, which relate in plane loads and deformations, decline over time reflecting the decline in overall mechanical properties. This decline is much more marked in the polyester material when compared to the phenolic, due to phenolic composites retaining elastic properties up to higher temperatures.

The $B$ matrix components describe the interaction between the in plane loads and out of plane bending and twisting. This value is initially zero due to the symmetry of the material in the through thickness direction. The $B$ terms rise to a peak as the CSM skin is burnt away causing a symmetrical imbalance. A second, larger peak is

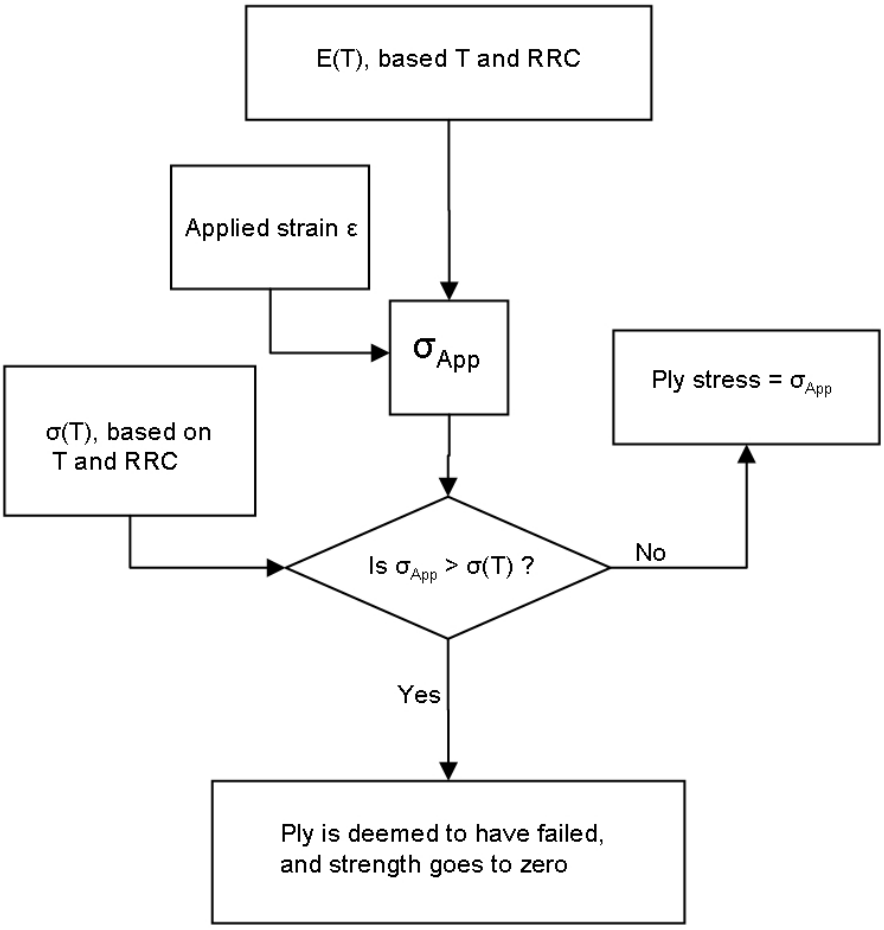


Figure 4.15: Flow chart of model for fire behaviour under load.

caused by further asymmetry as the UD core material is degraded. Finally, in the case of the polyester pultrusions, the $B$ matrix terms decay as the full section of the product passes its glass transition and begins to decompose. This double peak in the case of $B_{11}$ is not observed in laminates having a uniform structure throughout. Monolithic glass/polyester and glass/vinyl ester laminates showed only one single large peak [1, 27, 44]. The phenolic pultrusions also show a double peak, but the contribution of the CSM skins is less strong, and the final decay has only just begun to set in by the end of the simulation period, indicating significantly better stiffness retention.

The $D$ matrix components, governing bending resistance, decline with time for both resin systems, but again, the phenolic system shows a much slower rate of decline than the polyester. The influence of the progressive asymmetry can be seen with the small shoulders that can be observed on the curves. These coincide with the peaks in the $B$ matrix curves.

The bending stiffness of laminates is related primarily to the term $1/D'_{11}$ in the inverted $ABD$ matrix (equation 4.5). Figure 4.17 shows the evolution of $1/D'_{11}$ for the polyester and phenolic pultrusions. This is equivalent to the flexural stiffness parameter $EI$. Once again this declines over time reflecting the decline in overall mechanical properties. As with the $D$ matrix components, a shoulder is visible on the curves, again reflecting the progressive asymmetry. As with the $A$ matrix parameters, this decline is far more significant in the polyester material, due to the phenolic material maintaining its mechanical properties at higher temperatures.

Finally, figure 4.18 shows a comparison of the property retention of the two types of laminate, normalised to percentage values. The pultruded laminates tested in this project are, under normal circumstances, part of much larger pultruded sections. It has been assumed in preparing the data for figure 4.18 that the key strength parameter is the compressive strength, since most structural pultrusions will be loaded either in compression or flexure, which involves compression of some surfaces. This is the

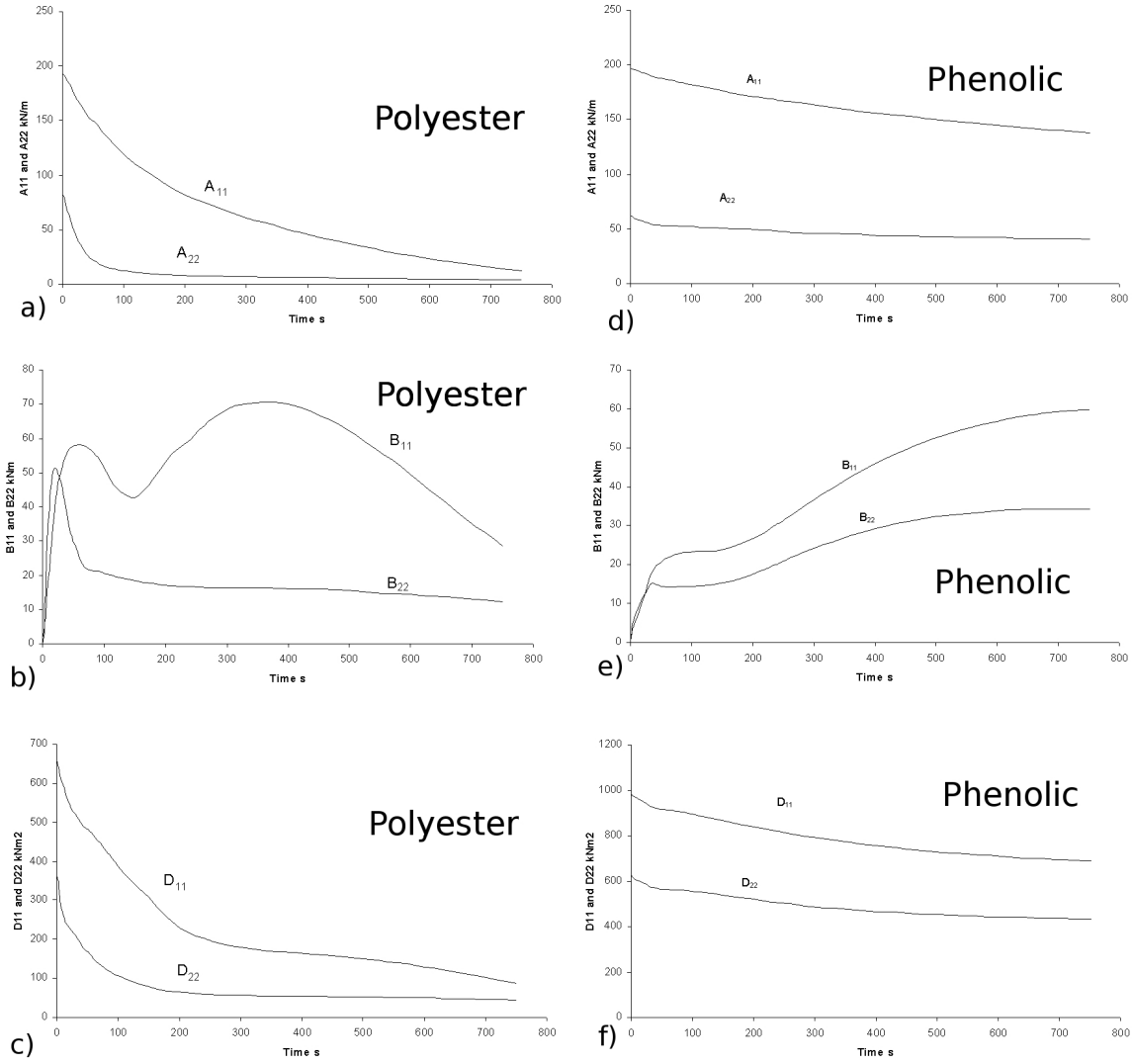


Figure 4.16: Modelled evolution of ABD matrix components with time for 8 $mm$ thick polyester pultrusion exposed to one sided heat flux of 50 $kW/m^2$: a) $A_{11}$ (upper curve) and $A_{22}$ (lower curve); b) $B_{11}$(upper curve) and $B_{22}$ (lower curve); c) $D_{11}$ (upper curve) and $D_{22}$ (lower curve). Modelled evolution of ABD matrix components with time for 8 $mm$ thick phenolic pultrusion exposed to one sided heat flux of 50 $kW/m^2$: d) $A_{11}$ (upper curve) and $A_{22}$ (lower curve); e) $B_{11}$(upper curve) and $B_{22}$ (lower curve); f) $D_{11}$ (upper curve) and $D_{22}$ (lower curve).

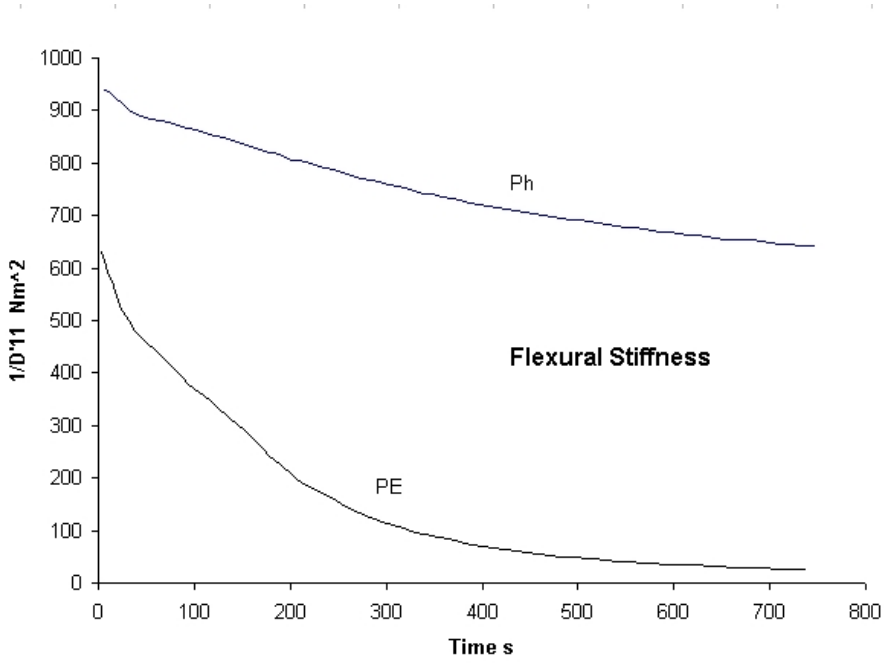


Figure 4.17: Modelled evolution of flexural stiffness $1/D'_{11}$ for 8 mm thick phenolic and polyester pultrusions, exposed to one sided heat flux of 50 $kW/m^2$.

parameter that has been normalised to produce the strength curves.

The key stiffness parameter was considered to be the $A$ matrix leading term, so this too was normalised. Figure 4.18 underlines some interesting conclusions. The first is that strength falls away much more steeply than stiffness in fire. The second is that the phenolic system does show significantly improved behaviour, compared to polyester. In the polyester case, both stiffness and strength decay within 800 s to very low values. By contrast, 72% of the phenolic stiffness and 22% of the strength are retained at that time. It appears therefore that, in a structural application, phenolic pultrusions can retain useful properties in fire, especially if the main requirement is stiffness. The strength would be acceptable after 800 $s$ if a sufficiently large safety factor [27, 47] were used. Significant safety factors are not uncommon in some composite structures.

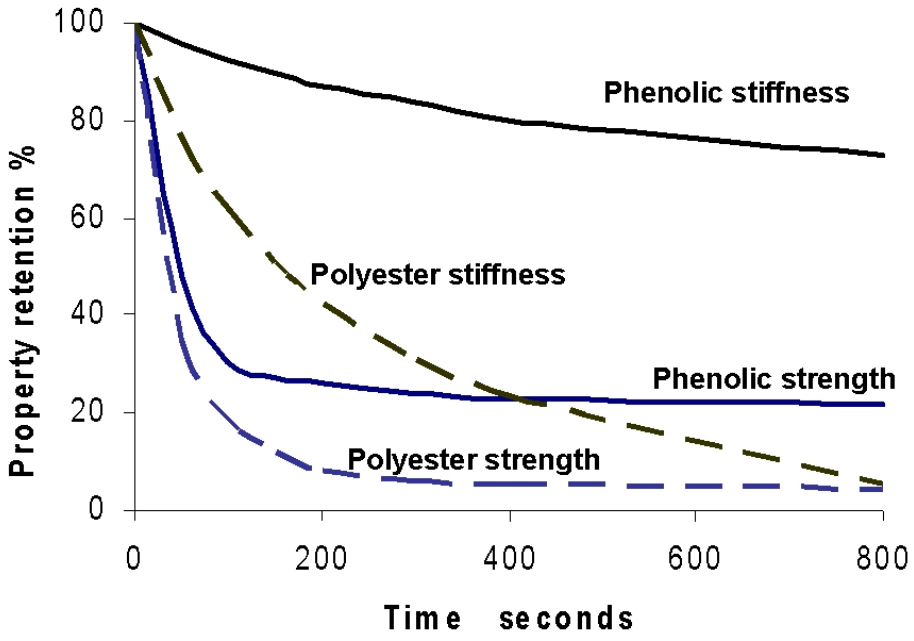


Figure 4.18: Normalised comparison of property retention for 8 $mm$ thick phenolic and polyester pultrusions, exposed to one sided heat flux of 50 $kW/m^2$; phenolic: continuous curves; polyester: broken curves.

# Chapter 5

# Apparent thermal diffusivity model (ATD)

## 5.1 Introduction

In this study, a novel fire model for composite materials was developed: the *apparent thermal diffusivity model (ATD)*. In the ATD, the phenomena occurring to a composite material exposed to fire are characterized using a single temperature dependent thermal diffusivity function, $\alpha(T)$. The apparent thermal diffusivity function of different composite systems was determined experimentally and theoretically. The possibility of outlining common features in the $\alpha(T)$ function for different materials was explored. The relationship between the effects of fire on composites and the shape of the apparent $\alpha(T)$ were studied.

This study develops a methodology for the measurement of the apparent thermal diffusivity of various composite systems over the thermal range needed for fire modelling, from ambient to ∼600 ℃. The function $\alpha(T)$ was used to predict the temperature profiles of composite components under conditions ranging from one to three-dimensional heat transfer cases.

The model was firstly implemented into a FORTRAN finite difference code to verify


Figure 5.1: Specimen for the step change test. Insulation material prevents heat transfer through the edges to to ensure one-dimensional heat flow.

its accuracy in analysing simple one-dimensional cases. The results were compared with the results obtained from COM_FIRE, an Henderson-based fire model developed at Newcastle University [16]. It was then implemented in a commercial finite element package to perform full three-dimensional analyses. In both cases the analyses were verified against experimental results.

The Henderson equation-based models are very effective when implemented in one-dimensional finite difference formulation. This approach allows the control of every single parameter and offers low computational burden. However, implementing multi-dimensional finite difference calculation is lengthy. Depending on the geometry of the model it can become a very difficult task. Furthermore small changes in the model geometry require a totally new implementation. These issues do not allow the use of these models within the modern parametric feature based design tools.

The Henderson-based models make use of the Arrhenius equation (equation 2.3). It often presents stability issues that can be solved narrowing the time steps used for

the calculation. As a result, the computational burden of the model increases.

The aim of the ATD model is that of overcoming the main issues identified in the previous models. It is easily extendible to two-dimensional and three-dimensional cases and its formulation does not include the use of the Arrhenius equation (2.3). These features make it a versatile, robust and efficient tool for the design of composite structures and the study of their fire behaviour.

## 5.2 Measurement of the ATD

To obtain the temperature dependence of the ATD, several characterization experiments are required for each composite (TGA, density, thermal conductivity etc). A novel experimental method is presented here for the direct measurement of the temperature dependent ATD, $\alpha(T)$.

### 5.2.1 Low temperature measurements

Simple but accurate thermal diffusivity measurements can be achieved by carrying out thermal step-change experiments in which a slab of material, initially at uniform temperature, is subjected to a sudden change in surface temperature. Slab samples, shown in figure 5.1, were placed in a temperature-controlled furnace at 80 ℃, allowing them to achieve a uniform temperature in air, over a period of about one hour. Following this, the sample were rapidly removed and placed in a bath of agitated water at 20 ℃, while the centreline temperature was recorded using a thermocouple and computer data capture. Water was chosen because it is a very effective heat transfer medium which does not damage the samples.

Because the step-change experiment required one-dimensional through-thickness heat flow it was necessary to ensure that this applied in the region of the measuring thermocouple. The sample geometries shown in Figure 5.1 were necessary to achieve this. Foam insulation was bonded around each rectangular sample to minimise heat

flow through the edge surfaces.

The measuring thermocouple was placed at the centre of the sample, in some cases using a hole drilled directly in one of the exposed surfaces. In other cases a centreline hole was drilled from the edge of the sample. In all cases the thermocouple was bonded in place with epoxy adhesive to prevent water entering the hole and affecting the temperature measurements.

The results of the step-change experiments were expressed in terms of the variation of the dimensionless centreline temperature, given by

$$\theta = \frac{T - T_0}{T_1 - T_0} \tag{5.1}$$

where $T$ is the centreline temperature, $T_0$ is the initial uniform temperature in the slab of material, and $T_1$ is the temperature suddenly imposed at the slab surface.

Theta, $\theta$, varies from zero at the start of the test, to 1 at long times, regardless of whether the slab is heated or cooled. The principal factor determining the variation of temperature with time is the Fourier number, equation 3.9. In this case $b$ is half the slab thickness (the distance from the surface to the centreline), $t$ is time and $\alpha$ is the thermal diffusivity in the through-thickness direction.

To extract reliable values of thermal diffusivity from these results it is necessary to use modelling. In the case of a material of constant thermal diffusivity, with perfect heat transfer at the surface there is a well-known analytic expression [34], from which the thermal diffusivity can be found directly. Unfortunately these two conditions are not adequately fulfilled in the case of FRP specimens using water as the heat transfer medium, so corrections are necessary.

The effectiveness of surface heat transfer is described by the Biot number

$$Bi = \frac{hb}{k} \tag{5.2}$$

where $h$ is the heat transfer coefficient at the surface, $b$ is the half-thickness of the

slab and $k$ is the thermal conductivity of the material.

For $Bi$ values in excess of about 100, the resistance to surface heat transfer can be neglected, so perfect thermal step-change conditions can be considered to apply at the specimen surface. This simple method works extremely well for materials, such as polymers, where the thermal conductivity is low enough to fulfil the condition. With FRP in water, however, $Bi$ is in the range 20-100, so a correction needs to be made for the effect of the surface resistance to heat transfer. The surface heat transfer coefficient in the present experiments was determined, from measurements on a block of high conductivity material, aluminium, to be $\sim$500 $W/(m^2\ ^\circ\mathrm{C})$. This value is also recommended for calculations involving water in these conditions [35]. A numerical finite difference model, assuming this value, was therefore implemented when extracting thermal diffusivity values from the results of the measurements.

The other important factor is the variation of the thermal properties of FRP with temperature. Even in the relatively narrow range of 20-80°Cthe thermal diffusivity cannot be considered constant. It was therefore necessary to assume in the processing of the results that thermal diffusivity varies linearly with temperature over this range.

A one-dimensional unsteady-state finite difference model was therefore written in FORTRAN to describe the variation of the centreline temperature in a flat slab, subjected to a sudden surface temperature change, with the following assumptions:

- The surface heat transfer condition with water is described by a heat transfer coefficient of $\sim$500 $W/(m^2\ ^\circ\mathrm{C})$.
- The through thickness direction thermal diffusivity of the laminate varies linearly with temperature.

The finite difference procedure was used to produce a least squares fit of $\theta$ against time for the step-change response of each sample tested. This required an iterative procedure, with trial values of the two thermal diffusivities, $\alpha_{20}$ and $\alpha_{80}$, at the extremes of the temperature range in the test.

### 5.2.2 High temperature measurements

The measurement technique developed here involves the evaluation of the thermal lag between the surface and core of a flat composite slab subjected to a changing temperature on its outer surfaces. It allows to measure the apparent thermal diffusivity of a composite up to 600 ℃.

#### Theoretical background

The experimental technique presented here lies on the Laplace's heat equation for a material with temperature-dependent thermal diffusivity:

$$\frac{\partial T}{\partial t} = \alpha(T)\frac{\partial^2 T}{\partial x^2} \tag{5.3}$$

Considering a flat slab of material, thickness $2x$, subject to a surface temperature that changes linearly with time. If the heating rate is $c$ , then:

$$c = \alpha(T)\frac{d^2 T}{dx^2} \tag{5.4}$$

Integrating with respect to $x$ gives:

$$cx + k_1 = \alpha(T)\frac{dT}{dx} \tag{5.5}$$

When $x = 0$ then $dT/dx = 0$. Therefore $k_1 = 0$, so:

$$cx = \alpha(T)\frac{dT}{dx} \tag{5.6}$$

Integrating again:

$$c\frac{x^2}{2} = \alpha(T)T + k_2 \tag{5.7}$$

When $x = 0$, $T = T_0$. Therefore $k_2 = \alpha T_0$. so:

$$c\frac{x^2}{2} = \alpha(T)(T - T_0) \tag{5.8}$$

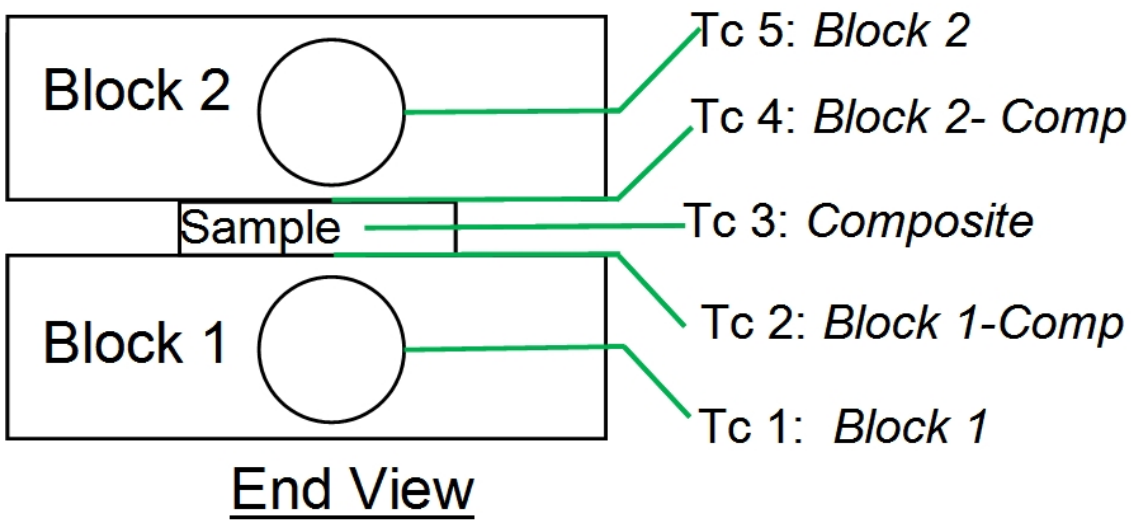


Figure 5.2: Schematic section of the testing rig for the measurement of the apparent thermal diffusivity. The thermocouple configuration is shown

This can be re-arranged to give:

$$\alpha(T) = \frac{cx^2}{2(T - T_0)} \tag{5.9}$$

In other words, the ATD, equation 5.9, can be measured directly as a function of temperature, using a slab with heated surfaces and measuring the temperature difference between the surface and the mid plane.

#### High temperature ATD experimental setup

To apply equation 5.9 approximately one-dimensional heat flow conditions need to be established through the thickness of the sample and a linear temperature profile needs to be applied to the faces. For this purpose a testing rig was designed as shown in figure 5.2.

Temperatures were measured on the faces and middle plane of the composite as it was heated to 600 ℃. The heating elements used were a pair of cartridge heaters, of 1 $kW$ power rating, figure 5.3. Each heater was wired to a variable transformer, or *variac*, capable of supplying an output voltage from 0 to 230 $V$ with analogue

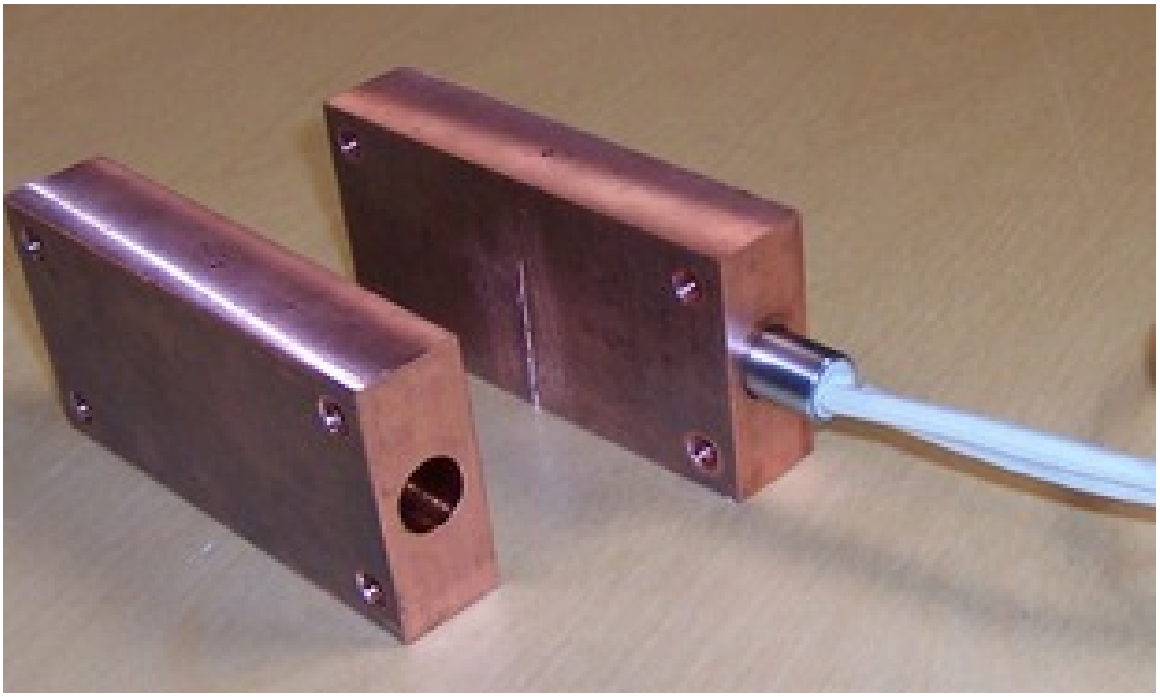

Figure 5.3: Copper blocks and cartridge heater used to impose a linear temperature ramp to the composite sample

adjustment. Keeping the power supply of the two heaters independent was essential to make the heating rates of the surfaces of the composite matching with accuracy. Two copper blocks were machined to transfer heat from the heaters to the sample and to hold the heaters and sample in place, figure 5.3. The measurement assembly, with the test sample between the copper blocks and the thermocouples in place, was wrapped in layers of ceramic fibres insulation to prevent heat losses, as shown in Figure 5.4. An alternative, more expensive, method of controlling the temperature would have been to employ a 3-term temperature controller for each block and to use a ramp generator, to generate a thermal signal to be followed. In the present case this was not found to be necessary. After some experimentation with the variacs it was found possible to achieve a well-matched temperature rise in each of the blocks. Applying a constant voltage to the cartridge heater produced a near-linear rate of change in temperature which was acceptable in the present case. The temperature difference between the surface and the centre of the composite needed to be measurable but

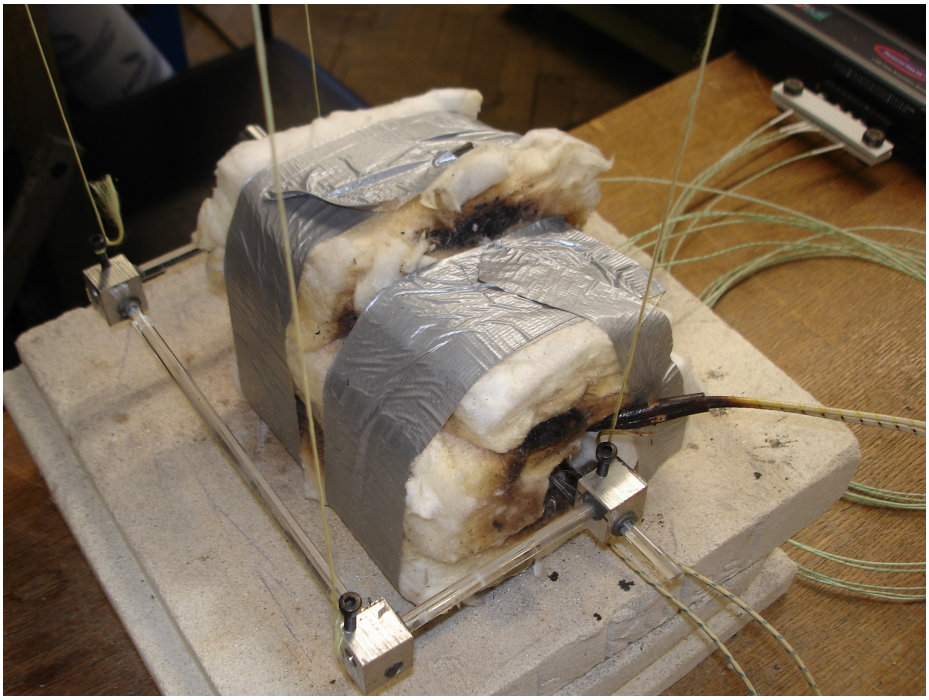

Figure 5.4: Measurement assembly. The test sample and the thermocouples held in place between the copper blocks. Layers of ceramic insulation prevent heat losses.

small enough to assure sufficient accuracy when plotting ATD against temperature. After some experimentation with heating rates and sample thickness this was found to be achievable.

### 5.2.3 Thermal laminate theory

Laminate theory for thermal transport was used to obtain an accurate estimate of the alpha along the $x$, $y$ and $z$ directions of the orthotropic laminates tested. Its formulation is relatively simple compared to that for mechanical properties, since conductivity and diffusivity are $2^{nd}$ rank, rather than $4^{th}$ rank properties. Assuming a uniform distribution of plies through the structure, the laminate conductivities are

given by

$$k_x = k_1 \sum f_i cos^2(\theta_i) + k_2 \sum f_i cos^2(\theta_i) \tag{5.10}$$

$$k_x = k_1 \sum f_i cos^2(\theta_i) + k_2 \sum f_i cos^2(\theta_i) \tag{5.11}$$

$$k_z = k_3 \tag{5.12}$$

where the $x$ and $y$ axes are the laminate in-plane axes, and $z$ is the through-thickness direction. Respectively, $k_1$,$k_2$ and $k_3$ are the ply parallel, transverse and through-thickness conductivities.

Because $\rho C_p$ is a scalar quantity, similar relationships apply for thermal diffusivity:

$$\alpha_x = \alpha_1 \sum f_i cos^2(\theta_i) + \alpha_2 \sum f_i cos^2(\theta_i) \tag{5.13}$$

$$\alpha_x = \alpha_1 \sum f_i cos^2(\theta_i) + \alpha_2 \sum f_i cos^2(\theta_i) \tag{5.14}$$

$$\alpha_z = \alpha_3 \tag{5.15}$$

For the laminates considered here, which contain only 0°, ±45°and 90°plies,this simplifies to;

$$\alpha_x = \alpha_1 \left( f_0 + \frac{1}{2} f_{45} \right) + \alpha_2 \left( \frac{1}{2} f_{45} + f_{90} \right) \tag{5.16}$$

$$\alpha_y = \alpha_1 \left( \frac{1}{2} f_{45} + f_{90} \right) + \alpha_2 \left( f_0 + \frac{1}{2} f_{45} \right) \tag{5.17}$$

$$\alpha_z = \alpha_3 \tag{5.18}$$

The values of alpha along the principal direction of the plies can be determined using equations 5.17-5.18. In this study CFRP laminates of different thickness and similar staking sequences were used, hence ply thermal properties were needed to obtain comparable values.

# Chapter 6

# Application of the ATD model: one and two dimensional case

## 6.1 One dimensional case

A glass/polyester composite was tested under one-dimensional heat transfer conditions and used as a first simple study case. Its thermal properties were measured as described in chapter 5 and implemented in a finite difference FORTRAN version of ATD. The model was validated by comparison with experimental results.

## 6.2 Materials

The laminate used to investigate the procedure was made using plain woven E-glass fabric (800 $g/m^2$) and polyester resin (Ashland Composite Polymers). The resin did not contain flame retardant fillers or additives. The composite was made using the vacuum-bag resin infusion process, cured under ambient conditions (20 ℃, 55% RH) and post-cured at 80 ℃ for two hours. The fibre stacking sequence of the laminate was [0/90] and the fibre volume content was 55%.

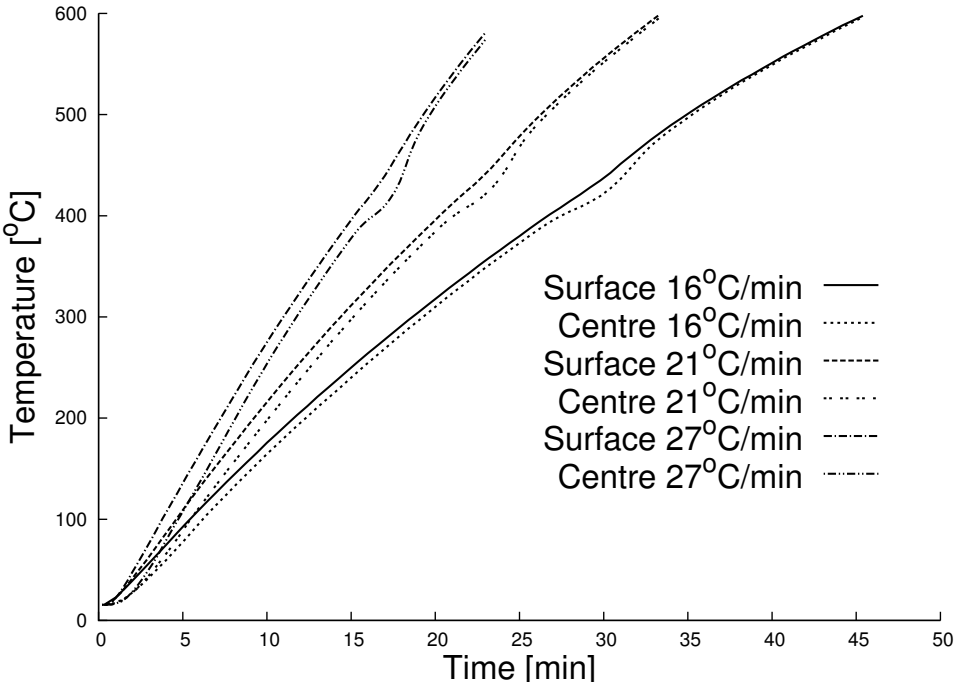


Figure 6.1: Surface and centre temperature profiles for polyester samples tested at 16C/min, 21.5C/min and 27C/min

## 6.3 Measurement of the ATD

### 6.3.1 High temperature ATD

Samples were tested in runs at three heating rates: 16 ℃/$min$, 21.5 ℃/$min$ and 27 ℃/$min$ up to 600 ℃, figure 6.1. At the end of each run the samples appeared to have been entirely depleted of resin. After cooling to room temperature the remaining fibre mat was then re-tested in order to evaluate the ATD of the bare fibres.

In figure 6.1 are shown the measured temperatures for each test. The upper line represents the imposed temperature and the bottom one the resulting temperature at the centre of the specimen. All the tests show the effects of the endothermic decomposition of the resin: the rate at which the temperature is raising decreases since the energy needed for the decomposition is absorbed in the process. Once all the resin has undergone decomposition the temperature rate increases again.

Values of apparent thermal diffusivity (ATD) from 100 ℃ to 600 ℃ were calculated using equation 5.9, figure 6.2. The lower limit of the measuring range is set by the

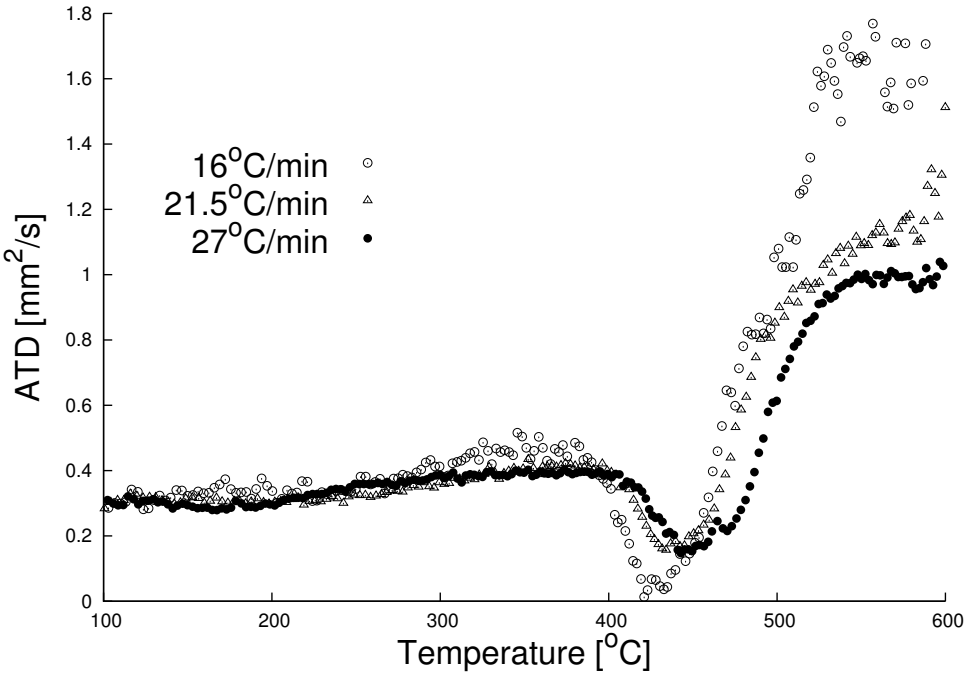


Figure 6.2: Polyester ATD profiles obtained for different heating rates

fact that at lower temperatures the heat transfer process is not fully established. The upper limit is influenced only by the operational range of the cartridge heaters. The apparent thermal diffusivity curves can be divided in three ranges belonging to virgin, decomposing and decomposed states [3]. The virgin state shows an almost constant value for the ATD. During the decomposition the ATD decreases as a result of the endothermic resin decomposition process. The ATD for the decomposed state at high temperature becomes the same as that of the fibre bed, as shown in figure 6.3 since, following decomposition the sample is mainly composed of fibres.

### 6.3.2 Low temperature ATD

Measurements of the ATD at low temperatures were carried out as described in paragraph 5.2.1. The samples measured 50 $mm$ × 50 $mm$ × 7 $mm$. Insulating foam was deployed along the edges of the samples to guarantee through-thickness one-dimensional heat flow.

In these tests, perfect step change boundary condition can not be considered.

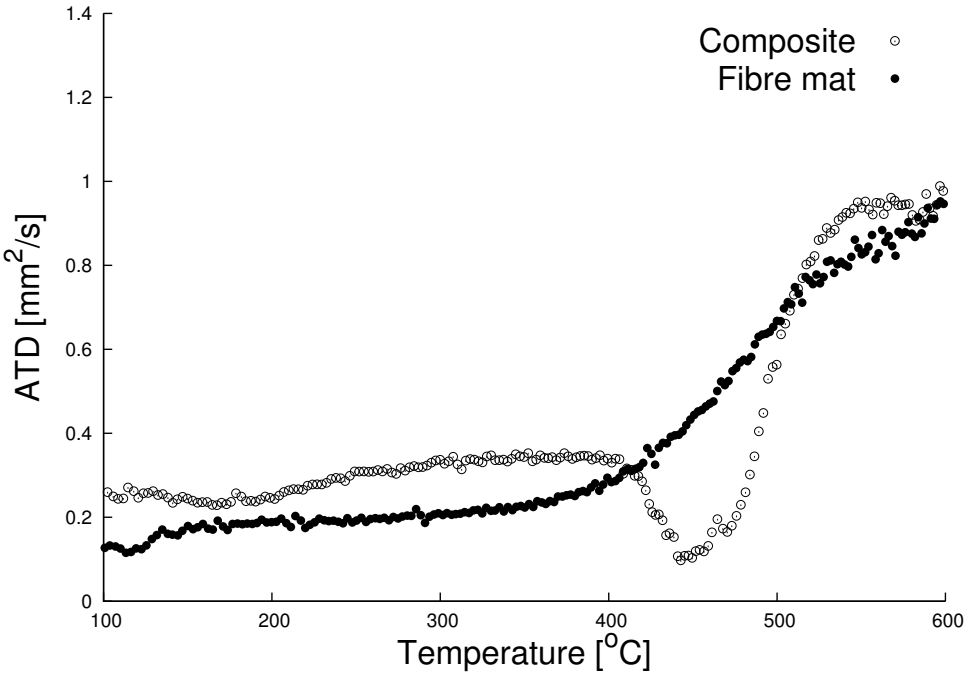


Figure 6.3: Polyester ATD graph at 27 ℃/$min$ for the composite and fibres mat

Inverse procedures were used to determine the value of the thermal diffusivity of the material.

Figure 6.4 shows the recorded mid-plane temperature of the sample varying from 80 ℃ to the isothermal bath temperature, 20 ℃.

## 6.4 One dimensional formulation of the ATD model: the Laplace heat transfer equation

### 6.4.1 Theoretical background

The analytical formulation of the ATD model is based on the Laplace heat transfer equation. Incorporating temperature dependent or 'apparent' thermal diffusivity (ATD) in Laplace's equation gives:

$$\frac{\partial T}{\partial t} = \alpha(T)\frac{\partial^2 T}{\partial x^2} \tag{6.1}$$

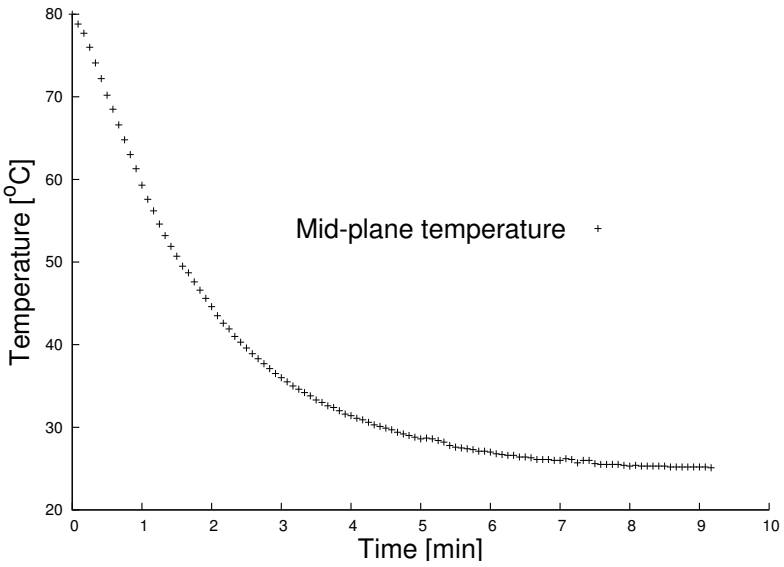


Figure 6.4: Mid-plane temperature of a polyester sample. The temperature of the sample was let stabilize in an oven for about one hour at 80 ℃. The sample was then dropped in water at ambient temperature

The thermal diffusivity is related to the thermal conductivity $k$, the specific heat $C_p$ and the density $\rho$ with the well known relationship:

$$\alpha(T) = \frac{k(T)}{\rho(T)C_p(T)} \tag{6.2}$$

These thermal properties evolve during heating from those of the virgin material through to the value for the final glass fibre remaining after resin decomposition.

### 6.4.2 Finite difference formulation of the Laplace equation

From the Laplace equation a 1-D finite difference model was developed. The $x$ direction considered is normal to the plane of the composite laminate. The 1-D configuration was chosen as first simple case study, easy to model and to characterise experimentally.

Considering that $T_i$ is the temperature of the generic node $i$ at the current time, $T_i'$ is the temperature of the same node after a period $\Delta t$, $T_{i-1}$ and $T_{i+1}$ are the temperatures for the nodes spatially adjacent to node $i$ at the current time, the finite

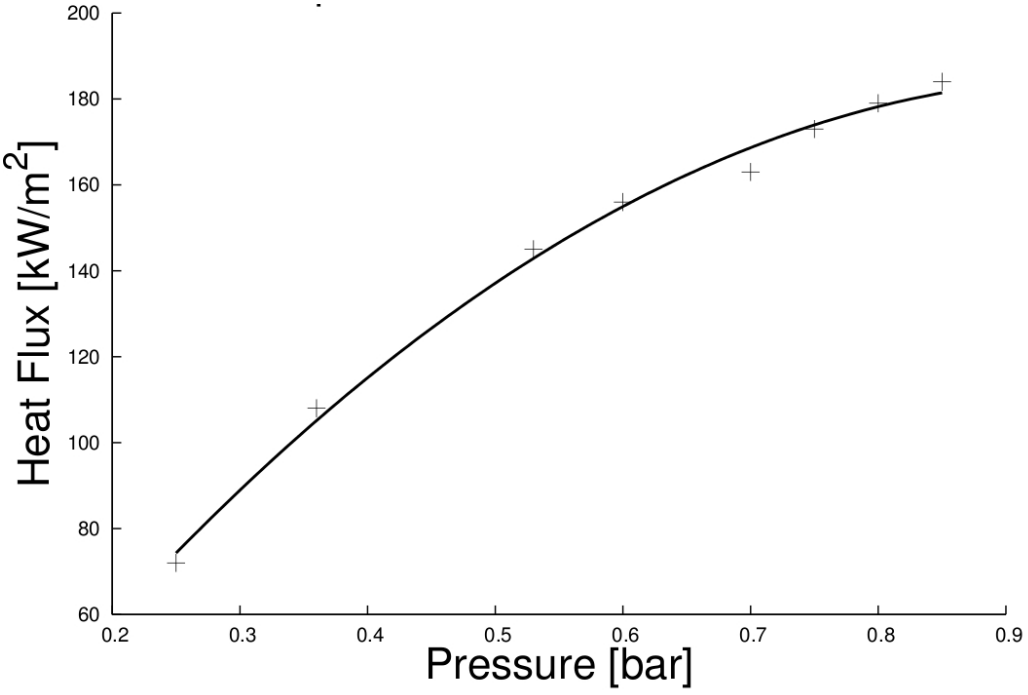


Figure 6.5: Calibration curve and data for the propane burner by means of a copper thermal capacitance calorimeter.

difference formulation of Laplace's equation is then [35]:

$$(T_{i-1} - T_i)A_p(T) + (T_{i+1} - T_i)A_n(T) = (T_i' - T_i) \tag{6.3}$$

where $A_p$ and $A_n$ are given by the apparent thermal diffusivity of the nodes $(i-1)$ and $(i+1)$ respectively, multiplied by $\Delta t/\Delta x^2$.

The thermal properties like thermal conductivity $k$, density $\rho$ and specific heat $C_p$

are calculated as average values between the node $i$ and the two adjacent nodes:

$$A_p(T) = \frac{\bar{k}_p(T)}{\bar{\rho}_p(T)[\bar{C}_p(T)]_p} \cdot \frac{\Delta t}{\Delta x^2}$$
$$A_n(T) = \frac{\bar{k}_n(T)}{\bar{\rho}_n(T)[\bar{C}_n(T)]_n} \cdot \frac{\Delta t}{\Delta x^2}$$
$$\bar{P}_p(T) = \frac{P(T_i) + P(T_{i-1})}{2}$$
$$\bar{P}_n(T) = \frac{P(T_i) + P(T_{i+1})}{2}$$
$$P = k, \rho, C_p$$

The temperature of the node $i$ after a time step $\Delta t$ can be calculated as follows:

$$T_i' = \Delta t[T_i(1 - A_p - A_n) + T_{i-1}A_p + T_{i+1}A_n] \tag{6.4}$$

For stability reasons [36] the time step $\Delta t$ has to obey to the following equation:

$$\Delta t \leq \frac{F_o \cdot \rho \cdot C_p}{k} \cdot \Delta x^2 \tag{6.5}$$

where $F_o$ is the Fourier number.

The thickness of the composite is modelled by $n$ nodes, usually 50, of which the temperatures are calculated per each time step. Equation 6.4 is used from node 2 to node $n-1$ at each time step $\Delta t$, temperatures for nodes 1 and $n$ are determined by the boundary conditions.

### 6.4.3 Boundary conditions

The heat transfer from the heating source to the composite during the exposure is the result of a thermal interaction between the hot surface of the composite sample and the source itself. When the heating source is represented by fire, heat is transferred mainly by radiative mechanisms. The energy balance at the hot surface of the

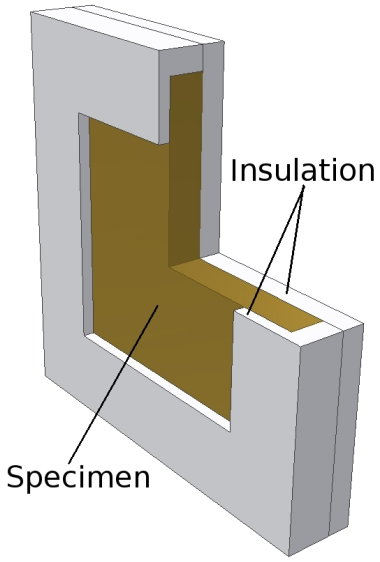


Figure 6.6: Schematic of deployment of the insulation around the specimen, a square of 100 $mm \times 100$ $mm$ is exposed to the heating source.

composite sample is described by the Stefan-Boltzmann law, augmented slightly by thermal convection from the heating source,

$$q = \sigma(\epsilon_s \alpha_m T^4 - \epsilon_m T_m^4) + h_{nc}(T_s - T_m), \tag{6.6}$$

where the subscripts $s$ and $m$ refer to the heating source and to the sample respectively.

For hot gases or flames undergoing combustion, energy is considered as transferred by selective emitters. In order to predict the emissivity of the heating source, thermocouples were placed close to the hot face of the sample. In fire situation, smoke particles may have emissivity between 0.7 and 0.9. Emissivity of the hot face of a FRP can be taken as 0.8 [33, 32].

## 6.5 Validation of the 1D ATD model

### 6.5.1 Experimental setup

A 15 $mm$ thick glass/polyester laminate was exposed to one-sided $50kW/m^2$ heat flux for 50 $min$. Temperature profiles at different depths, during time were measured.

The heat source was a calibrated propane burner. The calibration procedure involved heating up a thermal capacitance calorimeter [37] (copper block) with a standard cone calorimeter [5] at several constant heat fluxes. The heating rates that the cone calorimeter imposes to the copper block can be compared with the ones produced by the propane burner. In this way it was possible to relate propane pressure in the burner with the heat fluxes produced, figure 6.5.

The glass/polyester specimens were insulated on the non exposed face in order to achieve controlled and repeatable thermal boundary conditions. Insulation was used around the whole specimen except for an area of 100 $mm \times 100$ $mm$ on the exposed side, as in figure 6.6. This configuration was intended to ensure that the boundary conditions were as close as possible to those encountered in the standard cone calorimeter test procedure and that heat flow through the composite plate was close to one-dimensional over the exposed area.

Eleven thermocouples were placed through the thickness of the test pieces, along with one thermocouple on the exposed face to determine the hot surface boundary condition, as shown in Figure 6.7. At each point through the laminate thickness more than one thermocouple was used to improve accuracy and repeatability of the results. The hot surface measurement did not require redundant thermocouples because of the possibility of comparison with previous tests performed on the material under the same conditions.

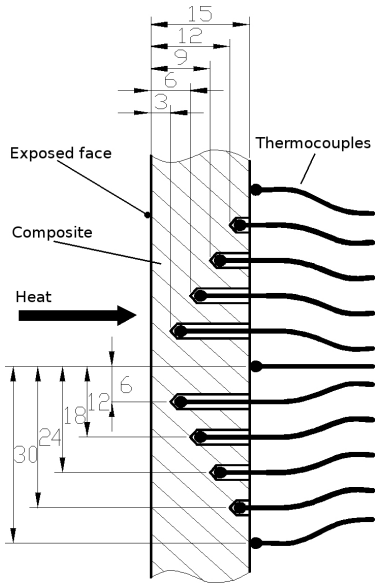


Figure 6.7: Experimental setup for through the thickness measurement of temperatures for a one-sided exposed GRP laminate through the thickness.

### 6.5.2 ATD model results

Figure 6.8 shows the experimental results compared with the numerical prediction obtained with ATD. The measurement and the calculation have been performed at the thicknesses specified in figure 6.7. Between 20 and 35$min$, from the fire exposure, the experimental curves show the usual decrease in the temperature rate due to the resin degradation and the convective effects due to the flux of volatiles. Both effects subtract energy to the composite decreasing the rate at which the temperature is rising.

From the temperature profile of the back face it is possible to observe that after about 35min of exposure the resin of the composite is totally degraded and the temperature starts rising at a higher rate.

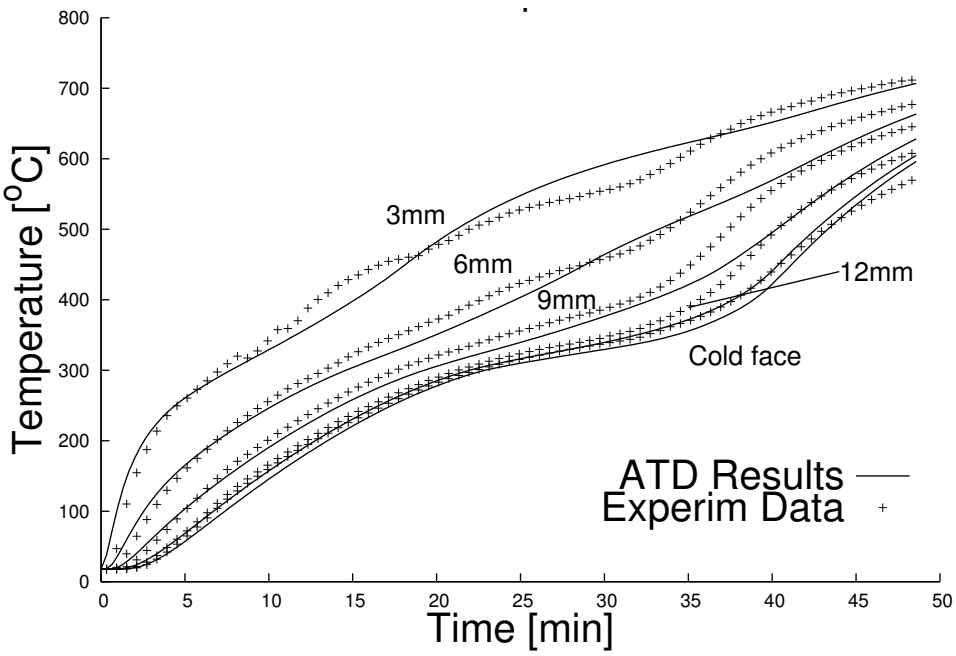


Figure 6.8: Experimental and ATD numerical results at different depths through the thickness of the composite.

## 6.6 Calculation of apparent thermal diffusivity (ATD) from experimental results

A verification of the apparent thermal diffusivity values can be performed by comparing them with a set of values obtained with a completely different method. The experimental temperature curves, obtained with the test described in paragraph 6.5.1, can be used to calculate the apparent thermal diffusivity of the material through a finite difference formulation of alpha:

$$\alpha(T) = \frac{\Delta T}{\Delta t} \frac{\Delta x^2}{T_{i-1} - 2T_i + T_{i+1}} \tag{6.7}$$

The values of apparent thermal diffusivity obtained through the two methods show a good match in figure 6.9. In the range of temperatures where the resin decomposition takes place, 350℃∼450℃, the apparent thermal diffusivity drops by an order of magnitude. This effect can be related directly with the decomposition plateau, figure

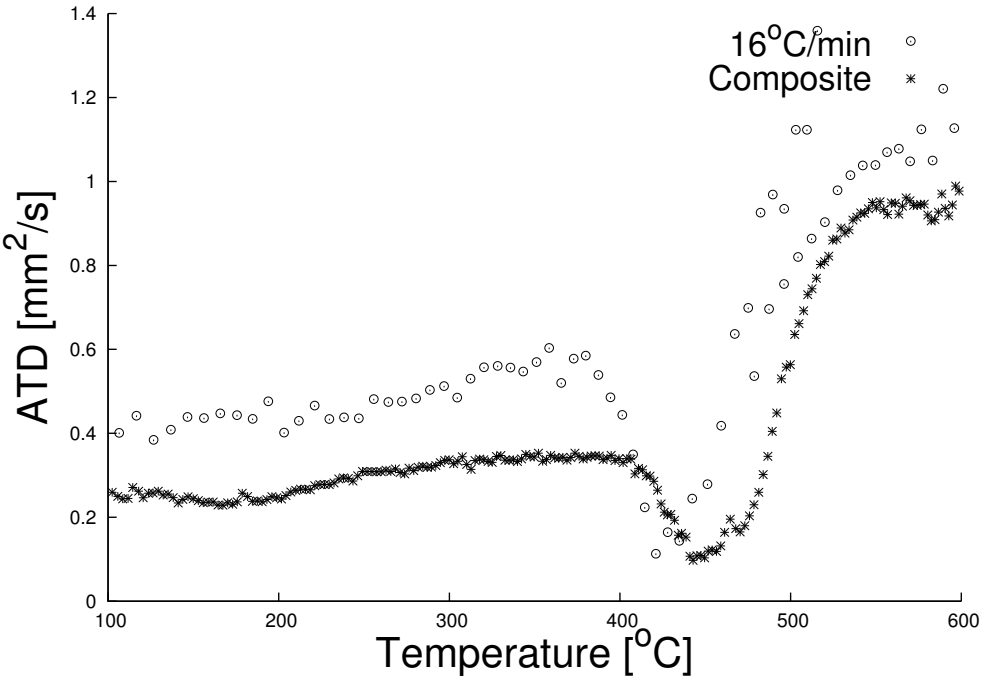


Figure 6.9: Experimental apparent thermal diffusivity of glass-polyester composite.

6.8.

## 6.7 Two dimensional case

Tests on glass/polyester pultruded I-beams were carried out. The specific boundary conditions allowed the establishement of two dimensional heat transfer conditions. The tests were modelled by implementing the ATD model in a commercial FE package.

### 6.7.1 Materials

The materials used were structural glass/polyester I-beams provided by Fiberline Composites. The nominal flange and web thickness measuring 8 *mm*. The sections show a structure similar to the box sections used in chapter 4. A unidirectional core aligned with the length of the beam provides strength and a continuous strand mat skin protects the core.

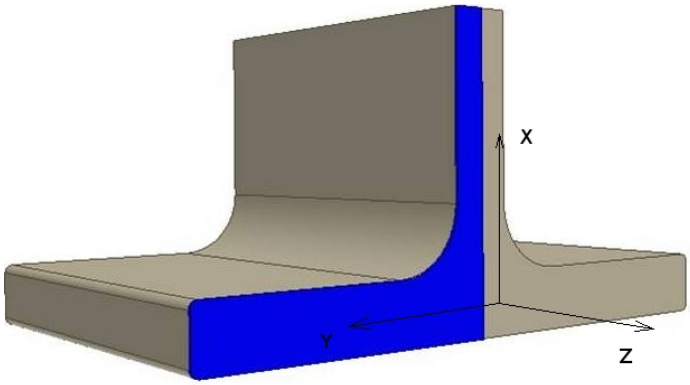


Figure 6.10: Schematic of the pultruded sections used to execute the two dimensional tests. FE techniques were used to model the blue area.

### 6.7.2 Experimental setup

The required heat transfer conditions were achieved applying a uniform heat flux of 50 $kW/m^2$ along the $x$ direction to the flange of a half I-beam pultruded section for 80 $min$, figure 6.10.

The remaining surfaces were insulated in order to obtain repeatable boundary conditions. The length of the specimen along the z direction was larger than 2.5 times the flange width (y direction). This was to ensure that there was no heat transfer perpendicular to the cross sections of the beam and two dimensional heat transfer can be established on these cross sections in the central region.

Thermocouples were deployed on the cold, or non-exposed, surface on 5 positions to monitor the temperature profiles during the exposure as shown in figure 6.11. Redundant thermocouples were used to test the repeatability of the measurements.

### 6.7.3 Modelling

The ATD model was used to provide an analytical description of the test. The two dimensional heat transfer conditions and the symmetry of the geometry allowed to analyse a half of the cross section as shown by the blue area on figure 6.10.

The FE model was composed of 2D solid elements, the ANSYS PLANE55. Twenty divisions were applied to thickness of the model. The other sides were divided accord-

| Kinetic parameters for polyester resin | |
|---|---|
| Pre exponential factor A $[1/s]$ | $2.72882 \times 10^6$ |
| Activation energy $[J/mole]$ | 113653 |
| $m_f$ [%] | 12 |
| Order of reaction [-] | 1 |

Table 6.1: Kinetic parameters for the decomposition of polyester.

ingly, to obtain elements with a near square shape. Radiation boundary condition were applied along direction x in figure 6.10 to the bottom edge of of the blue area, which represents the surface of the flange. The remaining surfaces of the model were isolated. To perform a convergence analysis in $P_1 - P_5$ the FE mesh needs to be refined several times. In these positions, nodes were required throughout the process. To achieved this, the cross section model in figure 6.11 was divided into areas with corners corresponding to the positions of the thermocouples in $P_1 - P_5$.

The thermal properties of the material needed to be expressed in terms of the single thermal conductivity , specific heat and density functions to be fed in the FE package. The way the density varies can be determined using Thermogravimetric analysis. If the exposure time is long enough a composite exposed to elevated heat fluxes reaches temperatures that trigger chemical reactions within the resin system. It degrades forming gaseous products. The resin decomposition process can be simulated using an $n^th$ order Arrhenius model, equation (2.3).

Figure 6.12 shows the results from the thermogravimetric analysis and the fitting obtained with the Arrhenius equation. The values of the kinetic parameters are shown in Table 6.1. These parameters can be derived from multiple heating rating techniques like Friedman's [38] or using multi-branch fitting techniques [39]. Although thermogravimetric tests are conducted at different heating rates resulting in different curves, kinetic parameters are independent from heating rates.

The thermal conductivity $k$ of the virgin and decomposed composite are different functions of temperature. The values used here were taken from Yu Bay *et al.* [40] that measured the thermal conductivity for glass reinforced polyester pultruded composites up to 720 ℃. The thermal conductivity functions for virgin and decomposed

composite were:

$$k_v = 0.33 + 4.4 \times 10^{-5} T \tag{6.8}$$

$$k_d = 0.0585 + 5.5 \times 10^{-13} T^4 \tag{6.9}$$

where $T$ is temperature.

During decomposition it is assumed that the thermal conductivity changes from the virgin to decomposed function following the relationship:

$$k = F k_v + (1 - F) k_d \; ; \; F = \frac{\rho - \rho_d}{\rho_v - \rho_d} \tag{6.10}$$

Subscripts $v$ and $d$ refer to virgin and decomposed respectively. Figure 6.13 shows the function of thermal conductivity for glass-polyester pultruded composites and its three stages: virgin, decomposing and decomposed. The specific heat was calculated using the equation that relates the thermal diffusivity with density, thermal conductivity and specific heat , equation 2.8.

### 6.7.4 Results

Tests results are shown in figure 6.14. Each data point set represents the temperature profile measured by the thermocouples located in the positions $P_1 - P_5$. As expected in $P_1$ and $P_2$, closer to the exposed face, the temperature rates are higher than the others The temperature values are quite similar at these positions. $T_2$ appears to be slightly lower than $T_1$. In fact the web behaves like a fin drawing heat to the cold end of the section, especially in the early stages of the exposure. Lower temperatures are recorded moving towards $P_5$. It is possible to conclude that a two dimensional temperature gradient is present on the cross section.

The temperature rates are affected by the effects of the decomposition. At every position, the resin appears to decompose at around the same temperature despite the different heating rates. Starting at 300 ℃ it exhausts the endothermic process

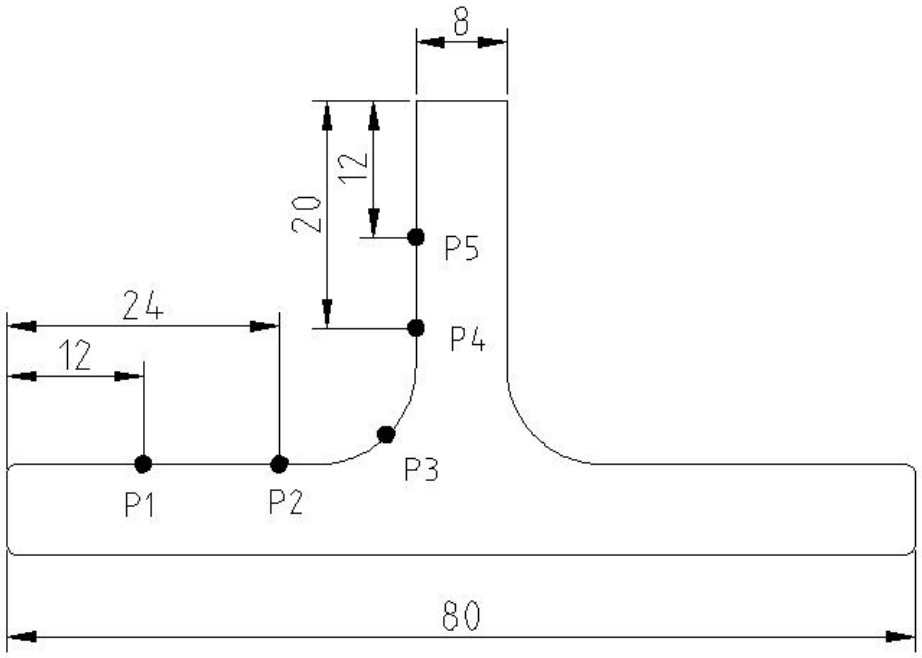


Figure 6.11: Schematic of the half pultruded I-beam section for the two dimensional tests. Dimensions and positions of the thermocouples (black dots) are shown.

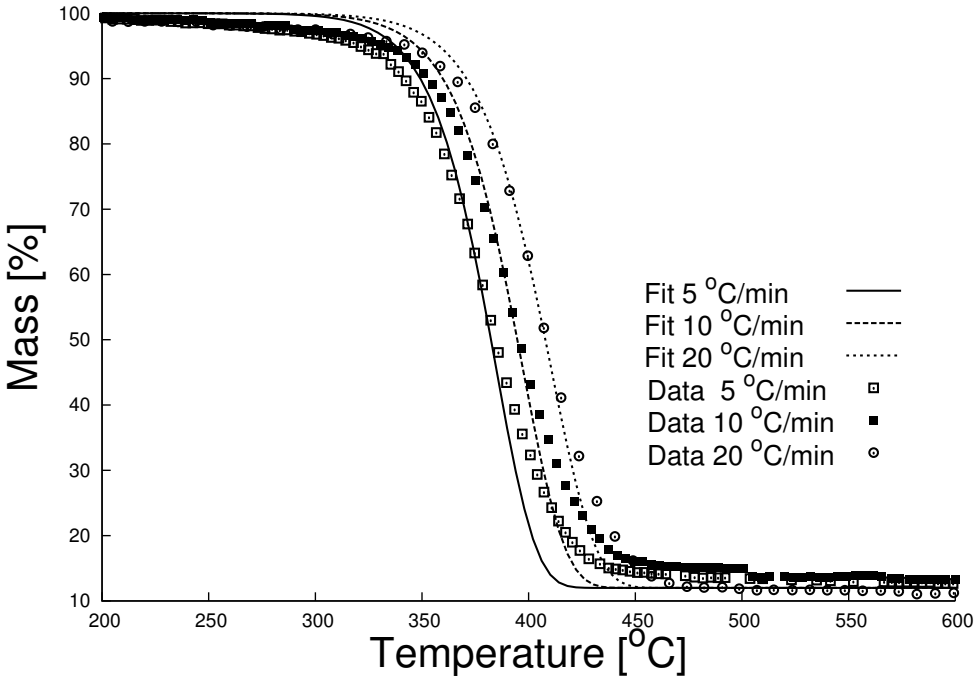


Figure 6.12: TGA results for three applied heating rates to glass polyester laminate and fitting.

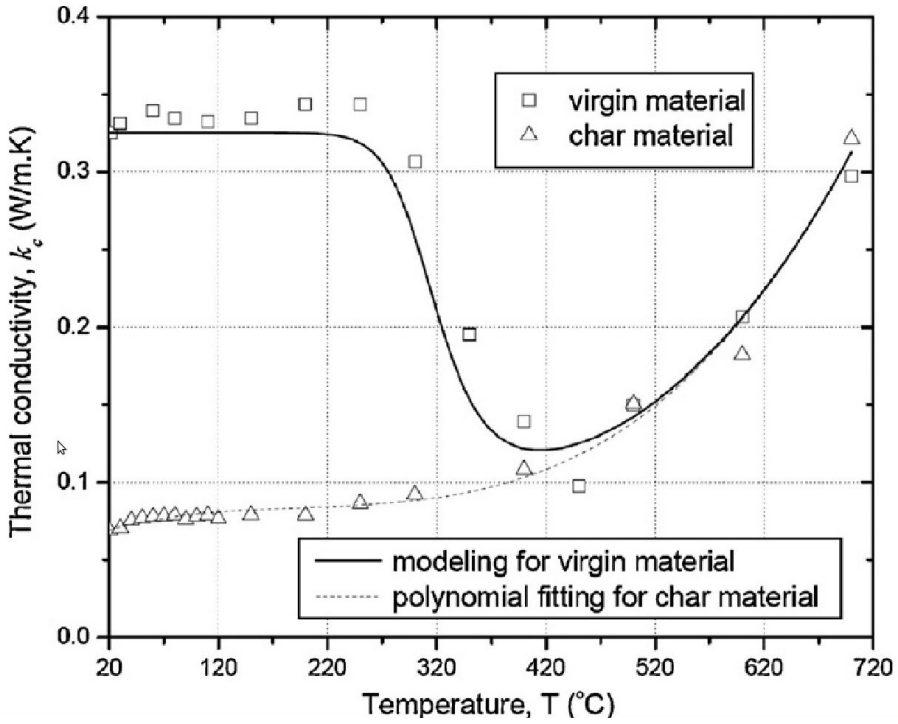


Figure 6.13: Temperature function of thermal conductivity of glass-polyester pultruded sections [40].

at around 450 ℃. After 80 *min* the temperatures reached the equilibrium and no sensible variations were recorded.

The temperatures predicted with the FE ATD model for this case are shown in 6.14 with solid lines. The model captured the decomposition of the resin. The use of a single function of temperature for the thermal diffusivity does not seem to have any effect on the accuracy of the prediction, despite the heating rates varying across the section. As observed the decomposition temperatureis scarcely sensitive to heating rate. This supports the applicability of the single ATD function approach to these materials.

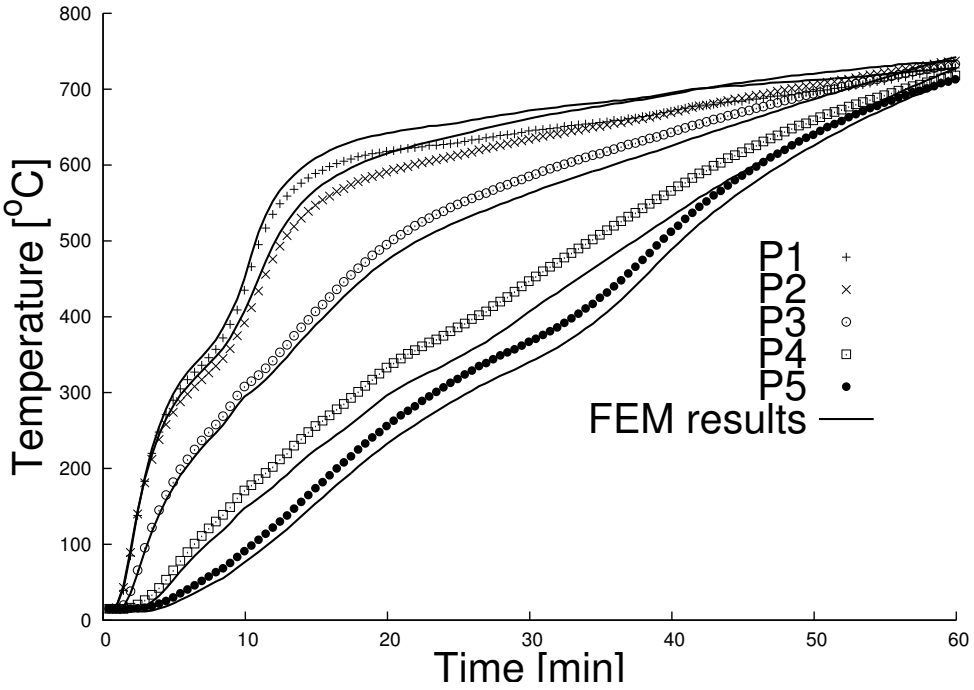


Figure 6.14: Experimental and FE results of the two dimensional tests performed on pultruded I-beam sections.

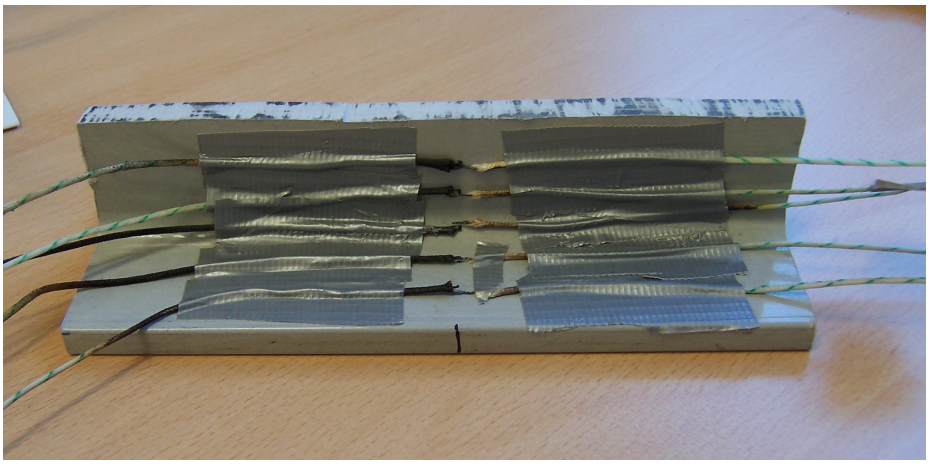

Figure 6.15: Deployment of thermocouples on pultruded polyester I-Beam section.

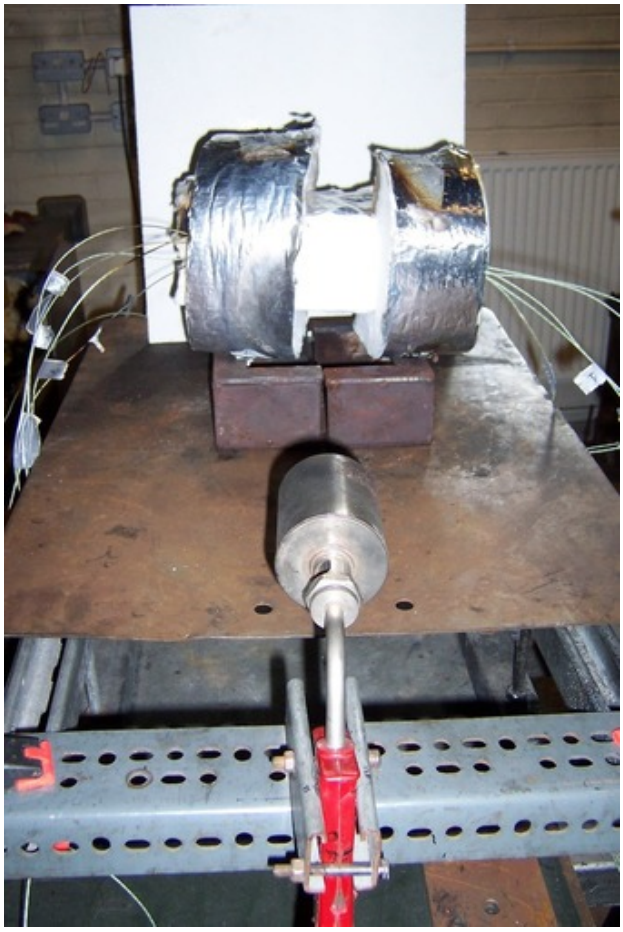

Figure 6.16: Experimental setup of the two dimensional heat transfer ATD test.

Figure 6.17: After the test the fibres of the pultrusion could be separated. No resin was left in the specimen as result of the fire exposure.

# Chapter 7

# Application of the ATD model: three dimensional case

This chapter describes the application of the ATD model to three-dimensional analyses on IMA/M21E CFRP wingbox composites. For this material, the in-plane values of the thermal properties are higher than the through thickness ones, due to the high thermal conductivity of the carbon fibre reinforcement and its high volume fraction. Given the orthotropic nature of the material, an accurate modelling of its fire behaviour requires the use of three dimensional analyses. The apparent thermal diffusivity of this material was measured along the directions 0 degrees, 90 degrees and the through thickness direction using the techniques described in chapter 5. These thermal properties were then implemented in a commercial Finite Element package and the results verified against three dimensional heat transfer fire tests.

## 7.1 Preparation of the samples

Measurements of the apparent thermal diffusivity were carried out for the materials along the three directions mentioned above.

The material was provided in three different thicknesses: nominally 6, 12 and 18 $mm$. The test requires that one dimensional heat transfer conditions are applied on

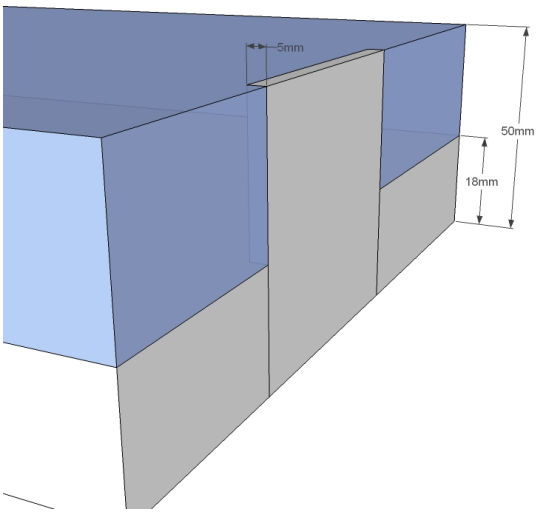


Figure 7.1: To measure the ATD along the in-plane directions samples were cut accordingly. The thickness of the laminates constitutes a limit for the width of the in-plane samples.

the direction along which the apparent thermal diffusivity is evaluated. In order to reduce the side effects the ratio between the thickness and the side needs to be about 1/10 [41]. Samples measuring 50x50x5mm were extracted from thick laminates along the three different orientations. However 50mm thick laminates should have been used to obtain the appropriate sample for the in-plane ATD measurements, see figure 7.1.

From figure 7.1, it is clear that the thickness of the laminate limits one of the dimensions of the sample. Due to the financial and logistic inconvenience of this option, smaller pieces were bonded to achieve the desired dimensions. For the sample used to measure the x (or 0 degrees direction) ATD, two types of pieces were cut from a 18mm laminate: one 18 x 5 x 50 mm and two 16 x 5 x 50 mm. The 18 mm piece constituted the middle part of the sample and the 16mm ones were deployed at either sides, figure 7.2.

Despite the transverse ATD samples contain some discontinuities compared with the through thickness ones, the following arguments justify the validity of the approach:

- the thermocouple located within the in-plane ATD samples, measures the tem-

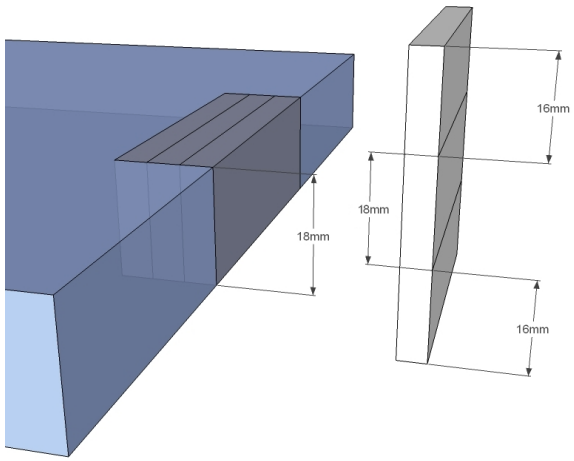


Figure 7.2: Samples for the in-plane measurement of the thermal diffusivity were made bonding together three cuts.

perature in the centre of the 18mm piece, away from the bonded regions;

- In the central region of the sample, the heat flow is parallel to the bonded surfaces and no temperature gradients are expected perpendicularly to them.

Hence the thermal transfer properties of the adhesive does not influence the temperature distribution within the sample in the central region. The results obtained with the two types of samples, continuous and discontinuous, are compatible and comparable.

## 7.2 High temperature measurements

The techniques described in paragraph 5.2.2 were employed to measure the apparent thermal diffusivity over a range between ∼100 to 600 ℃. The copper blocks were used to impose a linear temperature profile to the surface of the samples and the central temperature was measured. The samples were tested at three different heating rates: 16 ℃/$min$, 21.5 ℃/$min$ and 27 ℃/$min$ up to 600 ℃ along the three main directions of the composite. The samples were allowed to cool and a second run was performed to ensure that no decomposition effects could be seen.

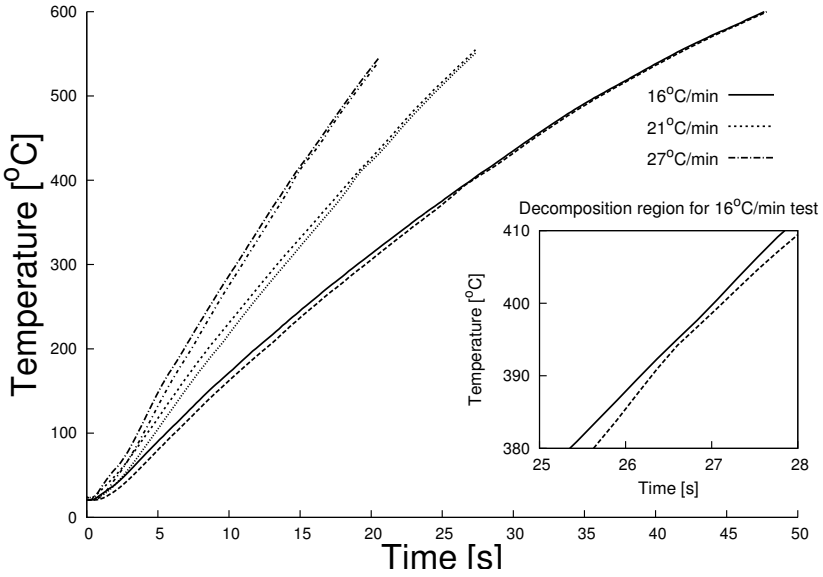


Figure 7.3: Temperature profiles for high temperature ATD measurement tests for the through thickness direction at three heating rates. The inset shows the temperatures in the decomposition region for the 16 ℃/*min* test. The central temperature of the sample appears to increase its rate during the process.

This procedure ensured that the the resin was completely depleted during the first run. Figure 7.3 shows the temperature profiles for the through thickness tests. During the degradation of the resin, the temperature rate inside the material appears to increase. It is clear that, in this case, the resin undergoes combustion. The heat developed by this process is greater than the amount absorbed by the endothermic process of decomposition. To prevent the combustion of the resin to occur tests were carried out in inert atmosphere using argon and nitrogen. Nevertheless the combustion of the resin still occurs.

To be able to extract the relevant information from the tests, modelling was needed. A one-dimensional finite different model was developed. The surfaces of the high temperature ATD test blocks impose with good approximation the linear temperature rate to the surfaces of the samples. Half of the sample was modelled since the thermal boundary conditions are symmetric. Twenty nodes were used to represent the thickness of the material.

The node representing the outer surface of the sample was imposed the temperature

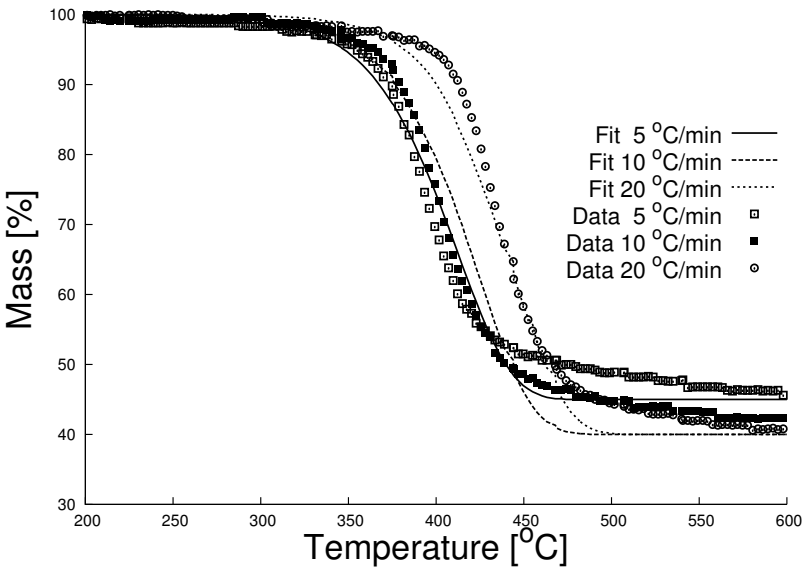


Figure 7.4: TGA data and fitting of IMA/M21E CFRP thermosetting composites.

measured by the thermocouple at the interface between the heating block and the composite. The node representing the middle plane was deemed isolated.

The density of the composite was modelled using the Arrhenius approach (equation 2.3): kinetic parameters were determined fitting the TGA test data, see figure 7.4. Using the Arrhenius equation and the proper kinetic parameters is then possible to predict the density profiles for heating rates different than those used in the TGA tests. The following finite difference formulation of the Arrhenius equation was used assuming the order of reaction $n = 1$:

$$\rho = \rho_i - A(\rho_i - \rho_f)e^{\frac{-E}{R\Delta T}} \tag{7.1}$$

where $\rho_i$ is the current value of the density, $\rho$ is the new value of the density, $\rho_f$ is the final value of the density, $A$ is the pre-exponential factor, $E$ is the activation energy, $R$ is the gas constant, $\Delta T$ is the temperature increment.

Density profiles relative to the high temperature ATD tests were determined at 16 ℃/$min$, 21.5 ℃/$min$ and 27 ℃/$min$ (figure 7.5). The specific heat and thermal

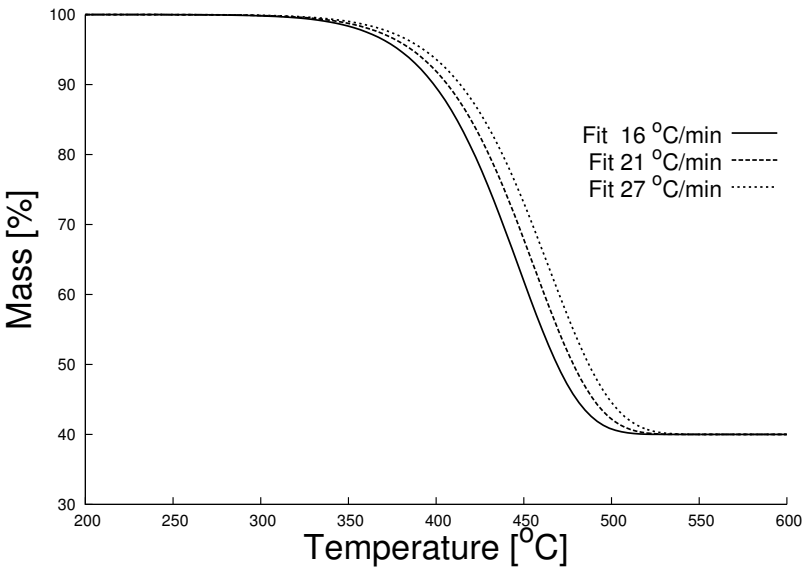


Figure 7.5: Density profiles prediction at 16 ℃/$min$, 21.5 ℃/$min$ and 27 ℃/$min$.

conductivity were calculated referring to the degree of decomposition,

$$X(T) = \frac{d\rho_{perc}(T)}{dT} \tag{7.2}$$

where $\rho_{perc}$ is the remaining percentage of the density at the temperature $T$. The relationships for the thermal conductivity and the specific heat become respectively:

$$k(T) = k_{virgin}(1 - X(T)) + k_{char}X(T) \tag{7.3}$$

$$C_p(T) = C_{p,virgin}(1 - X(T)) + C_{p,char}X(T) \tag{7.4}$$

Figure 7.6 shows the temperature results for the modelled high temperature ATD tests in the through thickness direction. In each case the temperature in the centre of the samples shows the effects of the endothermic resin decomposition process.

These results were used to calculate the apparent thermal diffusivity of the samples through equation 5.9, see figure 7.7

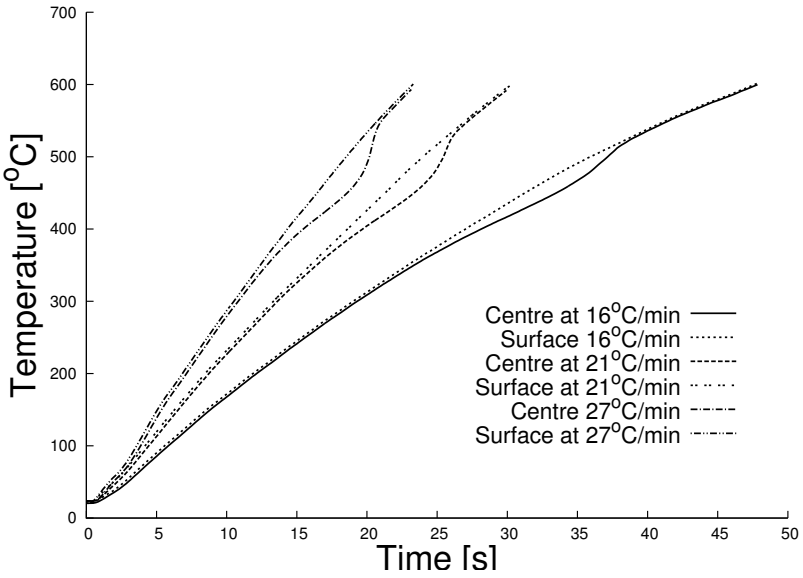


Figure 7.6: Modelled temperature profiles for high temperature ATD measurement tests for the through thickness direction at 16 ℃/$min$, 21.5 ℃/$min$ and 27 ℃/$min$.

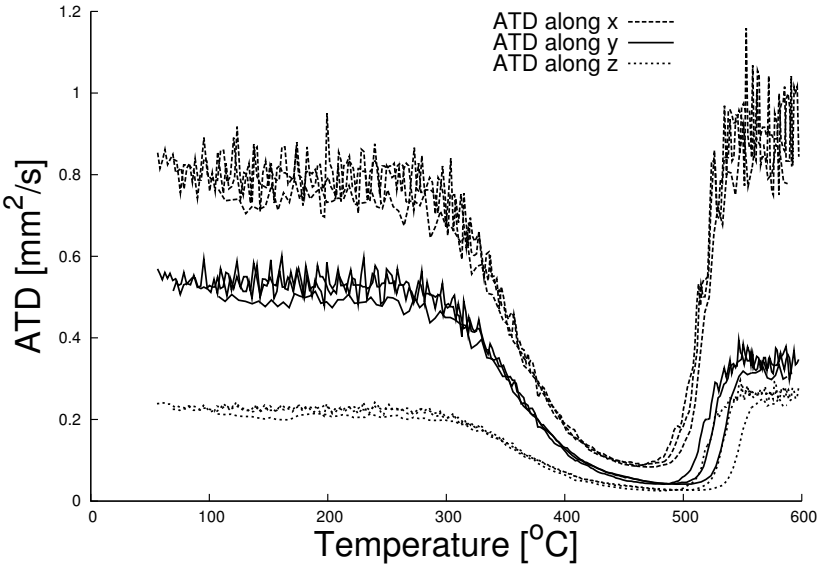


Figure 7.7: High temperature ATD curves for CFRP wingbox samples. Data sets for the three dimensions $x$, $y$ and $z$ are shown. Each one contains the results for the three heating rates used in this study: 16 ℃/$min$, 21.5 ℃/$min$ and 27 ℃/$min$.

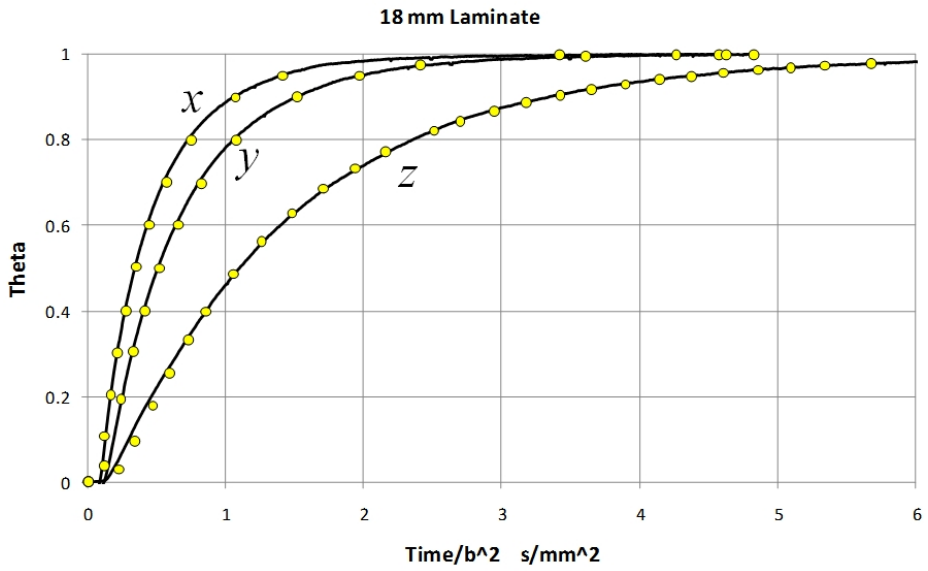


Figure 7.8: Dimensionless temperature response for 18 mm thick laminate in the three principal directions. Experimental curves with fitted points.

## 7.3 Low temperature measurements

Tests for the measurement of the apparent thermal diffusivity at low temperature were performed as described in chapter 5. Slab-shaped specimens were prepared for the three mentioned directions following the methodology of paragraph 7.1. Earlier, it was mentioned that the step-change experiment needs one-dimensional through thickness heat flow. Foam insulation was bonded around each rectangular sample to minimise heat flow through the edge surfaces. This was particularly critical when measuring the through-thickness-direction thermal diffusivity, as the in-plane diffusivities were significantly greater. The samples were instrumented with thermocouples measuring the centreline temperature. A thermal step change was applied.

The results were analysed using the parameter $\theta$ as per paragraph 5.2.1. To allow for comparison between results obtained with slightly different specimen thicknesses, the time scale in Figure 7.8 was scaled by dividing by $b^2$. The very different rates of variation of $\theta$ and shown in this figure result entirely from the significantly different values thermal diffusivity in the principal directions in the laminate.

The values of thermal diffusivity at the extremes of the temperature range of the

| Laminate thickness | $\alpha_x[mm^2/s]$ | | $\alpha_y[mm^2/s]$ | | $\alpha_z[mm^2/s]$ | |
|---|---|---|---|---|---|---|
| | 20 ℃ | 80℃ | 20 ℃ | 80℃ | 20 ℃ | 80℃ |
| 6.19 $mm$ | 1.70 | 1.03 | 1.05 | 0.68 | 0.47 | 0.35 |
| 12.38 $mm$ | 1.88 | 0.88 | 1.20 | 0.61 | 0.48 | 0.34 |
| 18.58 $mm$ | 1.74 | 1.08 | 1.02 | 0.78 | 0.46 | 0.30 |

Table 7.1: Values of laminate thermal diffusivity from step-change tests.

test were calculated using the inverse procedure explained in chapter 5. The closeness of the fit achievable can be seen by comparing the experimental curves and calculated points in Figure 7.8. Here examples of the variation of $\theta$ with time corresponding to heat flow in the three principal directions are shown.

Table 7.1 shows the values of thermal diffusivity obtained for the principal laminate directions from these tests. The most significant features of these results are the clear differences between the diffusivities in the three principal directions, with the z-direction values being substantially lower than the in-plane values, and the x-direction value being about 50-60% higher than that in the y-direction. The results can also be seen to be very temperature-dependent, with a substantial fall over the range from 20 ℃ to 80 ℃. This confirmed that the behaviour could not be modelled satisfactorily with a constant value of thermal diffusivity.

It can be seen that there is some scatter in the values in table 7.1. No formal statistical estimate was made, but the variability of the results appears to be about $\pm 5\%$. The test procedure and curve-fitting procedures were quite reproducible, as can be seen from figure 7.8. The laminates can also be expected to be of very consistent quality. The main origin of the variability, therefore, was probably the specimen preparation method, especially in the cases where samples were assembled by bonding together several layers or blocks of material. The reproducibility of the results is nevertheless good enough to enable these data to be used in thermal modelling procedures.

| Laminate thickness | $\alpha_1[mm^2/s]$ | | $\alpha_2[mm^2/s]$ | | $\alpha_3[mm^2/s]$ | |
|---|---|---|---|---|---|---|
| | 20 ℃ | 80℃ | 20 ℃ | 80℃ | 20 ℃ | 80℃ |
| 6.19 $mm$ | 2.33 | 1.37 | 0.42 | 0.34 | 0.47 | 0.35 |
| 12.38 $mm$ | 2.67 | 1.19 | 0.41 | 0.29 | 0.48 | 0.34 |
| 18.58 $mm$ | 2.46 | 1.38 | 0.30 | 0.48 | 0.46 | 0.30 |
| Mean values | 2.49 | 1.31 | 0.37 | 0.37 | 0.47 | 0.33 |

Table 7.2: Ply thermal diffusivity values, derived from the data of Table 1.

## 7.4 Thermal laminate theory

Table 7.2 shows estimates of the ply thermal diffusivities, based on the data of table 7.1 and thermal laminate theory, paragraph 5.2.3. The predictions for each laminate thickness have been averaged in the bottom line of the table to provide the most reliable estimates for the ply parameters.

There is considerable anisotropy of thermal behaviour at ply level. An approximate factor of 6 can be seen between the fibre and transverse directions. It is also interesting to note that the temperature-dependence of the thermal diffusivity appears to be greater on the longitudinal than the transverse direction.

Because of the anisotropy of the laminates the estimate for $\alpha_2$ is probably more sensitive to scatter in the results than that for $\alpha_1$, as its calculation involves differences between numbers of rather similar magnitude. The comparison between the transverse values, $\alpha_2$ and $\alpha_3$, therefore need to be treated with a little caution. It can, be seen that they are of broadly similar size and there may be some justification, depending on the ply architecture, in assuming them to be equal, as is often assumed in the case of elastic constants. However, closer comparison is precluded by the accuracy of the results.

Finally, the mean ply values of table 7.2 were used with laminate theory to produce best estimates of the laminate properties for use in subsequent modelling. These results are shown in table 7.3. This assumes that there are no systematic differences between laminates of different thickness, other than the differences predictable from the ply content. Although the figures given in the tables are restricted to two decimal places accuracy the underlying calculations were carried out using greater precision in

| Laminate thickness | $\alpha_1[mm^2/s]$ | | $\alpha_2[mm^2/s]$ | | $\alpha_3[mm^2/s]$ | |
|---|---|---|---|---|---|---|
| | 20 ℃ | 80℃ | 20 ℃ | 80℃ | 20 ℃ | 80℃ |
| 6.19 $mm$ | 1.79 | 1.00 | 1.07 | 0.68 | 0.47 | 0.33 |
| 12.38 $mm$ | 1.75 | 0.98 | 1.11 | 0.70 | 0.47 | 0.33 |
| 18.58 $mm$ | 1.78 | 1.00 | 1.08 | 0.68 | 0.47 | 0.33 |

Table 7.3: Best estimates of laminate thermal diffusivity values using laminate theory and averaged property values.

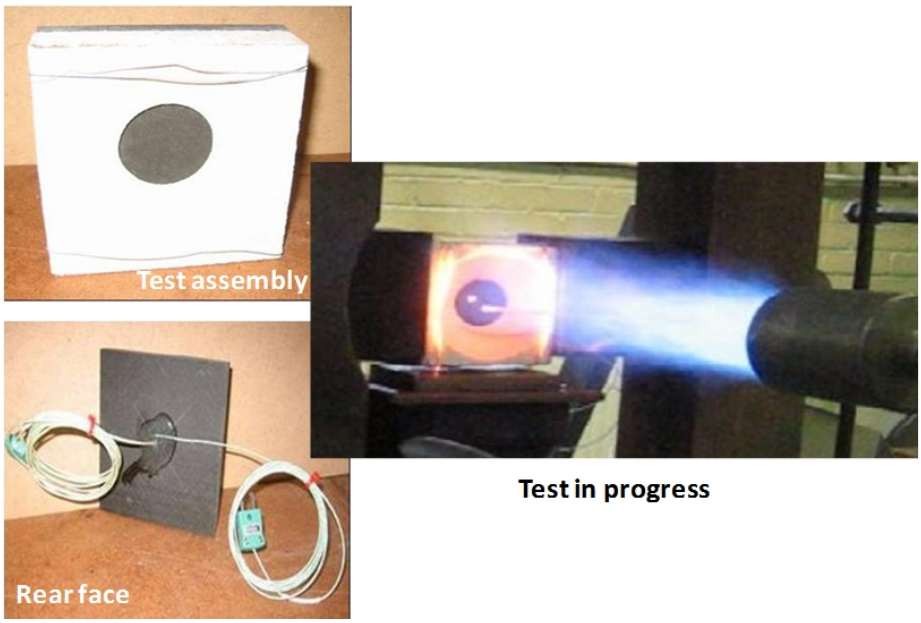


Figure 7.9: Bottom left: CFRP sample instrumented with thermocouples on the rear face. Top Left: test assembly; the CaSi mask exposes a circular region of the hot face of the sample. Right: test in progress.

order to avoid accumulation of errors. It is useful to note that the differences between the numbers in table 7.1 and table 7.3 are fairly small.

## 7.5 Modelling 3D cases using the ATD model

Experiments were carried out on the IMA/M21E CFRP wing box laminate samples. The in-plane thermal transport properties of the material are very different than the through thickness ones. This allowed to perform fire tests that require three dimensional modelling. The ATD was used and its suitability to model the behaviour of the material was verified.

The procedure involved exposing 100 mm square, 9 mm thick IMA/M21E carbon

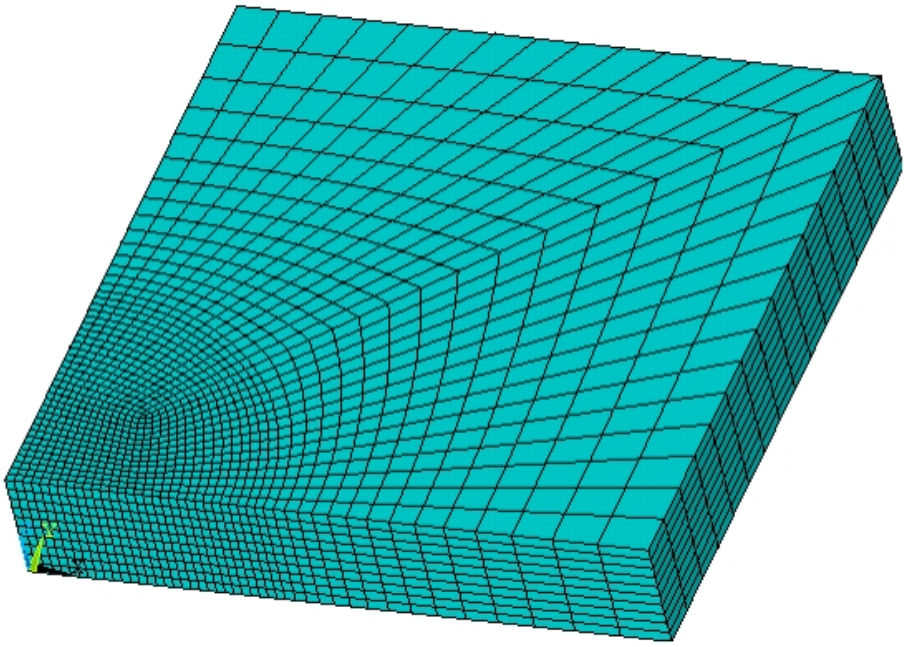

Figure 7.10: Finite element mesh used to model the fire behaviour of the CFRP samples.

fibre reinforced plastic (CFRP) specimens to a one-sided heat flux. Two heat flux levels were chosen, 185 $kW/m^2$ and 75 $kW/m^2$, provided by a calibrated propane burner. The highest value relates to severe hydrocarbon fires, due for example to crash landing fuel spillage. The latter value represents a less severe fuel event.

The tests comply with the regulatory requirements for the assessment of composite primary structure components on civil aircraft. The exposed area of the samples was a circular region of a diameter of 40 mm, delimited by a heat-resistant calcium silicate mask, as in figure 7.9. Specimens were exposed for 30, 60, 120, and 240 s and allowed to cool. The sample cold face was left uninsulated and in contact to air. The front and rear face temperatures were measured. This arrangement allowed to investigate whether the conduction of heat on the in-plane direction of the laminate would damage the material underneath the masked region [42]. Also, the model results were compared with the fire damage characterization which La Delfa [43] performed using ultrasonic non-destructive testing techniques and optical microscopy.

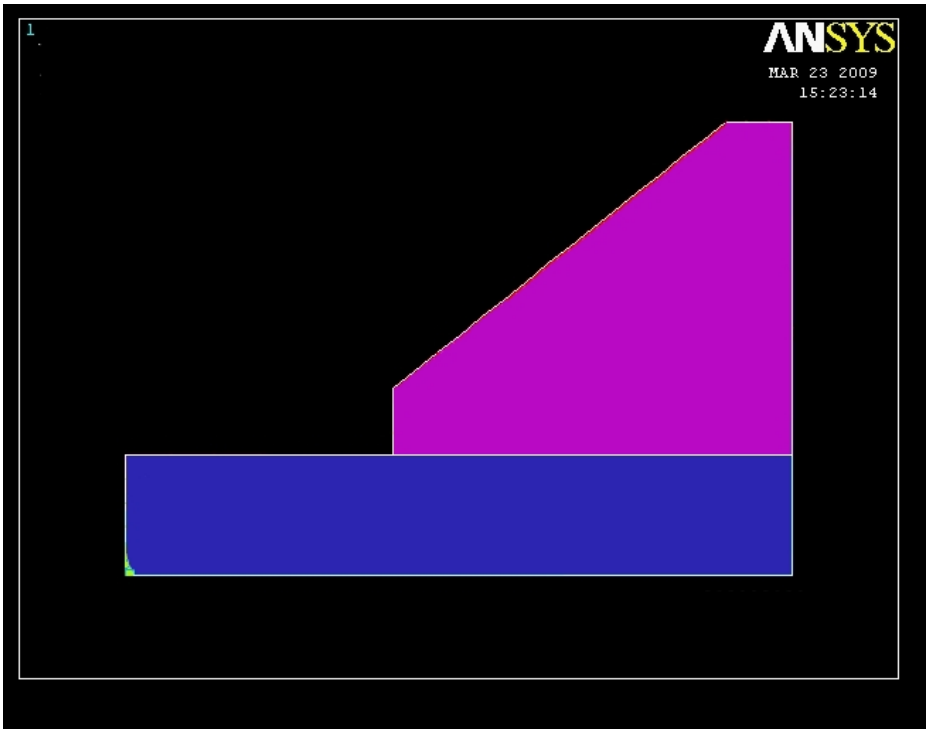


Figure 7.11: Mesh used for the analysis. The light blue mesh simulated the material properties of the composite and the purple elements simulated the CaSi mask.

To model this particular study case the values of ATD determined for this material were used to run an ANSYS FE model. The tests were modelled analysing a quarter of the sample given the symmetry of the boundary conditions. A finer mesh was used in correspondence of the exposed area, were larger temperature gradients were expected. Figure 7.11 shows a section of the model. Here the elements representing the composite and the CaSi mask are indicated with different colours. Radiative boundary conditions were applied perpendicularly to the upper surface of the composite and CaSi mask to simulate the incident heat flux of the burner. The face of the composite residing on the plane of symmetry were treated as isolated. The losses on the unexposed surfaces were modelled applying radiative heat transfer conditions allowing the model to exchange heat with a source at room temperature.

A convergence study was carried out. Firstly the analyses were performed on a very coarse mesh. The number of nodes on each side of the model were then doubled and the value of the calculated temperature, $T_c$, on the exposed face were then compared.

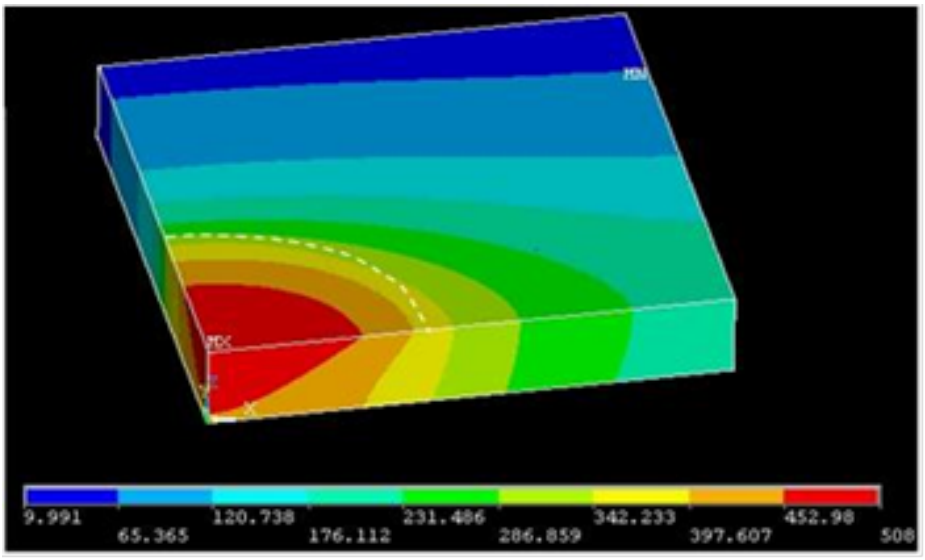


Figure 7.12: Temperatures for the CFRP sample after a 8 *min* exposure to the 185 $kW/m^2$ heat flux. The dashed arc represents the edge of the CaSi mask. The anisotropy of the model affects the in-plane and through thickness temperature distribution.

When the value of $T_c$ stabilized, with a variation of less than 3% , the FE model was deemed accurate, figure 7.10.

A data set was produced from the results of the high and low temperature techniques to cover the temperature range under examination. Most FEA packages enable thermal property information to be entered in tabular form, with appropriate values for the three orthotropic laminate directions. The high temperature ATD curves shown in figure 7.7 were simplified and represented by a small number of segments to improve the efficiency and stability of the FE model. [44, 43]

Figure 7.12 shows a contour plot of the temperatures for the CFRP sample after a 8 *min* exposure to the 185 $kW/m^2$ heat flux. Figures 7.13, 7.14 and 7.15 show the distribution of the temperatures on half the cross section of the sample and the CaSi mask, trapezoid area, after an exposure of respectively 100, 600 and 900 s.

The edge of the CaSi mask is represented by the dashed arc on the top surface of the model. The temperature rises well beyond the CaSi mask edge. The shape of the contours suggest that the heat propagation on the plane of the laminate is highly influenced by the in-plane thermal properties. The in-plane thermal anisotropy has

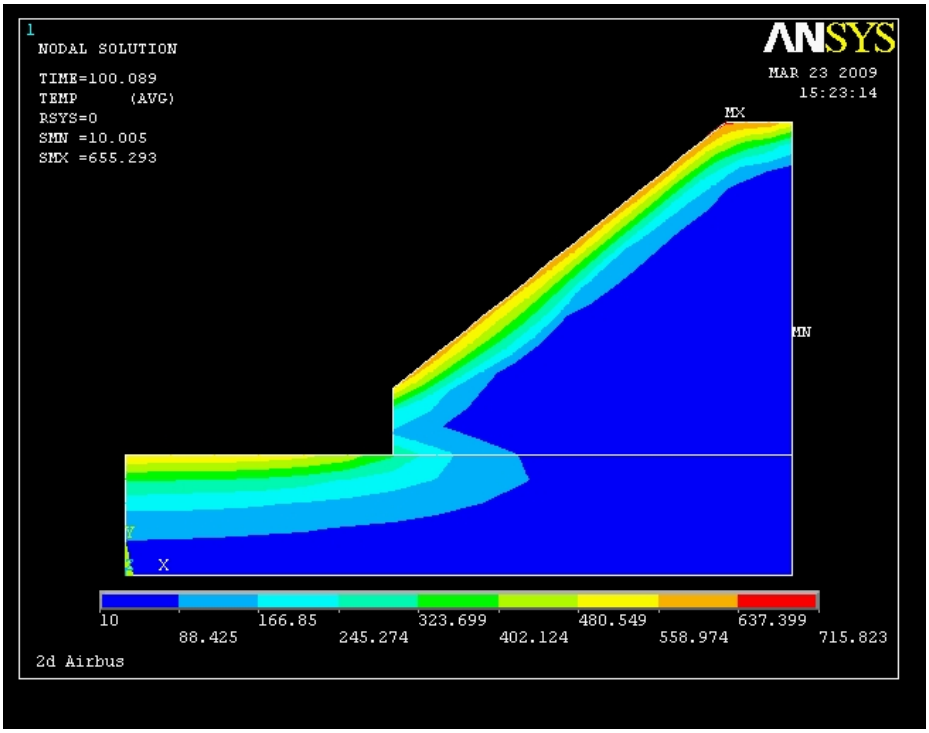


Figure 7.13: Contour plots of the temperature distribution on half cross-sectional area of CRFP sample. The result are refer to an exposure time of 100 s to 75 $kW/m^2$. The location of the calcium silicate mask is shown (trapezoid area).

clear effects on the temperature gradients of the plain of the laminate. La Delfa [42, 43] estimated the onset and finish of delamination using ultrasonic scanning on specimens with different exposure times. The modelling developed here was then used to attribute specific temperatures to the occurring of the delamination. Two estimates were made for these temperature: 350 ℃ or 420 ℃. The comparison between ATD modelling of the delamination and the ultrasonic measurements is presented in figure 7.16 for each heat flux.

These two temperatures were evaluated with thermogravimetric considerations: in fact the resin decomposition occurs within that range of temperatures.

For a heat flux of 185 $kW/m^2$, there is reasonable correspondence between the measured and modelled data. However, for the 75 $kW/m^2$ heat flux the model predicts that the delamination occurs earlier. The discrepancy may be due to the influence of the constraint offered by the structure of the material in the TGA test. TGA

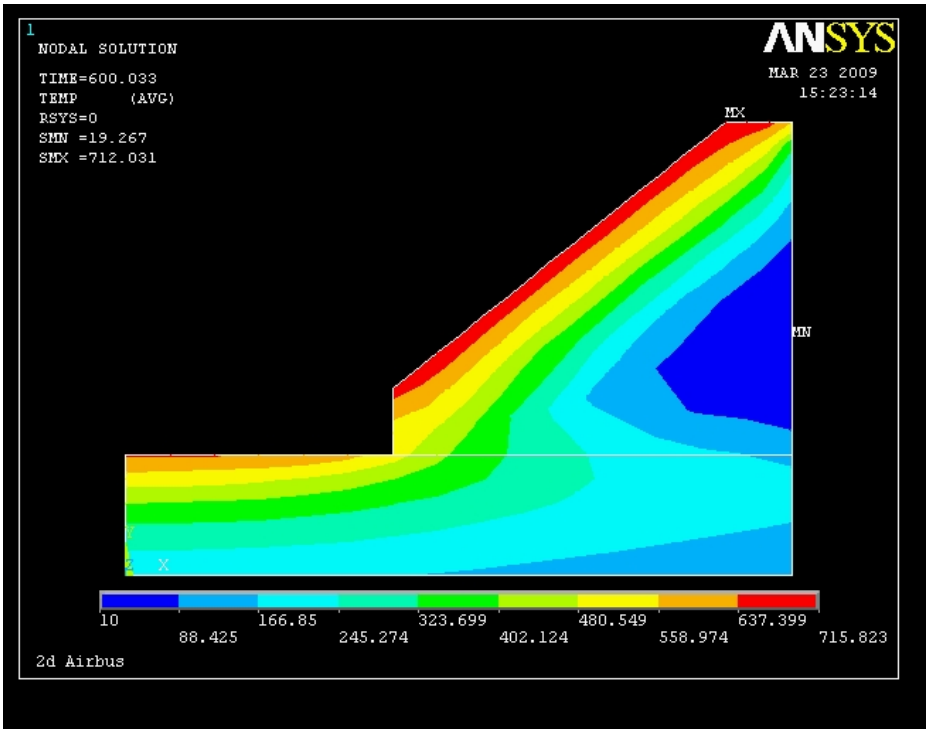


Figure 7.14: The result refer to an exposure time of 600 s to 75 $kW/m^2$.

samples have a very small mass. As a consequence the inner parts of the sample are surrounded by a much smaller quantity of mass when compared to a thick laminate. Possibly a very high heat flux is capable to mask this difference better than the lower 75 $kW/m^2$ flux.

The back face temperatures, measured by La Delfa , are shown in figure 7.17 together with the model results. The two data sets show good agreement.

To investigate the extent of the damaged zone, the samples were cut through the centre. The appearance of the samples shows that the damaged region extended well beyond the exposed area underneath the CaSi mask, indicating that the in-plane heat conduction is not negligible [42, 43].

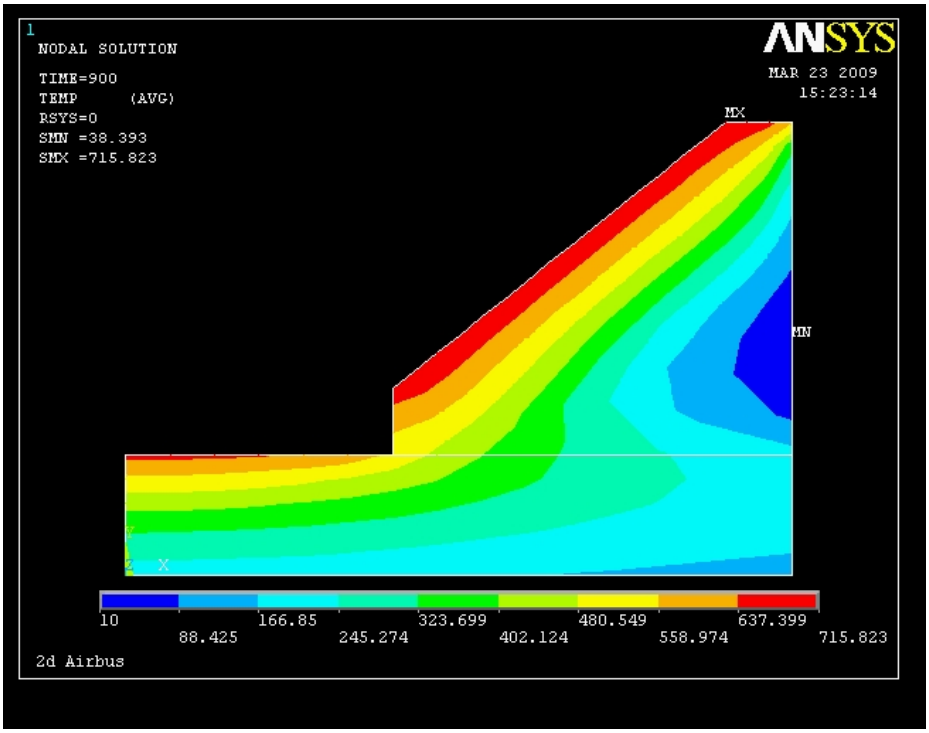


Figure 7.15: The result refer to an exposure time of 900 s to 75 $kW/m^2$.

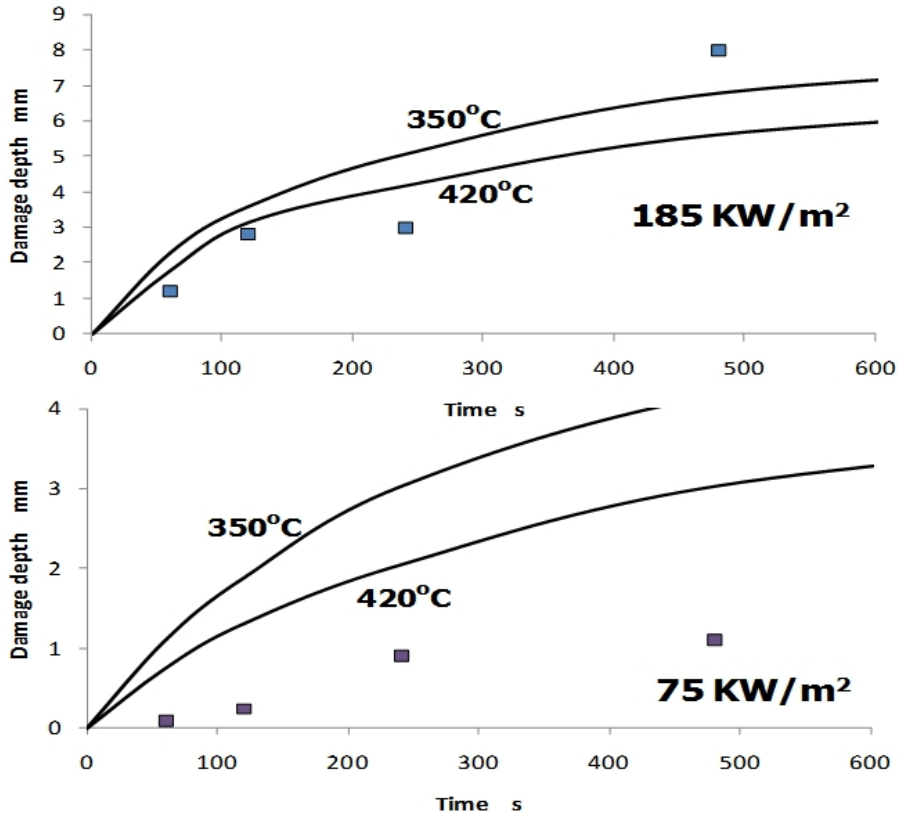


Figure 7.16: Depth of damage calculated assuming delamination occurring at 350 ℃ and 420 ℃, solid line [42], and from ultrasonic measurements [43], squared dots.

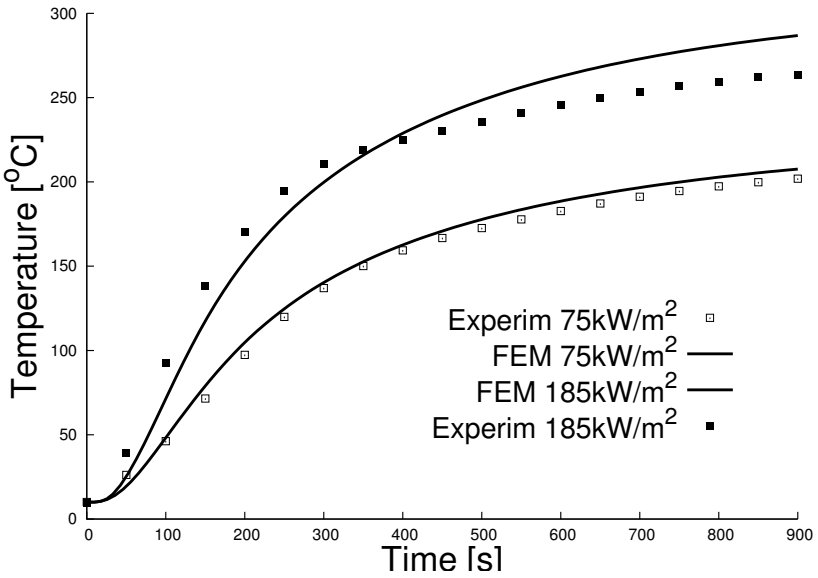


Figure 7.17: Back face temperature measurement and modelling for 185 and 75 $kW/m^2$ heat flux [42].

# Chapter 8

# Overall discussion and conclusions

## 8.1 Conclusions

Composite materials represent an effective lightweight solution to structural applications. The need of progressing the understanding of the fire behaviour of these materials was addressed in this research and its benefits identified together with the main shortcoming of the existing thermal models based on the Henderson equation.

The main objectives of this work were: to improve the modelling of phenolic composites and their decomposition process; investigate whether an apparent thermal diffusivity (ATD) approach to the characterization of the thermal properties of fibre reinforced composites over a wide range of temperatures is able to model accurately their behaviour in fire.

A two stage decomposition process was used to model the fire behaviour of phenolic pultrusions. Two sets of kinetic parameters were determined trough thermogravimetric investigation of the pultruded phenolic beams. Comparison with polyester pultrusion is provided.

Techniques were developed for the measurement of the ATD for glass fibre laminates, carbon fibre prepreg laminates and pultruded composite beams. The ATD thermal model was developed from the La place heat transfer equation and validated against experimental evidence produced from a selection of representative applica-

tions.

### 8.1.1 ATD One dimensional case

Basic phenomena occurring to a glass polyester composite in fire and their mathematical formulation were exposed in details. Resin degradation was modelled as a change of phase incorporated in the ATD which was modelled with a 3-stage function of temperature. The first stage can be attributed to the properties of the virgin state, from ambient temperature to the appearance of the decomposition phenomena. at these temperatures, the apparent thermal diffusivity remains fairly constant, a small rise can be observed approaching the decomposition. This stability can be associated to the thermal properties of the polymeric matrix. The second stage characterises the endothermic effects of the resin degradation. The resin sublimes subtracting thermal energy to the heating process. This causes the apparent thermal diffusivity to drop in that temperature region. The third region is fibre dominated because after the decomposition the samples contain almost no resin. At ambient temperature, the heat transfer properties of a glass fibre mat are poorer than the corresponding composites. At higher temperatures, the thermal diffusivity increases considerably as radiative heat transfer modes take over. This accounts for the high values of thermal diffusivity after decomposition. The results here presented confirm that neglecting the convective effect of the volatiles does not impair the accuracy of the calculation.

### 8.1.2 ATD Two dimensional case

Polyester pultruded sections were tested under two dimensional heat transfer conditions. Thermal properties were determined for these materials. The ATD approach was implemented into FE calculation to model the tests. Convergence studies were carried out to ensure the reliability of the results.

The results obtained from the models match well with the fire tests. Therefore it is possible to conclude that ignoring the convective effects of volatiles, avoiding the

burden of a permeability study of the material, allows an accurate description of its fire behaviour without affecting the reliability of the results.

### 8.1.3 ATD Three dimensional case

CFRP wing box composites were characterised along the three principal directions. The technique developed in chapter 5 proved capable of describing the thermal properties of the materials with the aid of TGA data and modelling. The decomposition region was clearly visible after the data processing. Thermal diffusivities were calculated from the temperatures. Along the three principal directions, the ATD assumes different values, decreasing from the x to the y and z orientations. The fibre orientation and thermal properties clearly dictate the thermal behaviour of the laminate.

FE three-dimensional analyses including the ATD formulation of the material were performed. Convergence study were applied to ensure the reliability of the results. Different heat transfer gradients cold be seen on the x, y and z directions, according to the values of ATD measured. The back face temperature measurement agree with the calculated values.

An attempt of relating the laminate damage onset with the temperatures was made. The ATD model calculation are overestimating the damage onset for the two heat fluxes considered. This suggests that damage occurs at higher temperature.

### 8.1.4 Two stage decomposing composites

The thermal model based on the Henderson equation can predict temperature evolution through a pultruded composite and the empirical *tanh* function (equation 4.1) can be used to describe mechanical properties. Both polyester and phenolic pultrusions retained a significant residual strength under tensile load, due to the residual strength of the glass fibres. However, pultruded composites, like other organic matrix composites, are particularly susceptible to compressive failure when subjected to fire, due to the loss of properties when the resin $T_g$ is reached.

The fire reaction properties reported here showed the phenolic pultrusions to perform better than polyesters in all fire reaction properties (time to ignition, heat release, smoke and toxic product generation).

The mechanical measurements under load in fire showed that phenolic pultrusions decayed at a much slower rate than the polyester, due mainly to the very shallow glass transition of the phenolic, but also the char forming characteristic of the phenolic. It appears that phenolics can retain a substantial degree of stiffness in fire (72%) along with 22% of strength after 800 $s$. These conclusions of course apply to 8 $mm$ thick sections in a 50 $kW/m^2$ fire. The model described here would probably be capable of modelling other thickness or heat flux conditions.

The fire integrity reported here for phenolic pultrusions is superior to that reported elsewhere for phenolic laminates [28]. The main factor influencing integrity appears to be water content. A secondary factor is fibre architecture.

## 8.2 Recommendations for future work

The study reported here delivered promising results for a better understanding of the fire behaviour of composites, answers that pose new questions.

The ATD measuring method developed here scopes two temperature ranges, from 20 ℃ to 80 ℃ and 80-100 ℃ to 600 ℃. This work showed that modelling capabilities depend on the width of the ATD temperature range. Therefore, more work is suggested to extend this range. Research could be conducted with the aid of refrigerating chambers and low melting point alloy baths to achieve measurements for a wider modelling range from below zero to decomposition temperatures. Furthermore the technique used here involved two complementary measurements to cover the modelling range. The use of a single method covering the entire range would advisable for a better understanding of the thermal characterization in the transition zone.

This research showed that the heat transfer properties for orthotropic CFRP com-

posited are highly influenced by the properties of the fibres in the different directions. Further studies might be undertaken to assess and model the dependence of the thermal properties from the laminate stacking sequence, especially along the through-thickness direction.

In this work, the use of modelling and indirect techniques for the evaluation of thermal property values was undertaken. This method involves the use of iterative guesses for the determination of the relevant values. It is deemed to be a time consuming approach depending on the complexity of the problem and the number of variables governing the specific problem. In the last few decades, the computational power offered by computers, allowed the spread and development of optimisation algorithms. At the present time, the application of these techniques to thermal problems does not seem to exist. Optimisation algorithms assess the fitness of guessed set of variable values/functions for the problem addressed. This approach could reveal unforeseen features of the thermal properties of composites, trigger new challenges and approach new horizons.

# Chapter 9

# List of publications

- R. C. Easby, S. Feih, C. Konstantis, G. La Delfa, V. Urso Miano, A. Elmughrabi, A. P. Mouritz, A. G. Gibson, Measurement and modelling of the response of pultruded phenolic composites to fire, in: Proceedings of Sampe, Paris, 2007. cacti forum

- V. Urso Miano, A. G. Gibson, Fire model for fibre reinforced plastic composites using apparent thermal diffusivity (ATD), Proceedings 13nth European Conference on Composites Materials, ECCM13, 2008.

- R. C. Easby, S. Feih, C. Konstantis, G. La Delfa, V. Urso Miano, A. Elmughrabi, A. P. Mouritz, A. G. Gibson, Failure model for phenolic and polyester pultrusions under load in fire, Plastics, Rubber and Composites 36 (9).

- V. Urso Miano, A. G. Gibson, A. P. Mouritz, S Feih, Simultaneous measurement of apparent thermal diffusivity and distortion of composites at high temperature, Proceedings of the 17nth International Conference on Composite Materials, ICCM-17, Edinburgh, 2009.

- V. Urso Miano, A. G. Gibson, Fire model for fibre reinforced plastic composites using apparent thermal diffusivity (ATD), Plastics, Rubber and Composites 38 (2/3/4) (2009) 8792.

- G. La Delfa, V. Urso Miano, A. Gibson, Characterisation and modelling of structural integrity of carbon fibre wing box laminate subject to fire, Plastic, Rubber and Composites 38 (2009) 367-373.

# Bibliography

[1] A. P. Mouritz, A. G. Gibson, Fire Properties of Polymer Composite Materials, Solid Mechanics and its Applications, Springer, 2006.

[2] V. Babrauskas, R. D. Peacock, Heat release rate: the single most important variable in fire hazard, Fire Safety Journal 18.

[3] R. C. Easby, S. Feih, C. Konstantis, G. La Delfa, V. Urso Miano, A. Elmughrabi, A. P. Mouritz, A. G. Gibson, Failure model for phenolic and polyester pultrusions under load in fire, Plastics, Rubber and Composites 36 (9).

[4] A. G. Gibson, Performance issues related to aerospace composites post-fire and post-crash fire behaviour, Fifth Conference on Composites in Fire (CIF5) Newcastle upon Tyne 2008.

[5] ISO, ISO 5660-1: "Reaction-to-fire tests - Heat release, smoke production and mass loss rate - Part 1: (cone calorimeter method)", International Organization for Standardization, International Standard Organization, Second Edition, 2002.

[6] J. B. Henderson, J. . Wiebelt, M. R. Tant, A model for the thermal response of polymer composite materials with experimental verification, Journal of Composite Materials 19 (1985) 579–594.

[7] A. G. Gibson, P. N. H. Wright, Y.-S. Wu, J. T. Evans, Laminate theory analysis of composites under load in fire, Journal of Composite Materials 40 (7) (2006) 639–658.

[8] S. Feih, Z. Mathys, A. G. Gibson, M. A. P., Modelling the tension and compression strengths of polymer laminates in fire, Composites Science and Technology 67 (2007) 551–564.

[9] A. Mouritz, S. Feih, Z. Mathys, A. G. Gibson, Mechanical property degradation of naval composite materials, in: ONR (Ed.), Modelling of Naval Composite Structures, SAGE Publications, 2006, pp. 2387 – 2410.

[10] A. G. Gibson, P. N. H. Wright, Y.-S. Wu, A. P. Mouritz, Z. Mathys, C. P. Gardiner, Modelling residual mechanical properties of polymer composites after fire, Plastics, Rubber and Composites 32 (2) (2003) 81–90.

[11] V. Urso Miano, A. G. Gibson, Fire model for fibre reinforced plastic composites using apparent thermal diffusivity (atd), Plastics, Rubber and Composites 38 (2/3/4) (2009) 87–92.

[12] J. B. Henderson, M. R. Tant, Measurement of thermal and kinetic properties of a glass-filled polymer composite to high temperatures, High Temperatures-High Pressures 18 (1996) 17–28.

[13] ASTM, Standard test method for determining specific heat capacity by differencial scanning calorimetry, 2004.

[14] H. C. Kung, A mathematical model of wood pyrolysis, Combustion and Flame 18 (1972) 185–195.

[15] K. A. Murty, Thermal decomposition kinetics of wood pyrolysis, Combustion and Flame 29 (1977) 311–324.

[16] N. Dodds, A. G. Gibson, D. Dewhurst, J. M. Davies, Fire behaviour of composite laminates, Composites: Part A 31 (7) (2000) 689–702.

[17] M. R. E. Looyeh, P. Bettess, A. G. Gibson, A one-dimensional finite element simulation for the fire-performance of grp panels for offshore structures, Interna-

tional Journal of Numerical Methods for Heat & Fluid Flow 7 (6) (1997) 609–625, no.8.

[18] A. G. Gibson, Y.-S. Wu, H. W. Chandler, J. A. D. Wilcox, P. Bettess, A model for the thermal performance of thick composite laminates in hydrocarbon fires, Revue de l'Institut Francais du Petrole 50 (1) (1995) 69–74 (special issue).

[19] B. Y. Lattimer, J. Ouellette, Thermal properties of composites for heat transfer modeling during fires, Proceedings of SAMPE 2004 Conference, Long Beach CA.

[20] Y.-S. W. A. G. Gibson, P. N. H. Wright, Fibre reinforced composite-steel connections for transverse ship bulkheads, Plastics, Rubber and Composites Processing and Applications 29 (10) (2000) 549–557.

[21] V. Urso Miano, A. G. Gibson, Fire model for fibre reinforced plastic composites using apparent thermal diffusivity (atd), Proceedeings 13th European Conference on Composites Materials, ECCM13.

[22] B. Y. Lattimer, J. Ouellette, J. Trelle, Thermal response of composite materials to elevated temperatures, in: ONR (Ed.), Modelling of Naval Composite Structures, Acclaim printing, 2006, pp. 1–48.

[23] J. B. Henderson, J. A. Wiebelt, M. R. Tant, G. R. Moore, A method for the determination of the specific heat and heat of decomposition of composite materials, Thermochimica acta 57 (1982) 161–171.

[24] R. C. Easby, S. Feih, C. Konstantis, G. La Delfa, V. Urso Miano, A. Elmughrabi, M. A. P., A. G. Gibson, Measurement and modelling of the response of pultruded phenolic composites to fire, in: Proceedings of Sampe, Paris, 2007.

[25] A. P. Mouritz, Z. Mathys, Mechanical properties of fire-damaged glass-reinforced composites, Fire and Materials 24 (2000) 67–75.

[26] A. P. Mouritz, C. P. Gardiner, Compression properties of fire-damaged polymer sandwich composites, Composites part A 33 (2002) 609–620.

[27] A. G. Gibson, P. N. H. Wright, Y. S. Wu, A. P. Mouritz, Z. Mathys, C. P. Gardiner, The integrity of polymer composites during and after fire, Journal of Composites Materials 238 (15) (2004) 1283–1307.

[28] S. Feih, Z. Mathys, M. G, A. G. Gibson, M. Robinson, A. P. Mouritz, Influence of water content on failure of phenolic composites in fire, Polymer degradation and stability 93 (2008) 376–382.

[29] D. Anderson, E. Freeman, The kinetics of the thermal degradation of the synthetic styrenated polyester, liminac 4116, Journal of Applied Polymer Science 1 (2) (1959) 192–199.

[30] H. L. Friedman, Kinetics of thermal degradation of char-forming plastics from thermogravimetry, application to a phenolic plastic, Journal of Polymer Science 6 (1965) –.

[31] T. D. Eastop, A. McConkey, Applied thermodynamics, Longman, London and New York 6 (1978) –.

[32] A. H. Buchanan, Structural Design for Fire Safety, John Wiley and Sons, 2001.

[33] Y. Wu, A. L. Naas, Calibration of heat flux emitted from flames of a small scale propane burner, Internal technical report, School of Mechanical and System Engineering University of Newcastle (2004) UK.

[34] H. S. Carslaw, J. C. Jaeger, Conduction of heat in solids, 2nd edition, Oxford Science Publications, 1959.

[35] D. R. Croft, D. G. Lilley, Heat transfer calcucations using finite difference equations, Applied science publishers, 1977.

[36] G. M. Dusinberre, Heat-transfer calculations by finite differences, Scranton, International Textbook Co, 1961.

[37] ASTM, Standard test method for determining heat transfer rate using a thermal capacitance (slug) calorimeter, ASTM E457-96(2002), Philadelphia, USA, 2002.

[38] H. L. Friedman, in: Proceedings of the $136^{th}$ American Chemical Society Meeting, Atlantic City, NJ, USA, 1959.

[39] http://www.gnuplot.info/.

[40] Y. Bay, N. L. Post, J. J. Lesko, T. Keller, Experimental investigations on temperature-dependent thermo-physical and mechanical properties of pultruded gfrp composites, Thermochimica Acta 469 (2008) 28–35.

[41] R. Volpes, G. Rodon, Fisica Tecnica, (Heat Transfer), 2nd edition, Dario Flaccovio Editore, 1994.

[42] G. La Delfa, V. Urso Miano, A. Gibson, Characterisation and modelling of structural integrity of carbon fibre wing box laminate subject to fire, Plastic, Rubber and Composites 38 (2009) 367–373.

[43] G. La Delfa, Aerospace composite materials in fire, PhD Thesis, Newcastle University, Newcastle, UK, (2009).

[44] T. N. A. Browne, A model for the structural integrity of composite laminates in fire, PhD Thesis Newcastle University, Newcastle, UK, (2006).

[45] J. Bausano, S. Boyd, J. Lesko, S. Case, Composite life under sustained compression and one sided simulated fire exposure: characterisation and prediction, in: Composites in Fire 3, Newcastle upon Tyne, England, 2003.

[46] A. P. M. A. G. Gibson, S. Feih, Z. Mathys., Tensile strength modeling of glass fiber - polymer composites in fire, Journal of Composite Materials 41 (2007) 2387–2410.

[47] S. Feih, Z. Mathys, A. G. Gibson, M. A. P., Modelling compression strengths of polymer laminates in fire, Composites part A 38 (2007) 2354–2365.

[48] A. S. Fiberline Composites, Fiberline design manual (2007) ).

[49] V. Babrauskas, Development of the cone calorimeter - a bench-scale heat release rate apparatus based on oxygen consumption, Fire and Materials 8 (2) (1994) 81–95.

[50] B. Budiansky, N. A. Fleck, Compressive failure of fibre composites, Journal of the Mechanics and Physics of Solids 41 (1) (1993) 183–211.

[51] B. Budiansky, N. A. Fleck, A. J. C, On kink-band propagation on fibre composites, Journal of the Mechanics and Physics of Solids 46 (9) (1997) 1637–1653.

[52] Advanced composite compression tests, boeing specification support standard (1986).

[53] A. G. Gibson, A. P. Mouritz, , M. Z, Journal of Composite Materials 38 (2004) 1283–1306.